Antennas for low-cost Ka-band ground terminal devices

THÈSE Nᵒ 7554 (2017)

PRÉSENTÉE LE 27 MARS 2017

À L'ÉCOLE POLYTECHNIQUE FÉDÉRALE DE LAUSANNE
À LA FACULTÉ DES SCIENCES ET TECHNIQUES DE L'INGÉNIEUR
LABORATOIRE D'ÉLECTROMAGNÉTISME ET ANTENNES

ET

À L'INSTITUTO SUPERIOR TÉCNICO (IST) DA UNIVERSIDADE DE LISBOA

PROGRAMME DOCTORAL EN GÉNIE ÉLECTRIQUE
DOUTORAMENTO EM ENGENHARIA ELECTROTÉCNICA E DE COMPUTADORES

POUR L'OBTENTION DU GRADE DE DOCTEUR ÈS SCIENCES (PhD)

PAR

Joana Rita ALVES DOS SANTOS SILVA

acceptée sur proposition du jury:

Prof. M. Figueiredo, président du jury
Prof. J. R. Mosig, Prof. C. A. Cardoso Fernandes, directeurs de thèse
Prof. J. Costa, rapporteur
Prof. A. Moreira, rapporteur
Prof. C. Peixeiro, rapporteur
Dr. N. Fonseca, rapporteur
Dr. H. Legay, rapporteur

TÉCNICO LISBOA

EPFL
ÉCOLE POLYTECHNIQUE
FÉDÉRALE DE LAUSANNE

Suisse
2017

UNIVERSIDADE DE LISBOA
INSTITUTO SUPERIOR TÉCNICO

ÉCOLE POLYTECHNIQUE FÉDÉRALE DE LAUSANNE

Antennas for low-cost Ka-band ground terminal devices

Joana Rita Alves dos Santos Silva

Supervisors: Doctor Carlos António Cardoso Fernandes
Doctor Juan Ramon Mosig

Thesis approved in public session to obtain the PhD Degree in
Electrical and Computer Engineering

Jury final classification: Pass with Distinction

Jury

Chairperson: Chairman of the IST Scientific Board

Members of the Committee:
Doctor Juan Ramon Mosig, Full Professor, École Polytechnique Fédérale de Lausanne, Switzerland
Doctor Jorge Manuel Lopes Leal Rodrigues da Costa, Associate Professor (with habilitation), Escola de Tecnologias e Arquitectura, ISCTE-Instituto Universitário de Lisboa, Portugal
Doctor António Manuel Restani Graça Alves Moreira, Associate Professor, Instituto Superior Técnico, Universidade de Lisboa, Portugal
Doctor Custódio José de Oliveira Peixeiro, Assistant Professor, Instituto Superior Técnico, Universidade de Lisboa, Portugal
Doctor Nelson Jorge Gonçalves Fonseca, Researcher, European Space Agency, The Netherlands
Doctor Hervé Legay, Head of Advanced Studies on Antennas, Thales Alenia Space, France, individual with recognized competence in the scientific area of the thesis

2017

We leave something of ourselves behind when we leave a place. We stay there, even though we go away. And there are things in us that we can find again only by going back there.

Pascal Mercier, *Night train to Lisbon*

To my parents, Ana e Carlos.
To my brother, Sérgio.
To my great-aunt, Lourdes.

To the memory of my dear aunt Isabel.

Acknowledgements

Abstract

The ever-growing demand for high-speed data links together with the increasing congestion in the traditional microwave spectrum are pushing for the exploitation of higher microwave and millimeter-wave (mm-wave) frequencies, including the so-called Ka band. Major investments came along, especially in the satellite communications industry, raising the technological constraints imposed on electronic equipment, mainly concerning performance, compactness and both reduced cost and weight.

The great antenna size reduction achieved at Ka band has boosted the research towards satellite-on-the-move applications (SOTM), aiming the development of ground terminal antennas for both commercial and personal use. Such antennas must work simultaneously at downlink and uplink Ka bands with circular polarization and also have beam steering capabilities to keep a steady connection with the satellite. In addition, the target is also achieving a cost-effective low-profile antenna.

The present thesis is focused on the design of feed antennas to be integrated in mechanical beam steering systems for the aforementioned application. Three different designs are here proposed and discussed. The first one, a wideband ridged horn antenna, was tested standalone and with a dielectric lens antenna. Once good results were achieved in both scenarios, reducing its height would be the next goal. Thus, the second design is a cavity backed patch antenna. A comparison between both feed antennas is performed, highlighting the pros and cons of both solutions, either standalone or with the same dielectric lens antenna. Here, the first studies with a planar lens antenna are shown. Finally, the third device consists of a ridged cavity antenna with a cross-slot on its top aperture. This time, the feed was successfully tested with a transmitarray which allows achieving a more compact antenna system than the first one here presented.

This thesis also analyzes two different manufacturing techniques, traditional milling technique and an innovative additive manufacturing (AM) technique based on metallized polymers called stereolithography (SLA). The present AM-SLA prototypes clearly illustrate the strong potential of this technology and pushes for its further assessment.

Keywords: feed antennas, ridged horn antenna, cavity-backed patch antenna, ridged cross-slot antenna, mechanical beam steering antennas, circular polarization, satellite communications,

satellite-on-the-move (SOTM), Ka band, milling, additive manufacturing (AM), stereolithography (SLA).

Resumé

La demande toujours plus importante de canaux de communication à grande vitesse, associée à la congestion croissante du spectre électromagnétique traditionel, poussent à exploiter des fréquences élevées ou millimétriques, en particulier en bande Ka. Des investissements importants ont accompagné ce mouvement, en particulier dans l'industrie des communications par satellites; les contraintes technologiques imposées aux équipements électroniques se sont alors accentuées, tant en ce qui concerne les performances que la compacité, le prix ou encore le poids.

La réduction de taille substancielle obtenue en bande Ka a motivé les recherches concernant le suivi de satellites en mouvement, avec pour objectif le développement d'antennes terrestres à la fois pour des usages commerciaux et personnels. Ces antennes doivent travailler simultanément en débit montant et en débit descendant (bande Ka) ainsi qu'en polarisation circulaire. Elles doivent également être capables de dépointer leur faisceau pour maintenir une connexion fiable avec le satellite. Enfin, le dernier but recherché est de minimiser l'encombrement et les coûts de ces antennes.

Cette thèse aborde la conception d'antennes intégrées dans des systèmes de dépointage mécanique pour les applications mentionnées ci-dessus. Trois différentes antennes sont proposées et discutées. La première, une antenne cornet *ridged* à large bande, a été testée seule et avec une lentille diélectrique. Lorsque les deux ont donné de bons résultats, la réduction de la taille s'est présentée comme l'objectif suivant. C'est pourquoi la deuxième antenne a été une antenne imprimée en cavité. Une comparaison entre les deux antennes est effectuée, mettant en évidence les avantages et les inconvénients des deux prises seules ou avec la lentille diélectrique. Ici, les premières études avec une lentille plane sont faites. Finalement la troisième antenne consiste en une fente en forme de croix au dessus d'une cavité *ridged*. Cette fois-ci, l'excitation a été testée avec succès à l'aide d'une antenne réseau qui a permis d'améliorer la compacité par rapport à la première solution.

Deux procédés de fabrication différents sont analysés, à savoir le fraisage traditionnel mais aussi une méthode de fabrication additive innovante basée sur des polymères métallisés: la stéréolithographie. Les prototypes obtenus ainsi illustrent clairement le fort potentiel de cette technologie et se présentent comme encourageants en vue d'autres recherches.

Mots clefs: antenne *feed*, antenne cornet *ridged*, antenne imprimée en cavité, antenne *ridged cross-slot*, antenne à dépointage mécanique, polarisation circulaire, communications par satellite, suivi de satellite, bande Ka, fraisage, fabrication additive, stéréolithographie.

Resumo

A exigência cada vez maior por ligações de dados de alta velocidade, juntamente com o aumento do congestionamento do espectro de microondas tradicional estão a promover a exploração de frequências mais altas nas gamas de microondas e de ondas milimétricas, onde se inclui a chamada banda Ka. Esta evolução está a ser acompanhada por grandes investimentos, especialmente na indústria de comunicações por satélite, que estão a aumentar as restrições tecnológicas impostas aos equipamentos electrónicos, principalmente em relação ao seu desempenho, compacidade e redução tanto de custo como de peso.

A grande redução no tamanho da antena que é possível na banda Ka impulsionou a investigação de comunicações por satélite a partir de plataformas móveis, sendo um dos objectivos o desenvolvimento de terminais de Terra direccionados quer para sistemas comerciais quer para uso pessoal. Estas antenas devem funcionar na banda Ka, tanto na frequência da ligação descendente como na frequência da ligação ascendente, com polarização circular e também devem conseguir orientar o feixe de forma a manter uma ligação estável com o satélite. Além disto, o objectivo passa igualmente por obter uma antena de baixo perfil que seja economicamente acessível.

Esta tese centra-se no desenvolvimento da fonte primária, que será posteriormente integrada num sistema mecânico para orientação do feixe de forma a satisfazer a aplicação descrita acima. Neste documento são propostas e discutidas três antenas. A primeira, uma corneta *ridged* de banda larga, foi testada sozinha e também com uma lente dieléctrica. Uma vez que foram obtidos bons resultados em ambos os casos, a redução da altura da corneta tornou-se no desafio seguinte. Deste modo, foi desenvolvida uma cavidade com *patches* no seu interior. As duas antenas são comparadas, destancando-se os prós e contras de cada uma, tanto na sua análise independente como quando integradas com a lente dieléctrica. Neste ponto é apresentado um estudo preliminar da cavidade com uma lente plana. Por último, a terceira antena consiste numa cavidade *ridged* com uma ranhura em forma de cruz na sua abertura. Esta fonte primária é testada com sucesso com um agregado de elementos transmissores, e juntos constituem um sistema mais compacto do que o primeiro aqui mencionado.

Esta tese também analisa duas técnicas de fabrico distintas, a tradicional técnica de fresagem e uma técnica inovadora de fabricação aditiva baseada em polímeros metalizados conhecida por estereolitografia. Os protótipos feitos com esta nova tecnologia são excelentes exemplos para demonstrar o seu imenso potencial e incentivam uma crescente aposta na mesma.

Palavras-chave: fonte primária, corneta *ridged*, cavidade com *patches*, cavidade *ridged*, antenas com orientação mecânica do feixe, polarização circular, comunicação por satélite, terminais de Terra móveis, banda Ka, fresagem, fabricação aditiva, estereolitografia.

Contents

Acronyms and abbreviations

ACTS	Advanced Communications Technology Satellite
AM	Additive Manufacturing
AMAZE	Additive Manufacturing Aiming towards Zero waste and Efficient production of high-tech metal products
BC	Boundary Conditions
BFN	Beam-Forming Network
CEPT	Conference of Postal and Telecommunications Administrations
CNC	Computer Numerical Control
COMSAT	Communications Satellite Corporation
CP	Circular Polarization
CS	Communication Satellite
DFS	*Deutsches Fernmelde Satellitensystem*
DMLS	Direct Metal Laser Sintering
DRA	Dielectric Resonator Antenna
ECC	Electronic Communications Committee
EIRP	Effective Isotropic Radiated Power
EPFL	*École Polytechnique Fédérale de Lausanne*
ESA	European Space Agency
ESOMP	Earth Stations On Mobile Platform
FCT	*Fundação para a Ciência e a Tecnologia*
FDMA	Frequency Division Multiple Access
FSS	Fixed Satellite Service

GEO	Geostationary Equatorial Orbit
GNSS	Global National Satellite Systems
HAPS	High-Altitude Platform Station
HDFSS	High Density Fixed Satellite Service
HTS	High Throughput Satellite
IST-UL	*Instituto Superior Técnico – Universidade de Lisboa*
IT	*Instituto de Telecomunicações*
ITALSAT	Italian Satellite
ITU	International Telecommunication Union
JAXA	Japanese Aerospace Exploration Agency
Ka	*Kurz*-above
KET	Key Enabling Technology
Ku	*Kurz*
LAN	Local Area Network
LEMA	*Laboratoire d'Éectromagnétisme et Acoustique*
LHCP	Left Hand Circular Polarization
LMDS	Local Multipoint Distribution Service
LP	Linear Polarization
NASA	National Aeronautics and Space Administration
NASDA	National Space Development Agency
PCB	Printed Circuit Board
RF	Radio Frequency
RiCSA	Ridged Cavity-backed Slot Antenna
RHCP	Right Hand Circular Polarization
RL	Return loss
SHF	Super High Frequency
SIW	Substrate Integrated Waveguide

SLA	Stereolithography
SLS	Space Laser Sintering
SOTM	Satellite-On-The-Move
TE	Transverse Electric
TM	Transverse Magnetic
Tx-array	Transmitarray
UHF	Ultra High Frequency
UWB	Ultra-Wideband
VSAT	Very Small Aperture Terminal
VSWR	Voltage Standing Wave Ratio

Chapter 1   Introduction

Eles não sabem, nem sonham
Que o sonho comanda a vida.

António Gedeão

This chapter contains the introduction to the thesis. First, the motivation and context of the research work are presented, followed by the description of the objectives. Then, the organisation of the thesis is described and the main original contributions are listed. Finally, the list of publications generated by this thesis is provided.

1.1   Motivation and context of the work

The interest in satellite communications has been greatly increased in the past years. Fig. 1.1 aims to demonstrate exactly this fact by marking on the map the countries with satellites and highlighting the huge difference between 1966 and 2016.

An attentive analysis of Fig. 1.1 leads to the conclusion that more than 55 countries have started to invest in satellite communications in the past 50 years. This is clearly associated to a parallel economic growth that was crucial to support the required technology advancement. But certainly, it is also strongly coupled to the key advantages of satellite communications that should be recalled now. The first one is the allowance of wireless communications between two widely separated points. Another unquestionable advantage is the global availability once the satellites are able to offer connectivity to more and more people from all around the world. Whereas the terrestrial services have a limited coverage, satellite communications target not only land markets but also maritime and aeronautical ones. The advantage is even bigger due to the association of wireless communications, global availability and high reliability. The independence of ground infrastructures contributes to see it as an unique and trustworthy way to ensure communications in a disaster scenario. Moreover, satellite communications can be considered as cost-effective since neither the number of users nor the distance between them have influence in

their associated cost. Then, it is no longer a surprise to rely on satellites to provide secure, efficient and resilient commercial, military, government and emergency communications [2], [3].
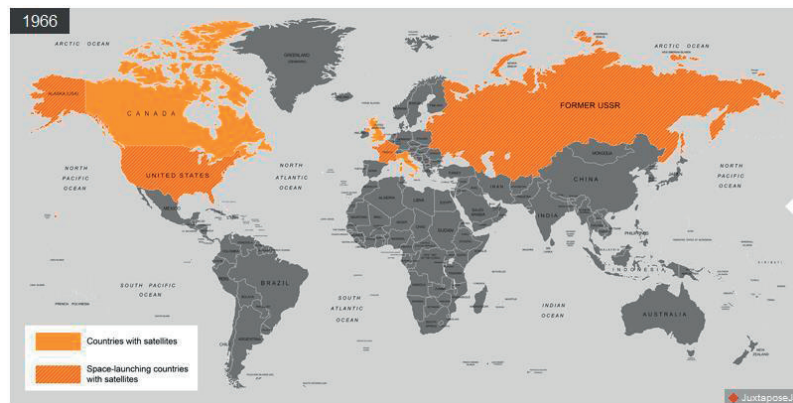
(a)
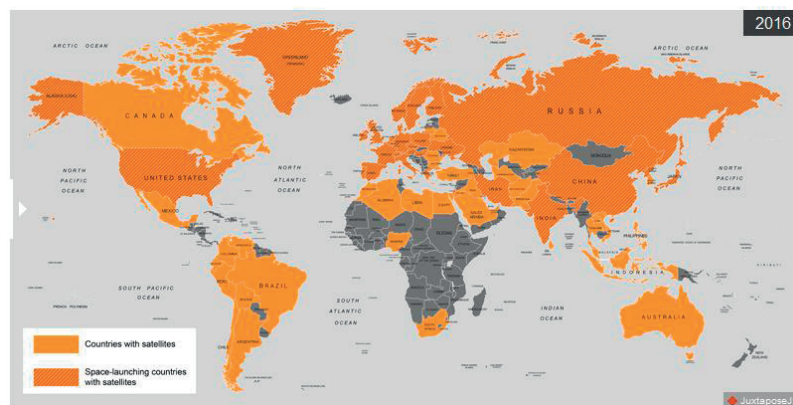
(b)

Fig. 1.1 – Countries with satellites: (a) in 1966; (b) in 2016 [1].

Historically, the idea of applying the already known Geostationary Equatorial Orbit (GEO) to satellite communications dates from 1945. At that time, the prediction of a worldwide coverage was described by the science-fiction writer Arthur C. Clarke in his paper entitled "Extra-terrestrial Relays - Can Rocket Stations Give World-wide Radio Coverage?" published in the Wireless World magazine [2], [4]. His network would need to count with three satellites as reported in the publication shown in Fig. 1.2.
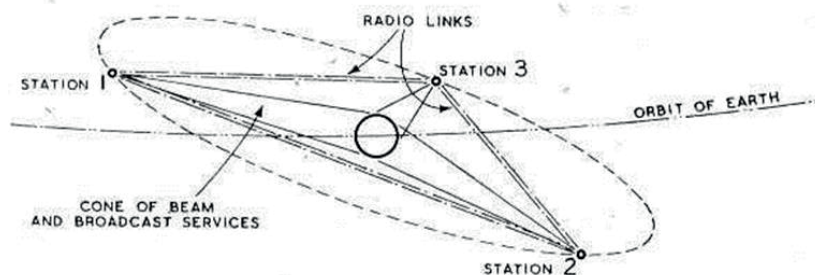
Fig. 1.2 – GEO satellite communications by Arthur C. Clarke: (a) first page of his publication; (b) his net-work conception [5].

This utopic idea turned into reality 20 years later with the launch of the first commercial GEO satellite named Intelsat-I, also known as Early Bird [2]. The satellite was built for the Communications Satellite Corporation (COMSAT) by the Hughes Aircraft Company and it was launched and tracked by the National Aeronautics and Space Administration (NASA) agency. In addition to be able to provide different broadcasting services such as telephone and television, it enabled direct communications between Europe and North America. The success of this mission helped to promote even more the satellite communications industry and since then, it has been evolving at a very fast pace. The next generations of satellites were precursor of a dramatic technological advancement. The biggest capability change until that moment came with Intelsat-IV that was much larger than all the previous ones. All of these changes were extremely valuable to place satellites as the primary means of international communication. In fact, this industry is permanently spearheading a technical struggle to satisfy the demands for higher capacity and speed-links of the global digital society that they created [2]. All those demands were the basis of the enormous pressure to improve and succeed along the past years, and in a way they are also linked to several technology life-cycles.

In line with those technology developments, the sector was also evolving along the Radio-Frequency (RF) spectrum, always increasing the frequency (see Fig. 1.3). The upper part of the spectrum, named Super High Frequency (SHF), concentrates the frequency bands of interest for satelites. Here, almost the majority of the bands are shared which means that the frequencies are also used by terrestrial links. Ku and Ka bands, in particular, have part of the band for ex-clusive use of satellite links [2]. By convention, the satellite band is divided in two parts: one for space to ground links (usually named by downlink band) and another one for ground to space links (commonly named by uplink band). The uplink band is allocated above the downlink one because in general, the higher the frequency, the more difficult is to generate RF power. So the

harder task (generating the required power at the highest frequency) is left to the earth station rather than to the satellite [2].
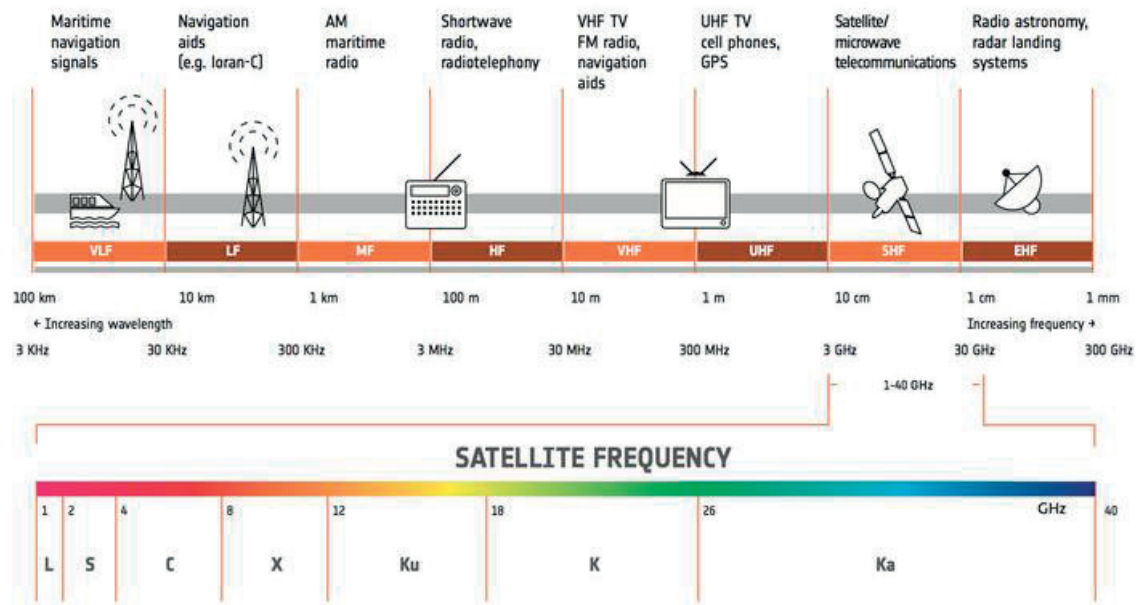
Fig. 1.3 – RF spectrum [6].

Regarding commercial satellite systems, the C-band was the first frequency range that was extensively used. For instance, the aforementioned satellites, from Intelsat-I (Early Bird, 1965) until Intelsat-IV (1975), were operating at this frequency band as shown in Fig. 1.4 [7]. Moreover, the availability of C-band microwave equipment developed for other applications was also a key factor for its adoption [2]. As the X-band is reserved for government and military use, the Ku-band was the next natural choice for commercial communications (see Fig. 1.4).

Herewith the development of the sector has consequently contributed for the increasing congestion of the traditional microwave spectrum. Then, together they turned to be the main reason to push for the exploitation of higher microwave and millimeter-wave frequencies, including the so-called Ka-band [8].

4

```
1965   INTELSAT I          Early Bird. 240 voice circuits, C-band, 130 MHz
1966   INTELSAT II         First to use FDMA, 240 voice circuits, C-band, 130 MHz
1968   INTELSAT III        1500 voice circuits, 4 TV channels, C-band, 300 MHz
1971   INTELSAT IV         4000 voice circuits, 2 TV channels, C-band, 500 MHz
1975   INTELSAT IV         6000 voice circuits, 2 TV channels, C-band, 800 MHz
       Atlantic Ocean Region
1980   INTELSAT V          12 000 voice circuits, 2 TV channels, C/Ku-band, 2144 MHz
1984   INTELSAT V          12 000 voice circuits, 2 TV channels, C/Ku-band, 2144 MHz
       Atlantic Ocean Region
1987   INTELSAT V          12 000 voice circuits, 2 TV channels, C/Ku-band, 2144 MHz
       Indian Ocean Region
1990   INTELSAT VI         TDMA with independent beams, 30 000 voice circuits, 6 TV
       Atlantic Ocean Region   channels, C/Ku-band, 3300 MHz
1992   INTELSAT K          TDMA with independent beams, 16 TV transponders
```

Fig. 1.4 – Summary of INTELSAT communications satellites [7].

1.1.1 Ka-band and emerging technologies

The Ka-band is officially allocated to the spectrum from 26.5 to 40 GHz, which corresponds to the frequency interval directly above K-band [9]. In fact, this detail turned out to define the band designator **Ka** which means *Kurz*-**a**bove. In turn, *Kurz* (**K**-band) means short in German and it was chosen in order to refer to short wavelength [10].

Although Ka-band transmission is being used in different areas such as Local Multipoint Distribution Services (LMDS), High Altitude Platform Stations (HAPS) and radars, its main application nowadays is indeed satellite communications [11]. The frequency allocation for satellite services is defined by the International Telecommunication Union (ITU). In order to simplify the complex procedure, the world is divided into the following three regions: Region 1 covers Europe, Russia, Arabic peninsula and Africa; Region 2 includes both North and South America and the Greenland area; and finally Region 3 englobes the rest of Asia, Australia and the south-west Pacific. The common spectrum intervals within all the regions for fixed-satellite services (FSS), including earth stations on mobile platforms (ESOMP) are shown in Table 1.I [12], [13]. According to the Electronic Communications Committee (ECC) from the European Conference of Postal and Telecommunications Administrations (CEPT), the frequency ranges 19.7-20.2 GHz and 29.5-30 GHz are reserved for both High Density FSS (HDFSS) and uncoordinated FSS earth stations exempted from individual licensing [13].

Table 1.I – Ka-band frequency allocation.

	Downlink [GHz]	Uplink [GHz]
Civil	17.7 - 20.2	27.5 - 30
Military	20.2 - 21.2	30 - 31

Historically, the first experimental communication satellite operating in Ka-band dates back to 1977. The launch of the first Communications Satellite (CS), also known as Sakura-1 (Fig. 1.5a), was carried out by the National Space Development Agency (NASDA) of Japan that was later merged into the Japanese Aerospace Exploration Agency (JAXA). Further missions were conducted by the next generation of satellites in order to maintain the Ka-band capability. The CS-2b (Sakura-2b) and CS-2a (Sakura-2a) satellites launched in 1980 and 1983, respectively, were used to serve public communications, emergency transmissions in disaster scenarios and also the connection with the remote Japanese islands. Later, in 1988, two CS-3 (Sakura-3) satellites were launched to replace the old CS-2. The Japanese investment in Ka-satellites was followed by the European Space Agency (ESA) with the launch of the largest civilian communications satellite, the Olympus (Fig. 1.5b), in 1989. Still from that time, it is relevant to mention the Italian Satellite (ITALSAT) program and their first satellite launch in 1991 (Fig. 1.5c), the German *Deutsches Fernmelde Satellitensystem* (DFS)-Kopernikus satellite system that was operational since 1992 (Fig. 1.5d) and also the Advanced Communications Technology Satellite (ACTS) launched by NASA in 1993 (Fig. 1.5e) [2], [11], [14]. Since then, the number of Ka-band satellite systems has been increasing.

| (a) | (b) | (c) |

| (d) | (e) |
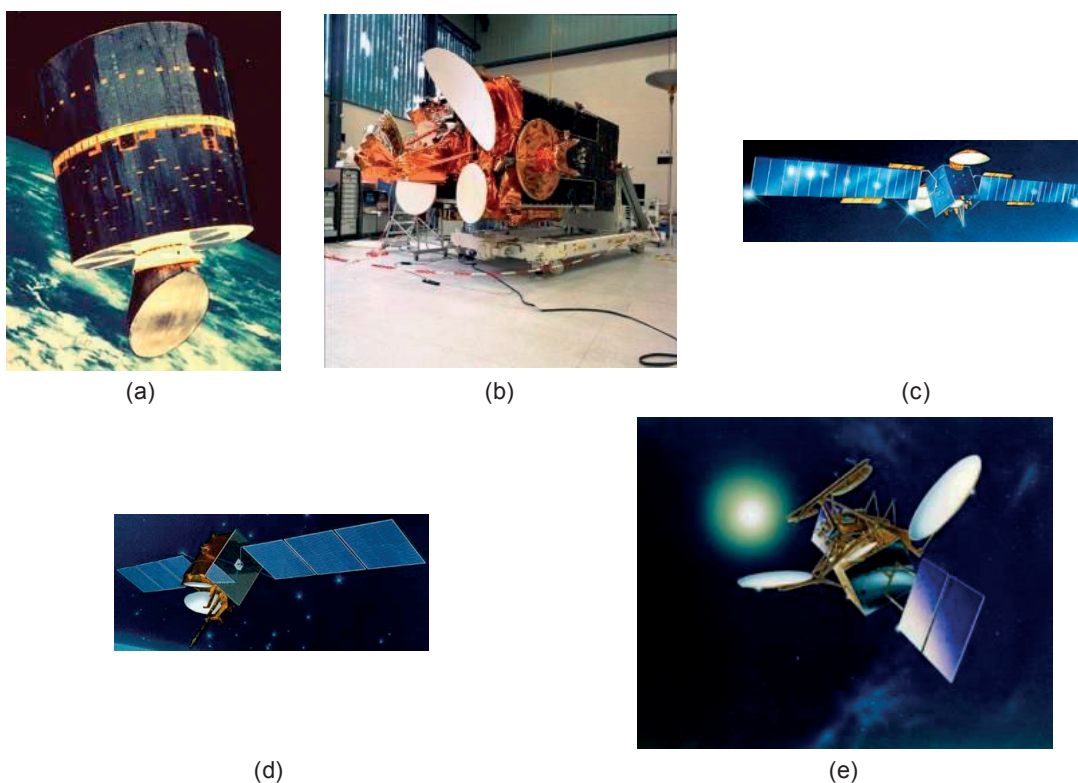
Fig. 1.5 – Ka-satellites: (a) CS-1 (Sakura-1) [15]; (b) Olympus [16]; (c) Italsat-1 [17]; (d) DFS-Kopernicus-1 [18]; (e) ACTS [19].

The satellite broadband market was a key aspect to continuously push the development of the Ka-band systems [20]. Here, the term broadband is understood as a high-capacity transmission technique that uses a wide range of frequencies to allow simultaneous data transfers. The benefits of broadband are recognized worldwide and satellite technology is being used to overcome the most difficult task which is to provide this broadband operation above any circumstance. The first High Throughput Satellite (HTS) operating at Ka-band, named Anik F2, was launched in 2004 by Telesat and it represented an important step to show the commercial viability of such systems [11], [21]. Currently, apart from Anik F2, there are several other broadband satellites operating at Ka-band such as, for instance, Ka-Sat (launched in 2010), Viasat-1 (launched in 2011) and Hylas-2 (launched in 2012). Moreover, the trend is far from disappearing with several new launches planned for the next years. For instance, both Hylas-3 and Hylas-4 from Avanti Communications, Viasat-2 and Eutelsat-35e are planned for next year [22], [23].

Actually, there are several reasons behind the adoption of Ka-band and, in general, the tendency of moving higher in frequency. The expansion towards Ka-band is often compared to the upheaval experienced in the past by this same industry on the occasion of the migration from L- and C-bands to Ku-band [9]. Yet, the Ka-band impact seems to be more significant due to its high versatility that has implied deep architectural changes. One of them is related to the beam coverage. While regional beams are the dominant architecture in C- and Ku-satellites, Ka-satellites mostly provide spot-beam coverage allowing frequency reuse operation [24]. Considering for instance the satellite Anik F2, the strong differences regarding the beam coverage between the previously mentioned three bands are depicted in Fig. 1.6, showing the spotty nature of the Ka coverage. Nevertheless, it is incorrect to assume that the spot-beam coverage started at Ka-band, since it was firstly exploited in C- and Ku-bands [24].
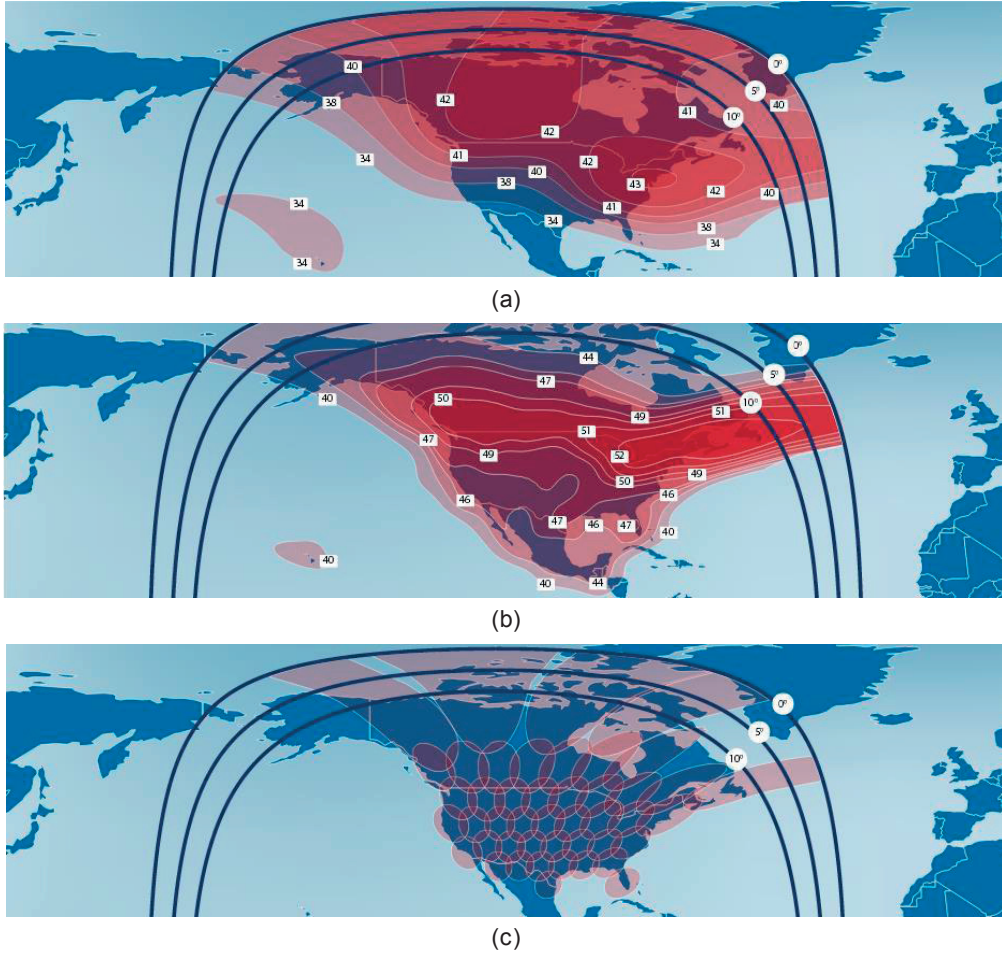
Fig. 1.6 – Coverage of North America with: (a) C-band; (b) Ku-band; (c) Ka-band [25].

However, considering spot-beams at higher frequencies (smaller wavelengths) is encouraged by a broader range of benefits. For instance, recalling the definition of antenna parameters [26], the gain is maximum at boresight and its value is given by:

$$G_{max} = (4\pi/\lambda^2)A_{eff}$$

where the wavelength is $\lambda = c/f$ (being c the velocity of light and f the frequency) and the effective aperture area of the antenna is $A_{eff} = \eta A$ (being η the efficiency of the antenna and A the aperture area). Considering a circular antenna with diameter D and geometric surface $A = \pi D^2/4$, the gain can be expressed by:

$$G_{max} = \eta(\pi Df/c)^2,$$

or in decibels (dBi) by:

$$G_{max}(dBi) = 10log\eta(\pi Df/c)^2.$$

It is obvious that, when compared with lower frequencies and for the same efficiency η, Ka-band requires smaller antennas to achieve the same gain. In other words, Ka-band systems provide larger gain for a given antenna size which results in economically and logistically attractive solutions. This is clearly visible in Fig. 1.7 that shows the maximum antenna gain, G_{max}, in dBi as a function of its diameter for different frequencies considering an efficiency of 60%. For example, for an antenna with 1 m of diameter, the gain is 39.8 dBi at 12 GHz (Ku band), 44.2 dBi at 20 GHz (downlink Ka band) and 47.7 dBi at 30 GHz (uplink Ka band).
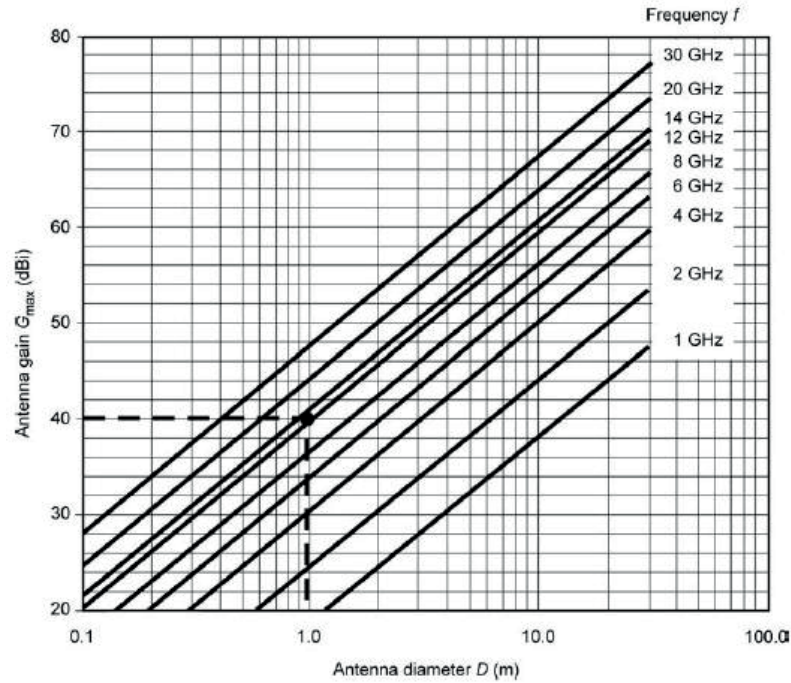
Fig. 1.7 – Maximum antenna gain as a function of its diameter (considering: η=0.6) [26].

The above results are for maximum gain usually reached at broadside (boresight direction). For other angles/directions the relevant information is contained in the radiation pattern. A very important parameter is the angular beamwidth of the antenna that is usually considered by a 3 dB gain drop with respect to the maximum value. The 3 dB beamwidth is associated to the ratio λ/D by a coefficient C that depends on the illumination law [26]. It is given by:

$$\theta_{3dB} = C(\lambda/D) = C(c/fD).$$

As an example, again for an antenna with 1 m of diameter and a coefficient C=70 which is a common value for reflector antennas when considering non-uniform illumination [26], the 3 dB beamwidth is 1.75° at 12 GHz (Ku band), 1.05° at 20 GHz (downlink Ka band) and 0.7° at 30 GHz (uplink Ka band). Therefore, in comparison with Ku-band, Ka-band enables narrower beams which then allow the provision of more beams within a given area as presented in Fig. 1.8. This reduction in the Ka-band footprint leads to a higher frequency reuse. In theory, if the beams are properly separated, their number determines the frequency reuse factor. However, continuous coverage relies on small beam superposition and in this case the common solution to avoid adjacent interference is to alternate frequencies and polarizations. Thereafter, the capacity at Ka-band is greater than in lower frequencies.

<table>
<tr><td>(a)</td><td>(b)</td></tr>
</table>

Fig. 1.8 – Spot-beam coverage of a GEO satellite at 10° East: (a) beamwidth of 0.4° at Ka-band; (b) beamwidth of 0.8° at Ku-band [23].

In parallel with these advantages, there are still some trade-offs to take into account when operating at Ka-band. High frequency is associated to higher space losses and is also the reason why Ka-band radiation is more sensitive to adverse weather conditions. In these cases, additional mitigation techniques, aiming total transparency to the end user, can be applied like in the case of scattered places receiving heavy rains. Moreover, and when compared with Ku-band solutions, Ka-band systems have more restrictive off-axis Effective Isotropic Radiated Power (EIRP) spectral densities [27]. Still, the trade-off between advantages and drawbacks is positive and, in most cases, Ka-band outperform the lower frequencies, especially regarding high-capacity systems.

1.1.2   Satellite-on-the-move (SOTM) terminals

The aforementioned Ka-band characteristics are also very interesting for the ground segment. This segment encloses the earth stations that are usually connected to the end user terminal through a terrestrial network. However, in the specific case of small stations known as Very Small Aperture Terminal (VSAT), the connection is directly established between the end user terminal and the satellite and this fact has largely widened the scope and possibilities of the ground segment (Fig. 1.9).
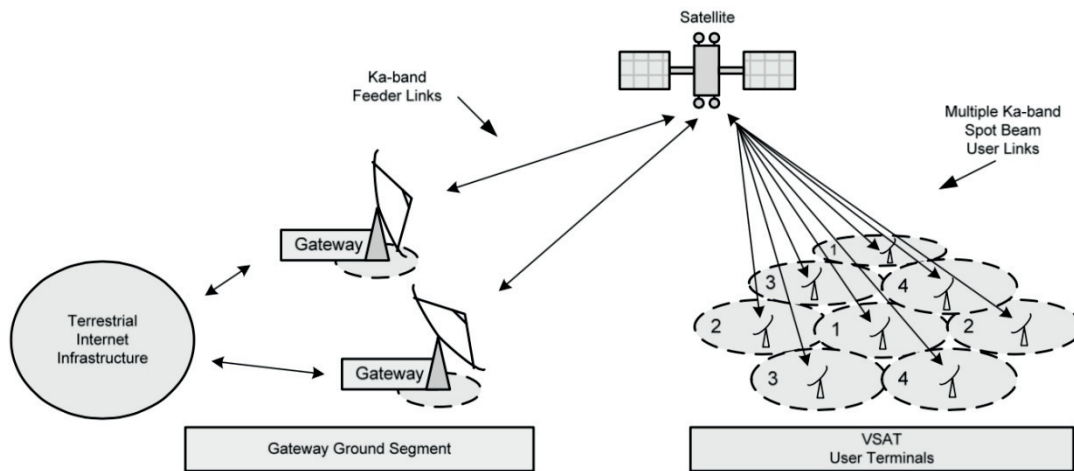
Fig. 1.9 – Ground system architecture [28].

The ground segment antennas have been evolving with several great reductions in size while the satellites have been increasing their capability and frequency of operation. At Ka-band, the dramatic size reduction has boosted the interest on SOTM applications mainly due to the customers' demands for higher speed links and the need of being always connected [9], [12], [29]. The SOTM terminals are vehicle-mounted and, obviously, the antennas must steer the beam in order to point always towards the satellite, keeping a steady link with it. Furthermore, SOTM pushed for the transition from Linear Polarization (LP) to Circular Polarization (CP) operation. Traditionally, at least in Europe, LP has been used in satellite transmissions; however in SOTM where the tracking of the satellite is needed, the use of LP would require an additional tracking axis [30]. The desired goal for this type of systems is to preserve good performance while trying to reduce the size of the antennas. Ka-band is bringing a new and large margin to progress in this category and research is being driven towards not only commercial moving platforms (e. g. high-speed trains, buses or airplanes) but also to personal use (e. g. small boats or all-terrain vehicles).

11

1.2   Objectives

The goal of this thesis is to develop compact and low-cost Ka-band antenna elements, while exploring innovative manufacturing techniques. The radiating elements should be capable to work simultaneously at both downlink and uplink Ka-bands with CP, either presenting wideband or dual-band behavior.

As previously explained, the characteristics of the Ka-satellites have boosted the interest in SOTM applications. Following this research line, the antennas proposed in this thesis were integrated as feeders in lens-based systems aiming to conciliate good performance, simplicity, low cost and low profile in a mechanical beam-steering solution. It is important to mention that the design of the lens antennas (and similar devices) used in this thesis is out of its scope. Here, the focus is the feeder and for this specific application, besides the aforementioned features, it must also have a stable phase center once it represents, together with the lens focal point, an important aspect of the entire antenna system.

For the sake of simplicity, the objectives were grouped in Fig. 1.10.
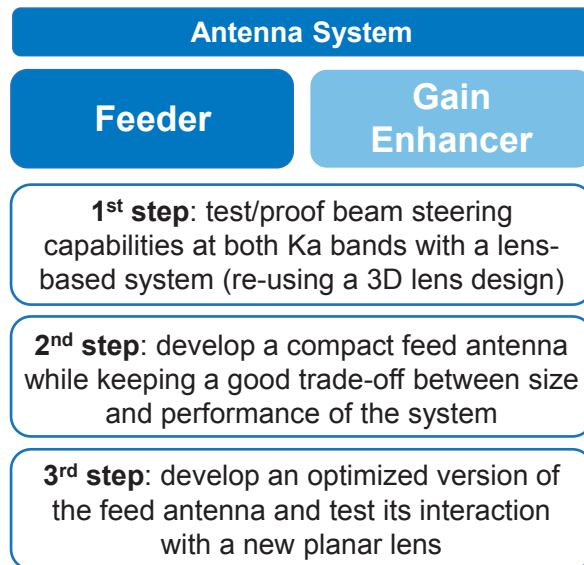
Fig. 1.10 – Objectives of this thesis.

1.3   Framework of the thesis

This thesis is one of the outputs of a joint doctoral initiative established between the Instituto Superior Técnico – Universidade de Lisboa (IST-UL), in Lisbon, Portugal and the École Polytechnique Fédérale de Lausanne (EPFL), in Lausanne, Switzerland. The former program was

oriented towards seven focus areas where both IST-UL and EPFL have strong competences, being "Antennas and EM devices for Wireless Applications" the one that enfolds this specific work. The scientific coordinators of the aforementioned area were both Professor Carlos A. Fernandes from IST-UL and Professor Juan R. Mosig from EPFL, who are also the supervisors of this thesis.

At IST-UL, the host laboratory of this thesis was Instituto de Telecomunicações (IT). This institute counts with several branches all over Portugal and develops expertise along four different scientific areas that are all managed by a Board of Directors headed by Professor Carlos Salema. This thesis is integrated in the area of Wireless Communications which is led by Professors Carlos A. Fernandes and Nuno B. Carvalho. One of the main research lines in this area is antennas, especially focused on satellite communications, Ultra-Wideband (UWB) body area networks and RF identification and localization. In the specific case of satellite communications, the laboratory has a great knowledge on lens-based systems.

At EPFL, the host laboratory of this thesis was Laboratoire d'Électromagnétisme et Acoustique (LEMA) that is headed by Professor Juan R. Mosig. As its name indicates, the two main areas of expertise are electromagnetics and acoustics. Regarding the first one, the laboratory has a deep know-how in computational electromagnetics, planar antennas, metamaterials, terahertz and graphene.

The goal of this collaboration is to take advantage of the combined expertise of both laboratories in planar feeders and lenses to fulfill the objectives described in the previous sections and in particular to develop Ka-band antennas that can be used as feeders for lens-based systems in order to achieve in the end a compact and cost-effective device for SOTM applications. The research performed during this thesis contributed for the following projects:

- o *KaLens*: Compact lens-based mechanically steered Ka-band user terminal antenna, funding by ESA;
- o *mm-SatCom*: Millimeter wave antennas for next-generation satellite mass services, funding by Fundação para a Ciência e a Tecnologia (FCT).

1.4   Outline and original contributions

The scheme of the different chapters of this thesis is illustrated in Fig. 1.11. The specific topics covered by each chapter and their original contributions are detailed next.
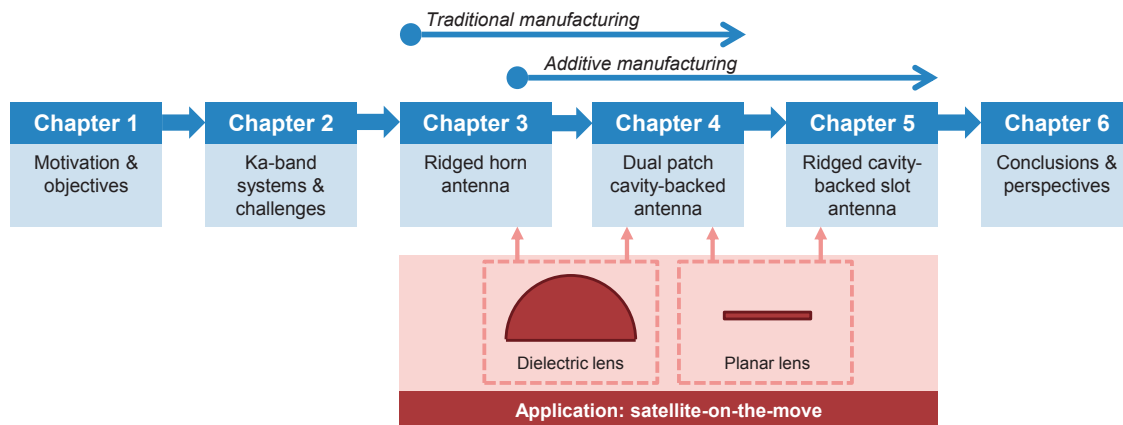
Fig.1.11 – Scheme of the different chapters of this thesis.

Chapter 2 – Ka-band antenna systems and challenges

Description: A state-of-the-art on Ka-band antenna systems is provided in this chapter. This overview serves to emphasize not only the new challenges at this frequency band but also to identify possible fabrication issues due to the limitations of the classical techniques. As an alternative solution and enabling technology, additive techniques are here discussed.

Original contributions: The concepts discussed in this chapter are not new. Nevertheless, the detailed literature review on the Ka-band antenna systems, applications and also on different manufacturing techniques allowed us to clarify the research line.

Chapter 3 – Ridged horn feed antenna for SOTM terminal

Description: A wideband ridged horn antenna and a dedicated coaxial-to-waveguide transition are proposed. A first prototype was manufactured using a classical technique named Computer Numerical Control (CNC) milling requiring the final antenna to be assembled from a set of different pieces; however the predicted wideband behavior was not achieved in the measurements. Then, a second prototype was fabricated as a single piece with success using a novel additive technology named Stereolithography (SLA). In this chapter, the horn is still integrated with a lens antenna in order to analyze a mechanical beam steering system for SOTM.

Original contributions: A Ka-band horn antenna is proposed and tested standalone and also in a lens-based system. The experience acquired and reported with both prototypes was relevant for this thesis but also for the community once this work was pioneered to demonstrate the strong potential of SLA at this frequency band.

Chapter 4 – Dual patch antenna

Description: A dual patch antenna is here presented. A trade-off analysis between this antenna and the horn presented in the previous chapter is performed. For the sake of completeness, the analysis was made for both cases: with and without the aforementioned lens antenna. This system is then further studied replacing the dielectric lens by a planar one.

Original contributions: The complete study demonstrates that planar antennas such as the example presented in this chapter are good feeder candidates and they must be considered when size is a strict requirement.

Chapter 5 – Ridged cavity-backed slot antenna

Description: The design presented in the previous chapter was the starting point for this one, aiming to conceive a compact fully metallic antenna with equivalent performance. The output is a ridged cavity-backed antenna. As a proof of concept, a dedicated beam-forming network (BFN) was also designed. This antenna is tested as the primary source of a transmitarray in order to propose a more compact system than the one shown in the Chapter 3.

Original contributions: The antenna is deeply explained through a modal analysis which shows the flexibility of the design. Once more, the prototype was fabricated resorting to SLA and the good results obtained aim to reinforce the potential of this technique especially to conceive compact RF components with complex inner shapes.

Chapter 6 – Conclusions and perspectives

This last chapter summarizes the work done during this Ph.D. thesis emphasizing not only the most important conclusions and original contributions but also the possible future research lines concerning the topics addressed here.

1.5   Publications

Papers in Journals

S. A. Matos, E. B. Lima, Joana S. Silva, J. R. Costa, C. A. Fernandes, N. J. G. Fonseca, and J. R. Mosig, "High gain dual-band beam steering transmitarray for satcom terminals at Ka band," *accepted for publication in IEEE Trans. Antennas Propag.*, Apr. 2017.

Joana S. Silva, M. Garcia-Vigueras, T. Debogovic, J. R. Costa, C. A. Fernandes, and J. R. Mosig, "Stereolithography-based antennas for satellite communications in Ka band," *Proc. IEEE (Special Issue: Additive Manufacturing of Radio-Frequency Components),* vol. 105, no. 4, pp. 655-667, Apr. 2017.

<u>Joana S. Silva</u>, E. B. Lima, J. R. Costa, C. A. Fernandes, and J. R. Mosig, "Tx-Rx lens-based satellite-on-the-move Ka-band antenna," *IEEE Antennas Wireless Propag. Lett.*, vol. 14, pp. 1408-1411, Mar. 2015.

Papers in Conference Proceedings

<u>Joana S. Silva</u>, M. Garcia-Vigueras, T. Debogovic, and J. R. Mosig, "Ka-band radiating element based on stereolithography," *accepted for publication in Proc. 11th Eur. Conf. Antennas Propag. (EuCAP), Paris, France*.

H. Hasani, <u>Joana S. Silva</u>, J. R. Mosig, and M. Garcia-Vigueras, "Dual-band 20/30 GHz circularly polarized transmitarray for SOTM applications," *in Proc. 10th Eur. Conf. Antennas Propag. (EuCAP)*, Davos, Switzerland, Apr. 2016, pp. 1-3.

E. de Rijk, <u>Joana S. Silva</u>, S. Capdevila, M. Favre, M. Billod, A. Macor, and A. von Bieren, "Additive manufactured RF components based on stereolithography," 36th European Space Agency Workshop in Antennas and RF Systems, ESA/ESTEC, The Netherlands, Oct. 2015.

<u>Joana S. Silva</u>, M. Garcia-Vigueras, M. Esquius-Morote, J. R. Costa, C. A. Fernandes, and J. R. Mosig, "A planar feed for SOTM Ka-band lens antennas," *in Proc. IEEE Antennas Propag. Soc. Int. Symp. (APSURSI)*, Vancouver, British Columbia, Canada, Jul. 2015, pp. 226-227.

<u>Joana S. Silva</u>, S. Capdevila, J. R. Costa, C. A. Fernandes, and J. R. Mosig, "Performance of a 3D-printed horn antenna working at Ka-band for satellite communications," *in Proc. URSI Atlantic Radio Science Conf. (URSI AT-RASC)*, Gran Canaria (Las Palmas), Spain, May 2015.

<u>Joana S. Silva</u>, M. Garcia-Vigueras, M. Esquius-Morote, J. R. Costa, C. A. Fernandes, and J. R. Mosig, "Lens-based Ka-band antenna system using planar feed," *in Proc. 9th Eur. Conf. Antennas Propag. (EuCAP)*, Lisbon, Portugal, Apr. 2015, pp. 1-4.

P. Robustillo, <u>Joana S. Silva</u>, J. R. Costa, C. A. Fernandes, and J. R. Mosig, "Comments on the phase center computation for Ka-band planar lens-antenna feeders," *in Proc. 9th Eur. Conf. Antennas Propag. (EuCAP)*, Lisbon, Portugal, Apr. 2015, pp. 1-2.

P. Gorski, <u>Joana S. Silva</u>, and J. R. Mosig, "Wideband, low profile and circularly polarized K/Ka band antenna," *in Proc. 9th Eur. Conf. Antennas Propag. (EuCAP)*, Lisbon, Portugal, Apr. 2015, pp. 1-3.

M. Tamagnone, <u>Joana S. Silva</u>, S. Capdevila, J. R. Mosig, and J. Perruisseau-Carrier, "The orbital angular momentum (OAM) multiplexing controversy: OAM as a subset of MIMO," *in Proc. 9th Eur. Conf. Antennas Propag. (EuCAP)*, Lisbon, Portugal, Apr. 2015, pp. 1-5.

<u>Joana S. Silva</u>, E. B. Lima, J. R. Costa, C. A. Fernandes, and J. R. Mosig, "Design and analysis of a Ka-Band coaxial-to-quad-ridged circular waveguide transition," *in Proc. 8th Eur. Conf. Antennas Propag. (EuCAP)*, The Hague, The Netherlands, Apr. 2014, pp. 7-9.

<u>Joana S. Silva</u>, E. B. Lima, J. R. Costa, and C. A. Fernandes, "Ground terminal antenna for Ka-band satellite communications," *in Proc. 7th Eur. Conf. Antennas Propag. (EuCAP)*, Gothenburg, Sweden, Apr. 2013, pp. 1613-1616.

<u>Joana S. Silva</u>, E. B. Lima, J. R. Costa, and C. A. Fernandes, "Antennas compactas baseadas em lentes com feixe orientável para terminais de terra na banda Ka," *in Proc. 6th URSI Seminar Portuguese Committee*, Lisbon, Portugal, Nov. 2012.

Chapter 2 Ka-band antenna feeding elements and challenges

Todo o mundo é composto de mudança
Tomando sempre novas qualidades.

Luís de Camões

This chapter provides an overview of Ka-band antennas highlighting the main challenges in this frequency band. First, a review of the literature is provided. It is followed by a brief discussion concerning the fabrication issues in Ka-band. Then, additive technology is here presented as an enabling technology.

2.1 Literature review

As discussed in the previous chapter, operation in Ka-band requires coping with the wide frequency separation between the downlink and uplink bands and also with CP. For the specific case of SOTM applications, beam steerable antenna systems are required and then, high gain and stable feed phase center should be considered as well. These characteristics are almost impossible to fulfill with a single antenna. Therefore, they are usually achieved by combining a primary antenna, also known as feeder, with a directive device such as lenses, reflectors, reflectarrays, transmitarrays or Fabry-Perot cavities. In the general approach, the feed antenna must already exhibit the required performance in terms of bandwidth and CP, while obviously the directive device is responsible to enhance the gain and narrow the beam. As for the beam steering, several possibilities are available being the mechanical and electronic solutions the most common ones. While in the first one, the relative movement between feed and directive device is producing the beam tilt, in the second one, the same is often done using complex RF electronic networks including specific active components.

As mentioned in the last chapter, the focus of this thesis is the feed antenna. Therefore, we

summarize now the state-of-the-art of these devices. Nevertheless, for the sake of completeness, we briefly review some interesting solutions of gain enhancers since the feed antennas proposed in this thesis will be tested in a similar scenario.

2.1.1   Feeders

Several Ka-band antenna elements that could also be used as feeders are already available in the literature. It is possible to group the proposed antennas considering several parameters. In the framework of this thesis, the groups will be based in the antenna's material and design strategy. Taking it into account, we arrived to the following main categories:

- Category 1: it encloses all-dielectric antennas;

- Category 2: hybrid antennas, mixing both dielectrics and metal, are here considered;

- Category 3: it reports all-metal solutions.

Regarding the first category, there are some examples in the literature. For instance, dielectric rod antennas are one of them. At Ka band, an example of this type of antenna is presented in [31] for active imaging systems (see Fig. 2.1a). Normally, metal cannot be avoided to feed the antenna and in this case, the feeding section is inserted into a metallic waveguide that due to design optimization does not require any horn antenna. Thus, the size of the antenna element is reduced which will be an advantage to achieve a smaller array arrangement. Another example of this type of antennas is reported in [32] at X-band; however, since the main material is dielectric, it could be easily scaled to higher frequencies. Another solution related with this category is Dielectric Resonator Antennas (DRAs) (see Fig. 2.1b). A complete review of the basic characteristics of these antennas is provided in [33]. Originally, DRAs were investigated for millimeter-wave frequencies [34] mainly due their small size, ease of fabrication, low cost and low losses. Nevertheless, since then they were also developed for lower frequencies. Again, metal cannot be avoided in the feeding network that often includes coaxial probes, metallic waveguides or microstrip lines. At Ka-band, DRAs were also used as a radiating element to develop reflectarrays as shown in [35], [36].
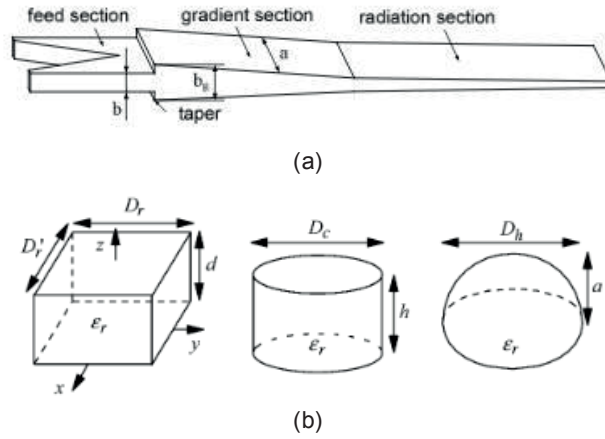
Fig. 2.1 – Dielectric-based antennas, examples taken from the literature: (a) dielectric rod antenna [31]; (b) common shapes of DRAs [33].

In line with the second category, several efforts have been carried out to design compact printed antennas at Ka-band. The main advantages of these designs are their low cost, low profile and light weight. Moreover, their popularity in many microwave areas has resulted in a mature and very well-known technology. The ease of fabrication by using Printed Circuit Board (PCB) technology is another positive aspect of this category. Though planar antennas are commonly associated to low gain, they can be easily integrated into arrays to overcome this issue. Nevertheless, there are some drawbacks. These designs usually exhibit significant substrate and conductor losses that are even more critical in higher frequencies. In order to avoid additional losses caused by the strong excitation of surface waves, the short wavelength in the millimeter wave frequency region imposes the adoption of thin substrates. The undesired surface waves can also be the source of a deterioration of the antenna performance especially regarding gain, cross-polarization and mutual coupling. On the other hand, thin substrates will imply narrow bandwidths and also more fragile structures that can become a serious problem in large arrays. Thus, the design of efficient antennas turns into a big challenge [37], [38].

Patch antennas are one of the most common solutions in this category. In many cases, aperture coupled patch antennas have been traditionally acknowledged as one of the more interesting versions of the patch family and this remains true in Ka-band [38], [39]. Basically these structures allow the separation of the patch and the microstrip transmission line by adding a ground plane layer in the middle of the dielectric layers. These two structures are electromagnetically coupled through a small aperture in the ground plane as depicted in Fig. 2.2. The employ of aperture coupled patch antennas is justified due to their attractive benefits such as broader bandwidth, protection of the radiating aperture from the feeding network and flexibility to apply different patch and aperture shapes. However, the adoption of several layers will increase the complexity of the design and its fabrication as well as the corresponding cost. Since the intro-

duction of this type of structure in 1985 [40], a very large number of designs have been proposed. At Ka-band, several examples with LP are available in the literature such as the elements presented in [41], [42]. When aiming at CP, normally the complexitiy increases, especially in the feeding network, as demonstrated in [43]-[45]. The complexitiy turns to be even higher when targeting not only CP but also broader bandwidth and higher gain. Stacked patch antennas is one of the strategies used to achieve bandwidth enhancement [46]-[48]. Apart from this strategy, to accomplish high gain, these types of designs are usually grouped in arrays [41], [42], [49], [50]. Nevertheless, some other modifications of the basic elements are possible in order to increase either the bandwidth such as the use of parasitic and capacitive patches [51], [52] and dual-ring patches [53] or both bandwidth and gain such as, for instance, backing cavities [51], [52], [54], [55]. Actually, backing cavities are a very popular solution at Ka-band not only due to the improvement in both bandwidth and gain, but also due to its benefits regarding surface waves, back radiation and isolation between elements in array arrangements. Two of the most interesting solutions among all the previously mentioned ones are presented in Fig. 2.3.
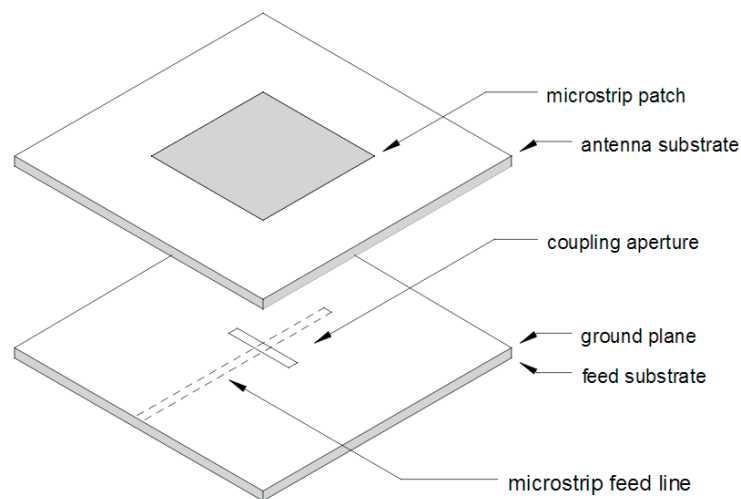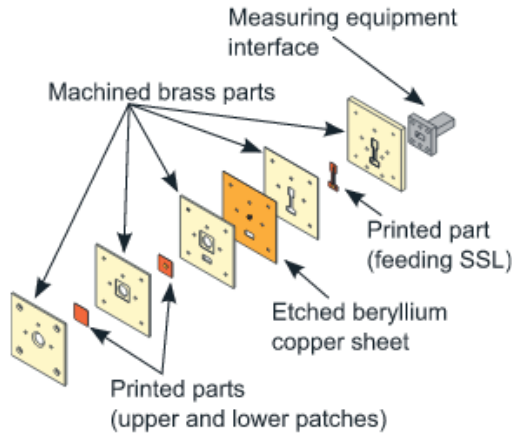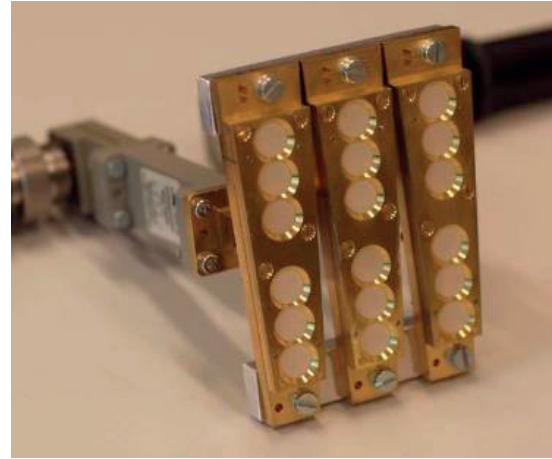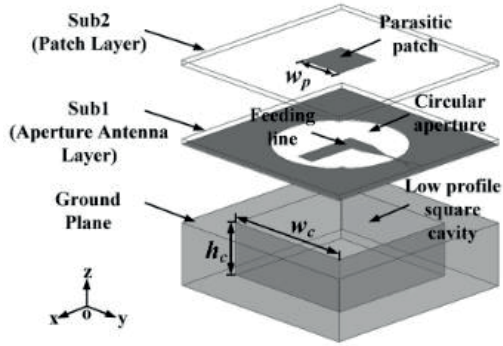

Fig. 2.2 – Geometry of an aperture coupled patch antenna [39].
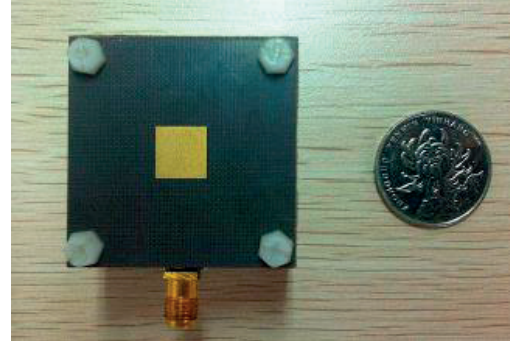
Fig. 2.3 – Hybrid solutions, examples taken from the literature: (a) aperture coupled patch antenna, single element [46]; (b) the prototype of the same element grouped in an array [11], [46]; (c) cavity-backed patch antenna [52]; (d) and its corresponding prototype [52].

Another solution of this second category is related with the concept of Substrate Integrated Waveguides (SIW) that was first proposed in [56] (see Fig. 2.4a). One of most attractive characteristics of this technology is the ability to combine the well-known advantages of conventional waveguides with the useful benefits of microstrip lines such as low cost, low profile and light weight. Therefore, they have received much attention. The basic principle behind this technology is the associations of the horizontal walls of the waveguide with both top and bottom metallizations of the substrate and the vertical walls with the metallized vias done through the substrate [57], [58]. At Ka-band there are several examples of LP SIW horn antennas such as [59], [60]. Regarding CP SIW antennas, the proposed ones are mainly based on SIW-slot antennas [61], [62]. From the authors' best knowledge, a CP SIW-horn antenna was firstly published this year in [63] (see Fig. 2.4b and Fig. 2.4c). Apart from all these antenna solutions, SIW technology can also be useful to improve the performance of the printed antennas by allowing the development of, for instance, more robust and complex feeding networks [64].

(a)

(a)

(b)

(b)

(c)

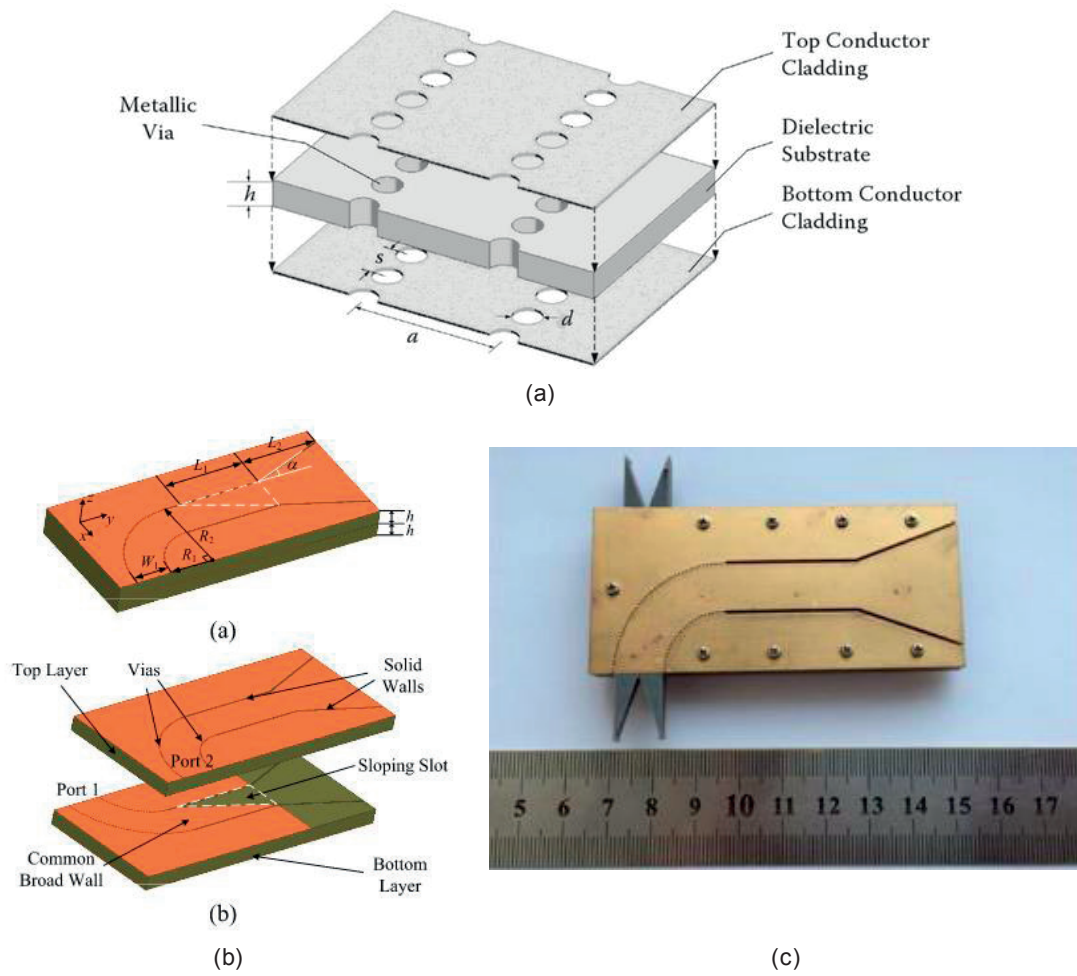Fig. 2.4 – SIW antennas: (a) example of the geometry of a SIW antenna [58]; (b) CP SIW-horn antenna, design [63]; (c) CP SIW-horn antenna, corresponding prototype [63].

A very interesting feed structure combining two PCB layers in the metal feed chain has been recently published [65] and it is shown in Fig. 2.5. The antenna was specially designed to serve as a feeder of a Cassegrain reflector for SOTM Ka-band applications.
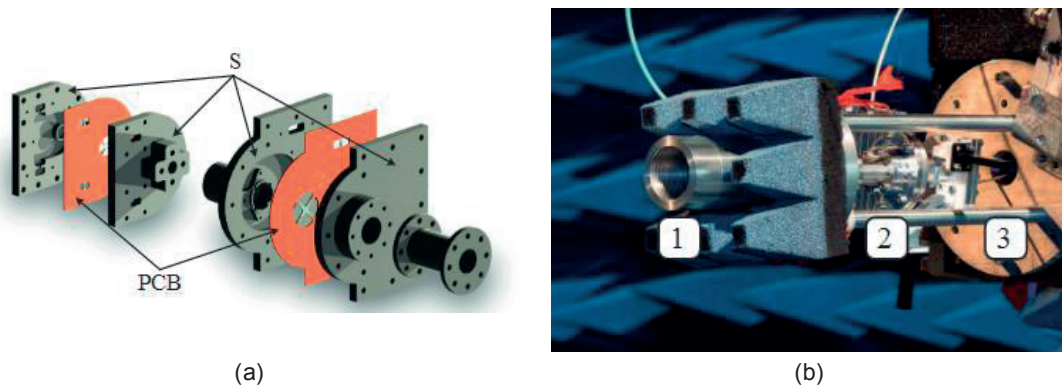
Fig. 2.5 – Hybrid feed chain [65]: (a) design; (b) prototype.

All these interesting solutions are mainly based on the use of dielectrics and hence should be considered for ground applications. When targeting the space segment, designs where the die-lectric parts are minimized or even fully metallic antennas are preferred in order to avoid unde-sired phenomena such as electrostatic discharge [66].

Hence the all-metal solutions (our third category) seem to be more flexible and to have a wider range of applications, provided that the pertinent technologies are available. These solutions are normally realized using traditional manufacturing techniques. In this category, probably, horn antennas are the most widely used in microwaves applications [67]. The advantages of this type of antennas, especially highlighted when compared with printed antennas, are wide bandwidth, good polarization purity, low losses and moderate gain. On the other hand, the bulky size can limit their implementation in certain applications. The first experience with a horn antenna dates from 1897 [68], [69]. After some years of interregnum, the World War II helped its revival in the late 1930s [68], [69]. There are several variants of this type of antennas that can be easily found in the market or in the literature. Besides the conventional either conical or pyramidal horns [70], [71]. that are commonly used as standard gain antennas in laboratory measurements and tests, there are other good examples that can favor wider bandwidth, higher efficiency, lower levels of cross-polarization, sidelobes and in some cases, even smaller size. For instance, the following examples have been proposed at Ka-band: ridged horns [72], [73] (see Fig. 2.6a), corrugated horns [74], [75] and choke horns [76], [77]. Moreover, Ka-band horn arrays have been also proposed in the literature [78], [79] (see Fig. 2.6b). Additionally to the fact of showing very robust performance, horn antennas are also well-known by their well-defined phase center. Hence they turn to be logical candidates to be used as feeders in antenna systems either in ground or space applications.
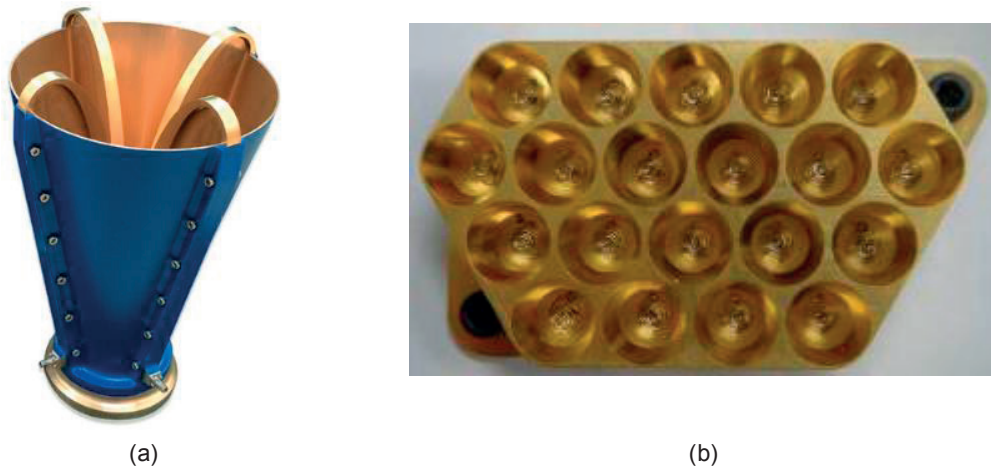
Fig. 2.6 – Horn antennas: (a) ridged horn [73]; (b) prototype of an array of horns [79].

Another common type of metal-based solutions used at Ka-band is slotted waveguide antennas (see Fig. 2.7) [80], [81].
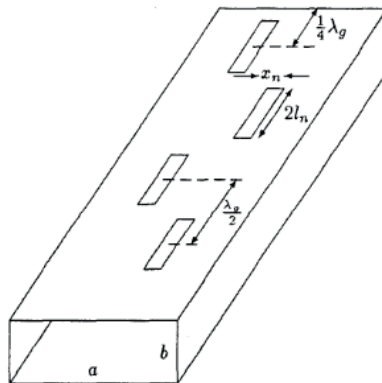
Fig. 2.7 – Example of a slotted waveguide antenna [81].

Nevertheless, these metal solutions are normally bulky and therefore, a volume reduction could be greatly beneficial in some Ka-band applications. For instance, cavity antennas could be a very interesting all-metal and more compact solution than the ones aforementioned. Despite of cavity antennas that include dielectrics such as the one presented in [82], here it would be interesting to consider similar designs to the ones shown in [83]-[86] for lower frequencies. These solutions have in common the sequential feeding technique that was used to achieve good quality CP. The corresponding antennas are presented in Fig. 2.8.

(a)   (b)

(c)   (d)
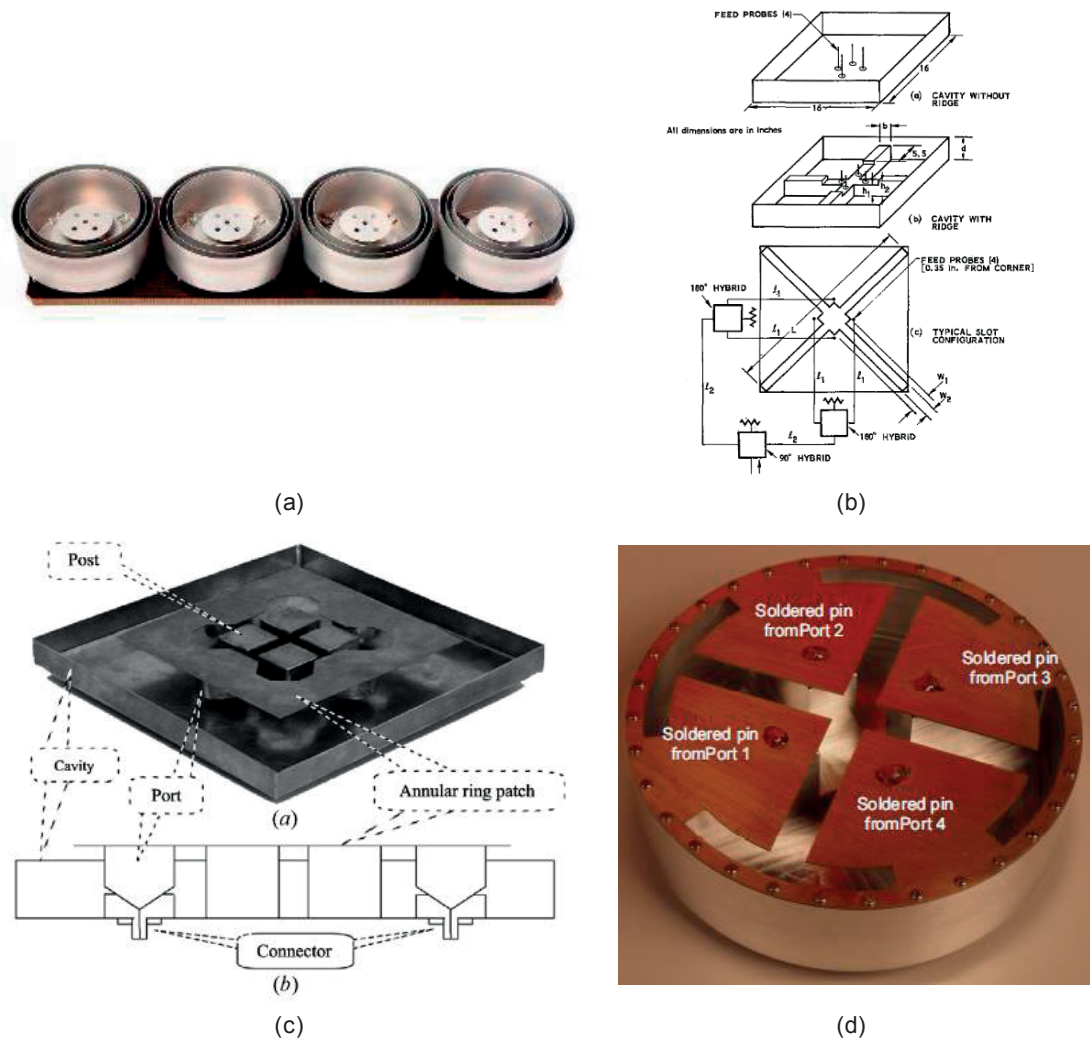
Fig. 2.8 – Cavity antennas: (a) taken from [83]; (b) taken from [84]; (c) taken from [85]; (d) taken from [86].

2.1.2   Gain enhancers

As aforementioned, these antenna elements are usually combined with more directive devices in order to achieve in the end higher gain systems. Such systems are related with the boost of small ground terminals market for mobile broadband applications in Ka-band once high gain antennas are required for the link budget. Moreover, beam steering capabilities are also required to keep a steady link with the satellite. Beam steering can be based upon electronic, mechanical or hybrid solutions. Electronic beam steering antennas [87]-[89] (Fig.2.9a), mainly consisting of phased arrays, allow very fast beam pointing and can be quite compact; however the feeding network tends to be complex, impacting on RF losses and terminal cost. In order to overcome these problems and also to reduce the cost of the device some techniques have been proposed in the literature such the one described in [90]. On the other hand, mechanical beam steering

antennas usually involve reflectors [91]-[94] and 3D lenses [95]-[99] (Fig. 2.9b). These solutions are simpler, have better performance related to losses and are more affordable than the electronic ones; however they are bulkier. In order to overcome this issue, the new challenge and trend is to design planar structures that would favor a lower profile and weight. Some interesting solutions are already available in the literature, such as flat Fresnel lenses or transmitarrays [100]-[104] (Fig. 2.9c). Besides the mentioned benefits, mechanical solutions need only one primary feed antenna in many cases which is a clear advantage over the phased arrays. For the sake of completeness, it is here important to refer that hybrid solutions have been investigated and an example is presented in [105] (Fig. 2.9d).
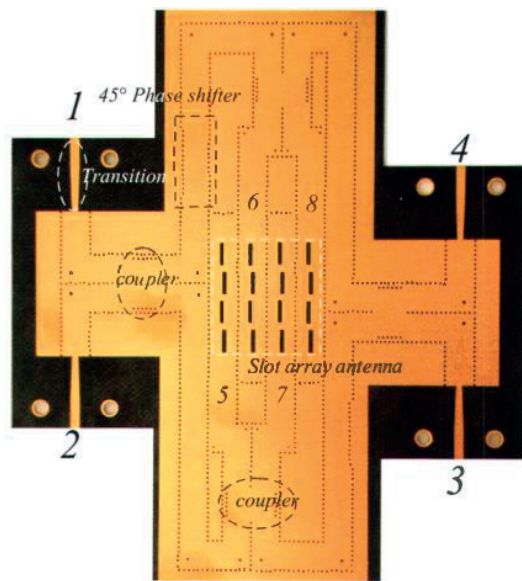
(a)

(b)
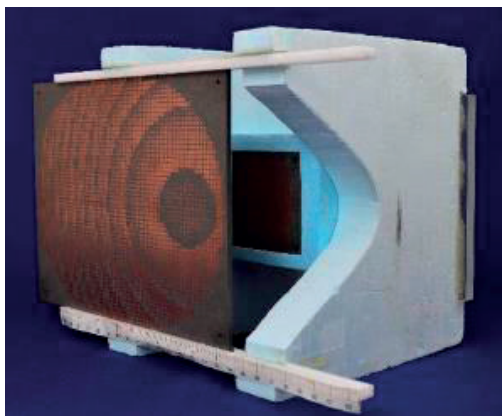
(c)

(d)

Fig. 2.9 – Beam steering solutions: (a) electronic [87]; (b) mechanical (3D lens antenna) [96]; (c) mechanical (planar lens antenna) [100]; (d) hybrid [105].

Since one of the main goals when developing antennas for Ka-band SOTM applications is to achieve a low cost terminal that could be appropriate for mass market production, mechanical solutions have became a very interesting research path. Following this line, a simple an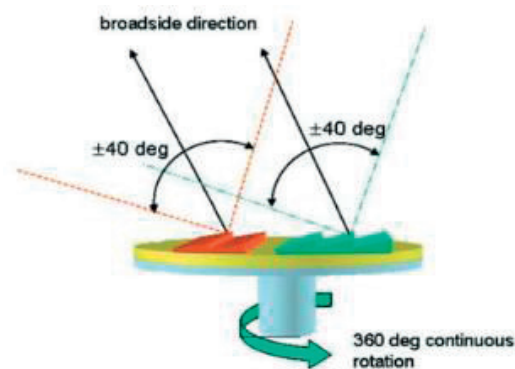d effective mechanical beam steering lens-based concept was developed in IT-Lisbon, one of the host institutions of this thesis [95], [96]. While in [95] the concept was demonstrated for scanning in azimuth, in [96] the concept was extended in the interest of scanning in elevation. The working principle of both solutions is the same, consisting on a primary feed antenna that remains stationary while the beam steering is obtained by moving the lens in front of it. The important detail here is that this movement must be done in such a way that the lens focal point remains always coincident with the feed phase center. Together with an appropriate lens design, it turns possible to obtain a beam tilt angle that is nearly the same as the lens tilt angle. Another important remark is that this antenna concept avoids the use of expensive devices such as rotary joints by keeping the feed in a fixed position. At the same time, this feature is also contributing to the adoption of a simpler setup.

Thanks to the expertise regarding lens-based antenna systems mainly of IT-Lisbon, the antennas developed in this thesis could be tested not only standalone but also as feeders of a lens subsystem.

2.2   Fabrication issues

Satellite communications fully metallic radiating systems, that typically are waveguide-based antennas and associated feed chain components, are usually fabricated employing traditional subtractive fabrication methods such as milling, turning, spark eroding, molding or shaping by plastic deformation. These manufacturing techniques are still the leading technology chosen in the industry specially when the wish of a mass production is combined with the requirement of operation at high frequencies. In the specific case of the satellite industry, these techniques are used not only for the ground terminals but also for the space segment where the imposed conditions are certainly harsher.

Nowadays, the market trends are taking the path towards strict requirements where the target is to have higher capacity at a lower cost. Considering the first wish, as mentioned before, the way to achieve it is to move higher in frequency which consequently requires an effort to ensure higher accuracy. On the other hand, cost-effective terminals can be achieved if we are willing to sacrifice the accuracy. Therefore, it is possible to understand that the nowadays requirements are a big challenge since they aim to bring together two opposite sides.

In line with these trends, the previously mentioned manufacturing methods start to present significant limitations. It is important to highlight that such limitations are not connected with the technique itself but they are the inevitable consequence of trying to keep the cost of the entire process as low and attractive as possible.

Difficulties stem mainly from the existence of very small and virtually inaccessible internal parts in the device that need to be very precisely machined. In order to access and machine these inner parts of the antenna, the classically adopted approach relies on splitting the piece into several sub-blocks, which are later assembled using screws and alignment pins. Good precision has proven to be achievable up to mm-wave frequencies; however it is normally at the price of bulky and heavy devices, high production costs and long lead times. Furthermore, in some cases, the conventional techniques pose several drawbacks concerning performance uncertainty due to the need for complex assembly procedures and non-negligible design limitations due to manufacturing constraints [106].

The complexity of the intermediate assembly step between the design and fabrication when using such technologies started to be highlighted in lower frequencies than Ka-band. For instance, in [107] the authors present a feed chain component for C-band where the assembly process is very demanding. Thus, it needed to be planned in detail once the performance of the device could suffer from misalignments. This requisite of carefully preparing the design of each block in order to be as perfect aligned as possible is also mentioned in [108], but this time in Ku-band. Despite being a hard process and apart from being possible to see its slight influence in the measured results presented in [107] and [108], globally they are in considerable agreement with the predicted results.

As expected, this issue is even more important in millimeter wave frequencies since the devices are more sensitive to the undesired asymmetries and misalignments. In [109], the authors explain in detail the problems related to the machining of feed chain components for Ka-band. The variations in the machining process are reported as the main source of errors that have a negative impact in the performance consistency. These contraints of the traditional manufacturing technique used in this case limited the design flexibility and obliged the authors to improve the device taking them into account. Another example is shown in [110] where ten different metal layers were needed to fabricate the W-band feed chain component. The manufacturing and assembling uncertainties are again pointed out as the reason behind the discrepancies between measured and simulated data.

The author of this thesis also experienced performance disparities between the theoretical model and the measured results for a horn antenna prototype at Ka-band. The used CNC milling technique did not allow the fabrication of the horn antenna in a single piece. Therefore, the design was split into several sub-blocks and its assembling procedure led to misalignments and bad contacts. These results are reported in the Chapter 3 of this document.

The harsh requirements of the new satellite antenna systems, mainly concerning high versatility, challenging performance, compactness, and both reduced cost and weight are contributing to highlight the limitations of the traditional manufacturing techniques. Furthermore, the fact that society and industry are evolving at very fast pace is becoming more and more incompatible with long lead times. All this justifies the search, development and use of innovative manufacturing techniques.

2.3 Additive manufacturing as enabling technology

Additive Manufacturing (AM) techniques, also known as 3D printing, refer to the process of building 3D objects directly from exported design data (models) by adding the material layer by layer [106], [111]. AM is considered by the European Framework Programme Horizon 2020 as one of the six Key Enabling Technologies (KETs). The KETs group is completed with photonics, industrial biotechnology, micro- and nanoelectronics, advanced materials and nanotechnology [112]. The experts believe that a fourth industrial revolution in Europe is on its way and furthermore that innovative manufacturing techniques will play an essential role in this re-industrialization [112]. In addition, AM is being supported because it promotes job creation and at the same time, it can be seen as a green technology once it decreases energy consumption and denies the use of toxic materials in considerable and measurable amounts [113].

Since 2009, when the European Commission published the first report on KETs, the confidence about their important role in the society has been increasing [114], [115]. In fact, in the Gartner's Hype Cycle which is a graph that aims to demonstrate the expectations in the adoption of emerging technologies, 3D printing appeared for the first time in 2010 (see Fig. 2.10a) [115]. The same type of graph exclusively made for 3D printing in 2015 mentioned that the applicability of this technology into prototyping would be reached in less than two years (see Fig. 2.10b) [116].
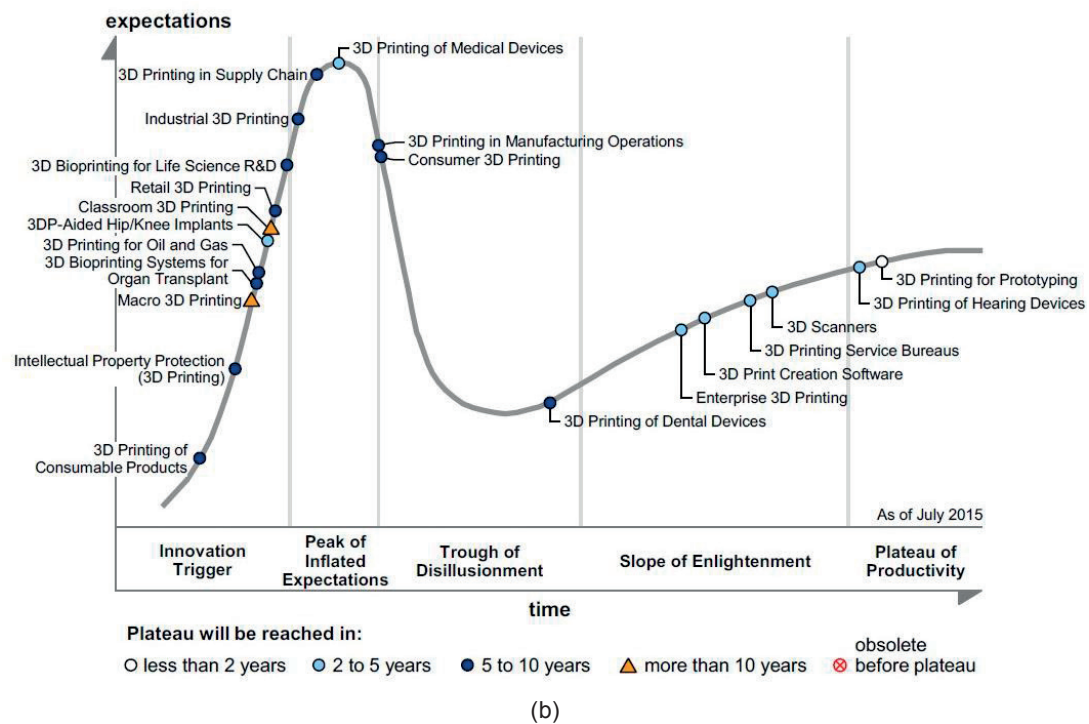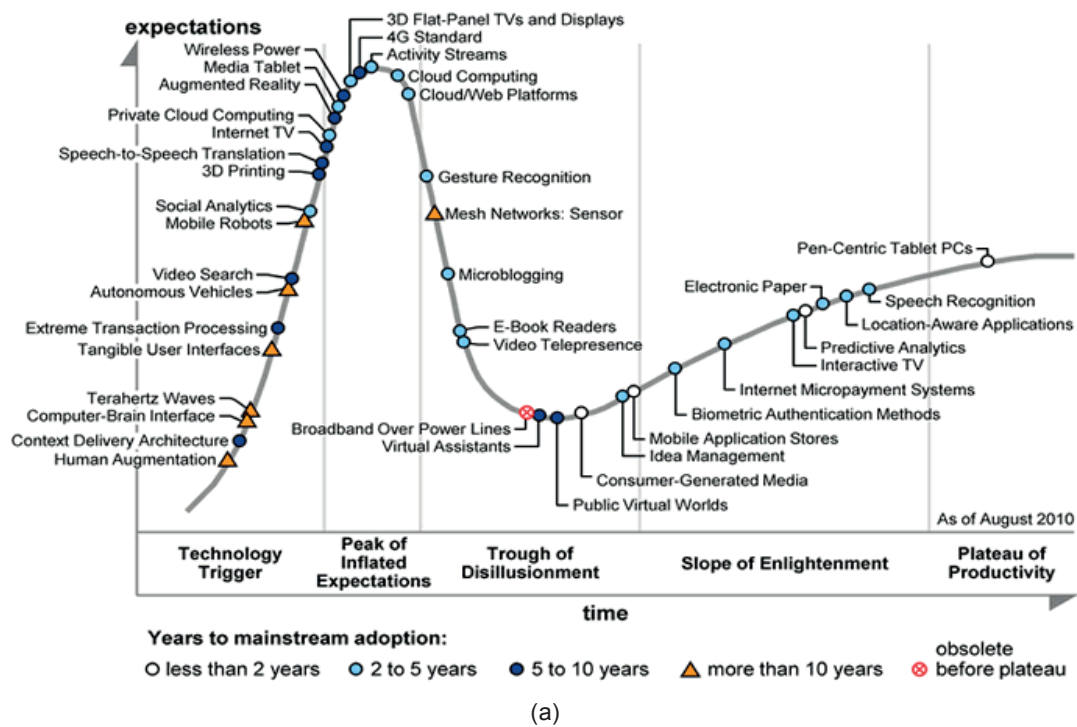
(a)

(b)

Fig. 2.10 – Gartner's Hype Cycle: (a) emerging technologies in 2010 [115]; (b) 3D printing in 2015 [116].

32

AM industrial applications are increasing exponentially and the number of funded AM-related projects has experienced a growth of 136% since 2014 [115]. In fact, AM has already radically changed the way to realize everyday life objects. This fact is obviously associated to the great advantages for a broad spectrum of applications. Fig. 2.11 shows the determining factors in the adoption of AM.
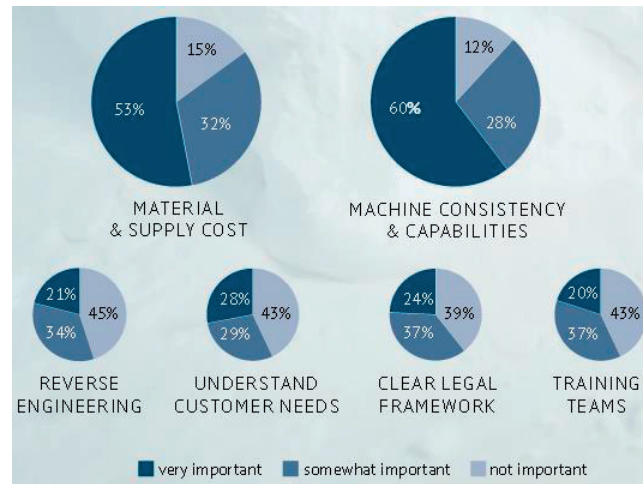

Fig. 2.11 – Determining factors in the adoption of AM [117].

Thus, the conception of modern satellite communications systems is one of the fields where these techniques seem the obvious and pertinent fabrication alternative to explore [118]-[121]. For instance, this is one of the topics that is being investigated in the €20 million collaborative project promoted by the European Commission: **A**dditive **M**anufacturing **A**iming towards **Z**ero waste and **E**fficient production of high-tech metal products (AMAZE) [120]. Being the largest and most ambitious initiative on this topic in Europe, it counts with 28 partners including EPFL, ESA, Fraunhofer Institute, Thales Alenia Space and Airbus Defence and Space.

In our domain, AM can become, when properly implemented, a promising alternative that offers several valuable advantages to simplify and improve the fabrication of antenna subsystems. These are enumerated next:

o Simplicity: AM allows an easier manufacturing process thanks to the direct transfer from the 3D model to the prototype. As even complex and demanding designs can be fabricated in a monolithic piece, there is no need for the common and time-consuming intermediate step normally used in traditional techniques to plan the best way to fabricate the device;

o Time efficiency: the removal of the previously mentioned intermediate step contributes

to make AM a faster manufacturing process. This technique leads to a dramatic reduction of the manufacturing time being able to introduce in advance the product in the market. The estimations tell that the lead times can be shortened by months [113];

o Design flexibility: AM increases the flexibility in the design process once complex internal features are no longer an issue. While conventional techniques promote the design for the fabrication, AM drives the design for function. Furthermore it can easily raise a greater customization in the manufacturing field without extra costs;

o Lighter weight products: external unnecessary parts that are common in prototypes made using conventional techniques are here avoided resulting in a great reduction of both size and weight of the devices. For this specific feature, techniques that use non metallic polymers as the basis material are very interesting. The weight reduction is estimated in 40-90% [113];

o Cost-effective: AM is such a simple and efficient manufacturing technique that can put in the market low-priced products;

o Repeatable process: the production process of every device can be easily replicated at any time, keeping the same dimensions and material properties.

During the last decades, the panorama of AM techniques is drastically evolving, being capable nowadays to distinguish between more than ten different types. Currently, the most exploited and commonly used approach for space-oriented metallic devices is Selective Laser Sintering (SLS) [122]-[124], with aluminum powder as the building material. Recent successful realizations have confirmed the SLS advantages in terms of design freedom, volume and cost reduction when conceiving antennas and RF components operating at Ka-band [124] and lower microwave frequencies [123]. However, these pluses are normally offset at high frequencies by large mechanical tolerances (around 250 µm [125]). Also, surface roughness (50 µm compared with the 20 µm achievable by milling [125]) can lead to high losses. Although losses can be reduced by introducing a post-fabrication procedure to smooth the surface such as sandblasting or electrolytic silver-plating, this post-processing involves higher costs and usually precludes monolithic fabrication. Nevertheless, in some cases the cost is still lower than the traditional manufacturing techniques and it is worthy to try it [124]. Direct Metal Laser Sintering (DMLS) has recently appeared as an improved version of SLS with surface roughness below 10 µm [111] and promising results have been obtained in high precision waveguide antenna arrays [126].

SLA, based on non-metallic polymer 3D printing, could be here a promising alternative [127], [128]. Basically, by using this technique, the device is created inside a tank full of liquid photopolymer where the polymerization process is activated by a laser. The build platform is being lowered while the device is being fabricated layer by layer [129]. Fig. 2.12 demonstrates the concept.
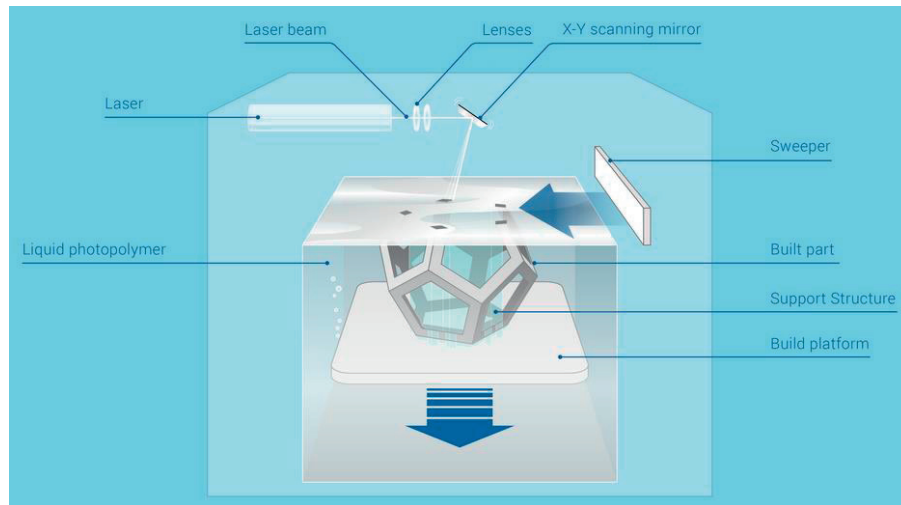
Fig. 2.12 – SLA concept [129].

In contrast to previously mentioned techniques, SLA allows at the same time: fine surface finish (around 1 µm), high manufacturing precision (around 25 µm) and mass savings thanks to the employment of light polymers as the building material. On the other hand, to achieve the sought-after electrical functionalities, SLA requires to be combined with a high-quality metallic coating procedure. This is nowadays possible thanks to an electro-less metallization process that allows homogeneous metallic coating, thus providing low levels of surface roughness and enabling realization of RF components and antennas from Ku- [130], [131] and Ka-bands [132], [133] up to 300 GHz [134]. This technique proves high performance even for highly convoluted geometrical structures. The W-band corrugated horn from [135], [136] serves here as an example.

In this thesis, the AM antennas were manufactured using this technique in collaboration with SWISSto12 [137], an innovative Swiss company specialized in SLA that spun off from EPFL in 2011. Its manufacturing process is here explained. The first fabrication step is the 3D-printing of the device body which is done through a polymerization as aforementioned. In this way local precision of ±25 µm can be achieved, with a maximum tolerance of ±200 µm on large dimensions (current setup is able to produce devices with volumes of approximately 300 x 300 x 350 mm). These values are likely to improve further as the printing technology is evolving. After printing and cleaning the polymer body, there is a preparation step, where the polymer surfaces are treated by chemical products in order to improve the adhesion of the subsequent metal coating. Afterwards, a uniform metallization of the entire device, including their complex inner shapes, is done through a chemical electroless process that results in a surface roughness below 1 µm. The metal used is typically copper, and the targeted metal thickness is 7-10 skin depths. Additionally, a very thin (100 nm) gold layer can be added for passivation. For Ka-band antennas, the metal layer deposited on the polymer body is more than 3 µm thick, which is enough to ensure full RF conductivity since the skin depth of copper at Ka-band roughly ranges between 0.4 and 0.5 µm. The basic test to validate the quality of metallization is an adhesion test where

one attempts to peal the metal off by using a scotch-like tape (ASTM Standard D3359-09). Another test consists of thermal cycling where the device is subjected to several cycles between extreme temperatures (e.g. −55°C to 75°C for airborne standard EUROCAE EDB14G). This test can be challenging since the polymer and metal have different coefficients of thermal expansion which puts the coating continuity in risk. Yet, the tests are passed successfully thanks to the choice of polymer materials and the developed plating process.

Chapter 3 Ridged horn feed antenna for a SOTM terminal

Enquanto não alcances, não descanses
De nenhum fruto queiras só metade

Miguel Torga

The first antenna proposed in this thesis is discussed in this chapter. First, an introduction is provided in order to recall the target application and to discuss the antenna concept we are looking for. Then, the design of the feed system is presented, followed by its integration in a lens-based system in order to achieve a mechanical beam-steering antenna. Finally, the corresponding prototypes and measurements are presented.

3.1 Introduction

As previously mentioned in this manuscript, Ka-band has aroused lots of interest in SOTM applications and consequently influenced the research towards this direction. The antenna systems developed for such application are intended to be placed on the top of moving platforms (e.g. planes, high-speed trains or buses) and therefore are obliged to fulfill, as main requirement, beam-steering capability, in order to keep up the link with the satellite. In addition to the beam-steering capability, the antenna system should operate simultaneously at both downlink (19.7 – 20.2 GHz) and uplink (29.5 – 30 GHz) Ka-band with CP. Here, we are also aiming to combine these features with others, such as simplicity, compactness and low cost.

Regarding the beam-steering, as also previously discussed, there are different ways to achieve it. This thesis can be viewed as a step in a global research strategy, which started looking for cost-effective antennas and considering a mechanical approach, where the beam steering is obtained by the tilt of a 3D dielectric lens. The first application of this idea was made in [96]. The

focus of the publication was the study of an appropriate lens design and the target application was indoor multi-gigabit local area networks (LANs) at 60 GHz.

The next evolution step was to replicate this antenna concept at the downlink Ka-band, while trying to enlarge the scanning interval originally achieved at 60 GHz (0° to 45° in relation to the zenith [96]). One key aspect was the concurrent design of a feed antenna able to produce already a tilt in its own beam. This initial progress was successfully accomplished by the PhD candidate in her master thesis [97], [138].

The above developments on a Ka-band lens-based antenna system are the starting point for this doctoral thesis. As previously mentioned, operation around both 20 GHz and 30 GHz is one of the objectives. This means that the feeder must be either dual-band or show enough broadband. In addition, after integration with the gain enhancer subsystem (in this case, a 3D dielectric lens), the produced beam tilt should be coincident in both frequencies. We could achieve it by placing two independent feeders, each one associated to a frequency band; however, this would be only an intermediate step in our preferred strategy, where we aim at a single feeder.

Inspired by the previous activities [96], [97], we keep as feeder in a first stage a horn antenna based on waveguide technology. First, we demonstrate theoretically that it is possible to achieve beam-steering capabilities at both downlink and uplink Ka-bands with a single feed and a single lens. Moreover, it is also possible to achieve approximately the same beam tilt angles for the two widely separated frequency bands. Prompted by these theoretical predictions, our last challenge is to validate the theoretical concept through the manufacturing of a prototype.

3.2 Feed antenna design

3.2.1 Quad-ridged horn antenna

Horns are probably one of the most popular and widely used antennas, especially because such designs are normally intuitive and versatile [68]. Their first use dates back from the late 1800s and the first experiment with such a device was reported in 1897 [139]. After a period of disinterest for horns, mainly due the success of Marconi's transatlantic wireless transmission experience and subsequent exploitation of lower frequencies, their resurgence is linked to the World War II once the research in microwaves became popular in the late 1930s [68]. The first journal publication about a horn antenna dates back to 1939 [140]. Since then, a large number of publications have been written describing the fundamental theory, optimized designs and possible applications.

Horn antennas are widely used as feeders for reflectors and lenses, elements of phased arrays and also as standard antennas for calibration and measurements, especially at Ultra High Frequency (UHF) and microwave frequencies. These antennas are known by having high gain and

directivity, large bandwidth and low loss. Concerning the geometry, horns are flaring metal waveguides, where the flare is the key point since it has a strong influence in the electromagnetic performance. Typical designs include E-plane, H-plane, pyramidal and conical horns (Fig. 3.1).
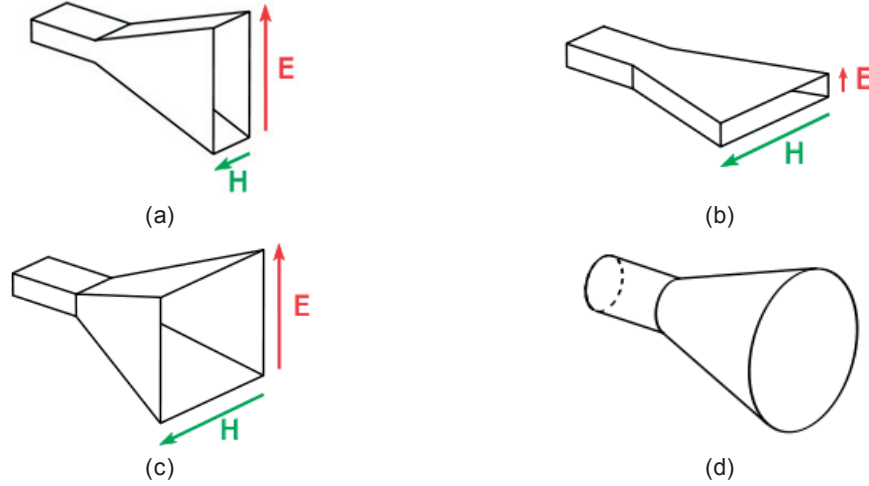

Fig. 3.1 – Typical horn antennas [141]: (a) E-plane; (b) H-plane; (c) pyramidal; (d) conical.

In some cases, the performance of typical horn antennas can be improved by adding corrugations or ridges on their inner walls. In fact, these type of devices started to appear with the need of broadband antennas. Corrugated horns have already proved their contribution in terms of bandwidth, sidelobes level and cross-polarization [68]. Nevertheless, the use of ridges was the first approach used to lower the cutoff frequency and increase the bandwidth [142].

The feed antenna proposed in this chapter is precisely a quad-ridged horn. This choice can be justified by the previously highlighted characteristics, especially the fact of yielding larger bandwidth. In addition, horns have a well-defined phase center, which is normally located close to the aperture plane. It must be taken into account that the phase center is one critical performance parameter associated to feed antennas that will be used with focused devices. In such systems, maximum aperture efficiency is obtained by making coincident the feed phase center with the focal point of the lens or reflector.

The first step in order to design the proposed horn antenna is to define the diameter of the waveguide. According to waveguide theory [143], a diameter of 8 mm will allow operation in the uplink Ka-band, more specifically from 26.5 to 33 GHz. Then, we have considered this value to calculate the corresponding cutoff frequency by using the following formula:

$$f_c = \frac{1.8412c}{2\pi a}$$

where, f_c is the cutoff frequency of the TE_{11} fundamental mode of the circular waveguide in Hz, c is the speed of light in metres per second and a is the radius of the circular cross section in metres. The obtained value is f_c = 22 GHz, which means that the downlink Ka-band is not achievable. Thus, the adoption of the ridges is here justified in order to increase the bandwidth of the horn antenna, by lowering the cutoff frequency. Previous studies on this matter were performed in [138]. For the sake of simplicity, we want to use as few ridges as possible while keeping the required symmetries. This results on four cross-disposed ridges to preserve modal symmetries and CP. The optimization of the quad-ridged horn aiming to cover both downlink and uplink Ka-bands is done through several simulation tests and the final dimensions of the ridges are 2.9 mm in depth and 1 mm in width (Fig. 3.2, Fig. 3.4). As expected, the ridges help to achieve the desired broadband behavior (Fig. 3.7).

In addition to the bandwidth requirements, this feed antenna should be designed to help the lens to extend its original scanning interval (0° to 45° in elevation [96]) as aforementioned. In line with this objective, the horn aperture is cut at a slant angle β with respect to the original aperture plane as shown in Fig. 3.2a. The fact of having a slanted aperture in a fixed horn means we lose the ability to follow the lens in its azimuthal rotation. So, in order to overcome this drawback (while avoiding expensive rotary joints) this optimized aperture requires its detachment/separation from the horn's body as shown in Fig. 3.2b and Fig. 3.4. It is important to refer that this azimuthal scan will be achieved by a synchronous rotation of the horn aperture with the lens. Another point to highlight in this discussion is the fact that this slanted aperture inducts higher order modes which we can not control. We adopted here a pragmatic analysis where a modal analysis was not performed. The horn was designed to perturbe the fundamental mode of the ridged waveguide, TE_{11}.

Several optimization tests were performed using a full wave commercial software [144] in order to find the best combination of the aperture slant angle β and the flare angle ϕ as detailed in [97], [138]. First, we understood that the slanted aperture has a negative impact in the cross-polarization level. The non-slanted horn (example depicted in Fig. 3.2a) has lower cross-polarization levels at both 20 GHz and 30 GHz as shown in Fig. 3.3a and Fig. 3.3b, respectively. These levels will deteriorate when increasing the aperture slant angle β as also documented in [97]. We were also able to check that when using a slanted aperture, the horn flare angle ϕ also influences the beam tilt: if we define a small value for ϕ, we obtain a greater beam tilt at both frequency bands. However if we use a bigger flare angle ϕ and a conventional horn aperture we could improve the gain and benefit in terms of phase center stability, respectively. Here, it is important to highlight that this antenna concept was an outcome of a research initiative without any associated project to define the requirements and therefore a compromise was established. The compromise is to achieve the maximum beam tilt with, at least, a gain of approximately 10 dB at both frequency bands, a cross-polarization level of, at least, −10 dB and a phase center with a low σ value at both bands. In order to explain the meaning of σ, we resort to the explana-

tion given by CST Microwave Studio [144], since we have used this software to design the antenna as well as to calculate its phase center. In their algorithm, the σ corresponds to the maximum standard deviation of the phase center location.

The final values for the slant and flare angles are β = 45° and ϕ = 4.3°, respectively, and both are depicted in Fig. 3.2b. With this horn design we are able to tilt the beam, achieving α_{beam} = 18° at 20 GHz and α_{beam} = 11° at 30 GHz. The corresponding radiation patterns are illustrated in Fig. 3.3.

(a)   (b)
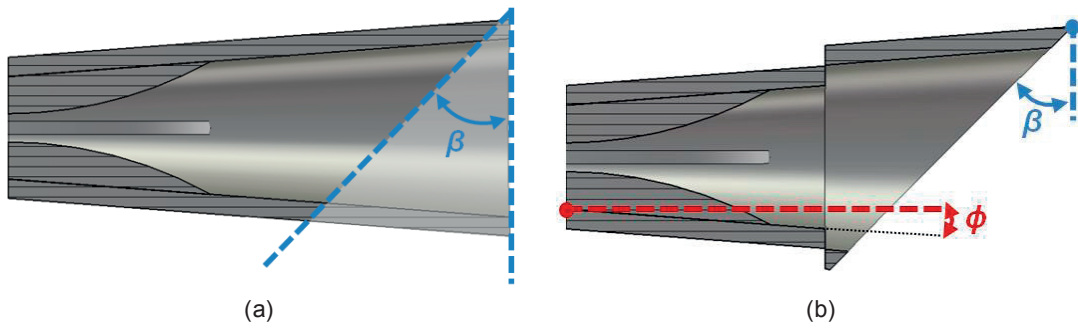
Fig. 3.2 – Optimizations in the horn design: (a) slanted aperture, approach used to tilt the beam; (b) separated slanted aperture, approach used to counter the asymmetry.
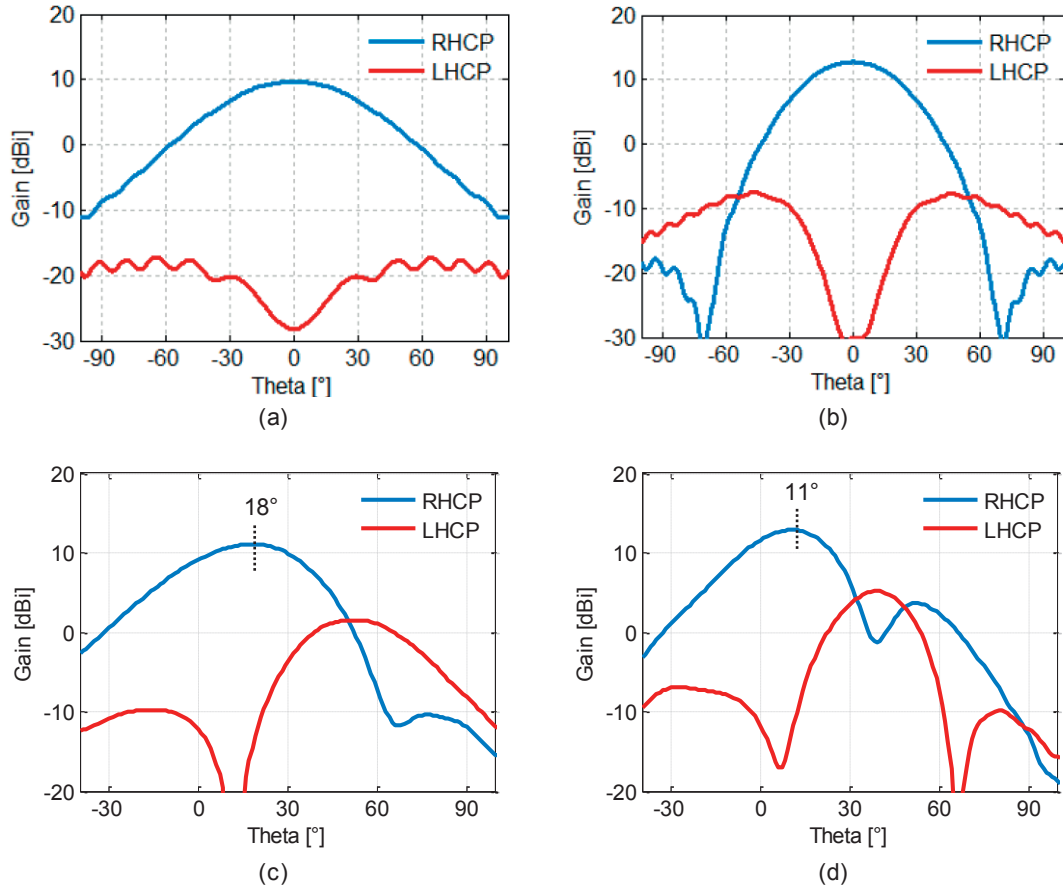
Fig. 3.3 - CP radiation patterns associated to the horn designs presented in Fig. 3.2: (a) model of Fig. 3.2a (non-slanted horn) at 20 GHz; (b) model of Fig. 3.2a (non-slanted horn) at 30 GHz; (c) model of Fig. 3.2b (slanted horn) at 20 GHz; (d) model of Fig. 3.2b (slanted horn) at 30 GHz.

Further simulation tests helped us to understand that the wall thickness of the horn slanted aperture also has an influence in the beam tilting at downlink. But much more relevant than that was the influence of the transition between the fixed ridged horn and its movable slanted aperture. The most efficient way to improve the beam steering at both frequencies was to make it as smooth as possible. Following this approach, it was kept the same flare angle ϕ for both pieces; and in order to allow the azimuthal rotation, it was added an air gap of 0.75 mm between both fixed and movable parts. After these modifications, which were adopted in the final design depicted in Fig. 3.4, the beam tilt was $\alpha_{beam} = 27°$ at 20 GHz and $\alpha_{beam} = 14°$ at 30 GHz. All the relevant dimensions of the quad-ridged horn antenna are detailed in the caption of corresponding figure.

The radiation patterns of the final horn antenna are illustrated in Fig. 3.5. Comparing both Fig. 3.3 and Fig. 3.5, it is possible to verify that the modifications in the horn aperture improved the beam tilt at both bands, increasing 9° at 20 GHz and 3° at 30 GHz. They also improved the

cross-polarization level, especially at the lower frequency. On the other hand, they contributed to a small and negligible decrease in gain. Nevertheless, the target was reached: achieve a maximum beam tilt while keeping approximately 10 dB of gain and -10 dB of cross-polarization level at both frequencies, as detailed in Table 3.I.

As it can be seen in Fig. 3.6, the phase center location is close to the horn aperture, which is usual in horn antennas. Therefore, we can conclude that the 45°-slant aperture is not affecting much the phase center. It is placed above the slanted aperture at downlink while at uplink its position is inside the antenna (Fig. 3.6). The difference between both cases is 6.3 mm, which is reasonable. Please note that more details about the horn phase center will be presented in the following chapter since they will be compared with the results of another antenna design.

The active S-parameters of the final antenna are presented in Fig. 3.7. In order to have the CP results in the full wave software, two modes were defined at the same antenna waveguide port (with a 90° phase shift between them). Therefore, each curve represents the active S-parameters associated to each mode. For the purpose of completeness, the two modes are presented in Fig. 3.8.

(a)

(b)
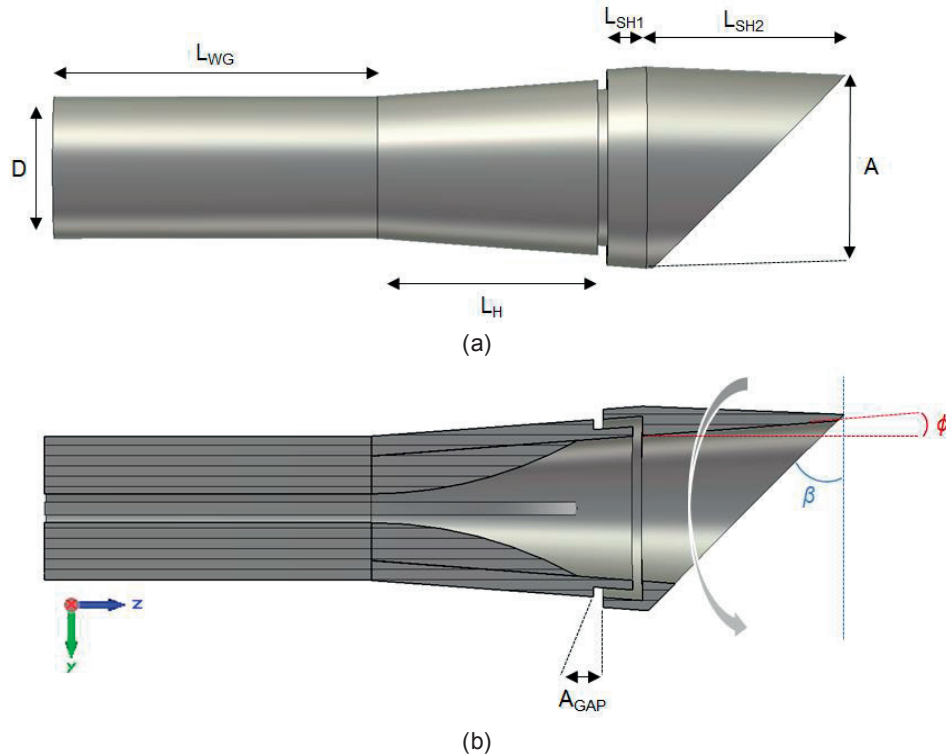
Fig. 3.4 – Quad-ridged horn antenna: (a) side view; (b) YZ cutting plane, side view. Dimensions in *mm*: D (inner diameter) = 8; L_{WG} = 25; L_H = 17; L_{SH1} = 3; L_{SH2} = 15.4; A (inner aperture) = 13.7; A_{GAP} = 0.75; β = 45°, ϕ = 4.3°.
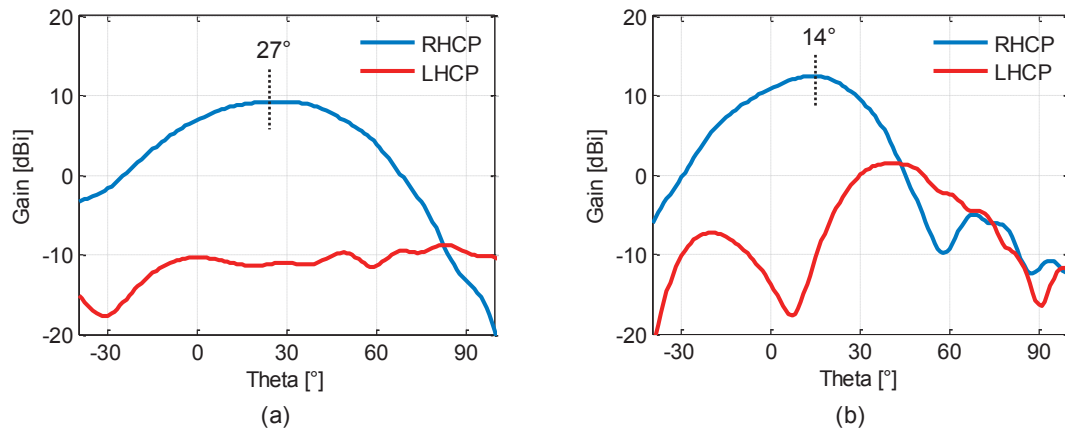
Fig. 3.5 – CP radiation patterns of the final horn antenna: (a) at 20 GHz; (b) at 30 GHz.

Table 3.I – Performance indicators of the horn antenna.

Frequency [GHz]	α_{beam} [°]	G [dBi]	Cross-pol. level [dB]
20	27	9.6	-18.9
30	14	12.5	-11.1
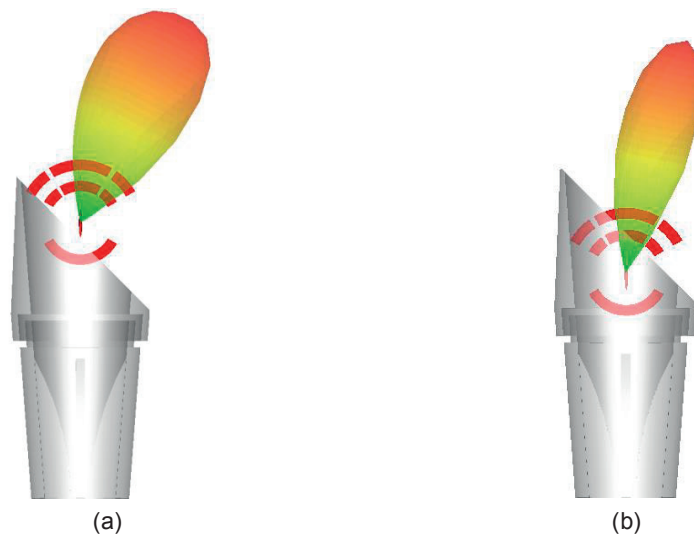
Fig. 3.6 – Phase center position: (a) at 20 GHz; (b) at 30 GHz.
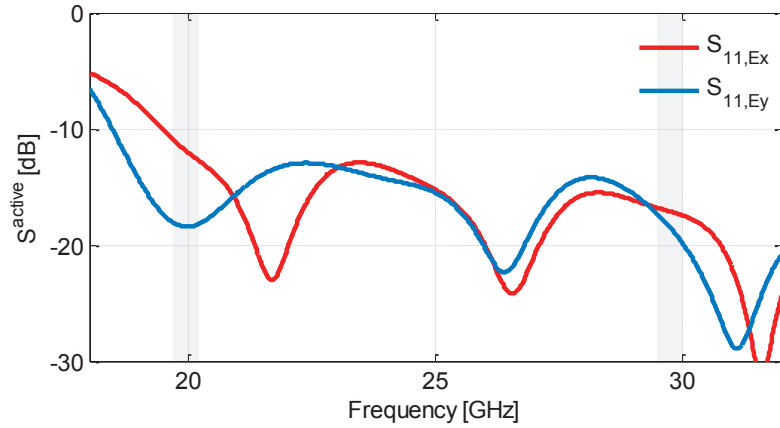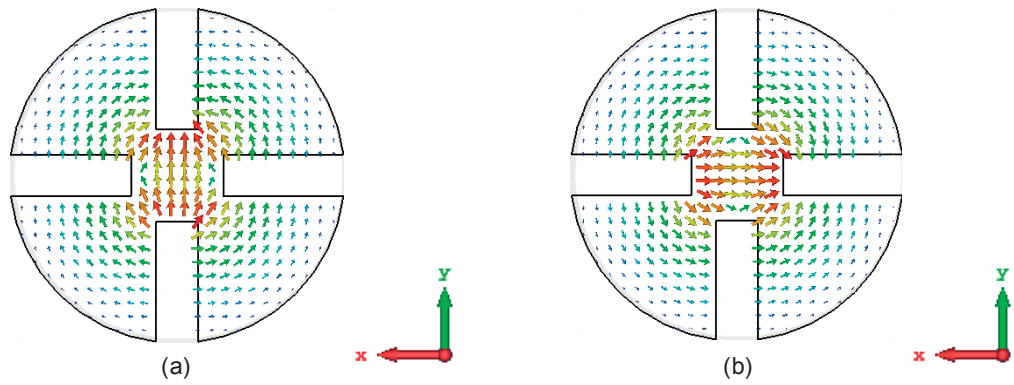
Fig. 3.7 – Active S-parameters of the final horn antenna.

(a)   (b)

Fig. 3.8 – Modes definition: (a) first mode, E-field in y-direction (Mode E_Y); (b) second mode, E-field in x-direction (Mode E_X).

3.2.2   Coaxial-to-quad-ridged waveguide transition

In order to feed the horn antenna previously presented and perform the measurements, we have designed a dedicated wideband coaxial-to-waveguide transition. Several examples of this type of devices can be found in the literature. For instance, a coaxial-to-double-ridged waveguide transition operating from 18 GHz to 40 GHz is presented in [145]. Another example of a double-ridged transition working from 8 GHz to 18 GHz is introduced in [146]. However, in both cases, the structures have a rectangular cross-section which is not appropriate to feed directly devices with two symmetry planes. Yet, these examples are here mentioned because they served as a source of inspiration for our design.

The proposed coaxial-to-quad-ridged circular waveguide transition comprises two different sections as presented in Fig. 3.9. The relevant dimensions are detailed in its caption. The first section of the waveguide, which we called mode launcher section, has a double-ridged configuration and in its bottom, closing the device, it counts with a shallow conical back-cavity. As it can be seen in Fig. 3.9, this section is fed by a EZ-86 coaxial cable and the excitation of a LP wave is made in the narrow gap δ between the ridges. In the part of the section, the ridges present a larger cross-section in order to accommodate the coaxial cable; and they end with a triangular prism shape that offers a smoother transition to the back cavity. These cross-sections are tapered towards the device open-end for having enough space to add the second pair of ridges. A tuning pin is included in the design for laboratory bench fine tuning.

The second part of the structure is a transitional section where the second pair of ridges is added. The launched mode is expected to be stably propagating in this section and unperturbed by the orthogonal pair of ridges. To accomplish it, the height of the second pair of ridges is increased linearly along z-axis until a perfect two-symmetry plane structure is obtained at the device open-end as depicted in Fig. 3.9b. Thus, this transition in its top aperture have the same configuration of the quad-ridged horn antenna.

The role of the ridges is to extend the bandwidth as already discussed in the description of the antenna. In turn, the back-cavity is here added to improve the return loss. The transition was optimized in a full wave software [144] and the simulations have shown that the return loss level and the bandwidth are extremely sensitive to the geometry parameters, especially in the mode launch section. Considering this type of broadband designs, this fact was already expected once it is commonly reported in the literature. In our case, the most critical parameters to obtain a satisfactory return loss are the position of the coaxial cable, the shape and height of the back-cavity, the dimensions of the ridges in the bottom of the launch section and the corresponding gap between them.

Therefore, in order to compensate a possible negative influence of fabrication tolerances in the return loss curve, we decided to introduce the tuning pin in the design. As illustrated in Fig. 3.10a, the zero position, represented by pin=0, corresponds to the alignment of the tip of the pin with the longitudinal axis of the transition. Negative positions corresponds to increase the pin depth inside the structure; for example, pin=-0.1 means pushing the pin by 0.1 mm. The same convention is applied in the opposite direction for positive positions. Fig. 3.10b presents the input reflection coefficient for the designed coaxial-to-quad-ridged waveguide transition for different depths of the tuning pin and it is clearly visible its influence. Nevertheless, even without the pin the transition exhibits a broadband behavior, covering both downlink and uplink Ka-bands.
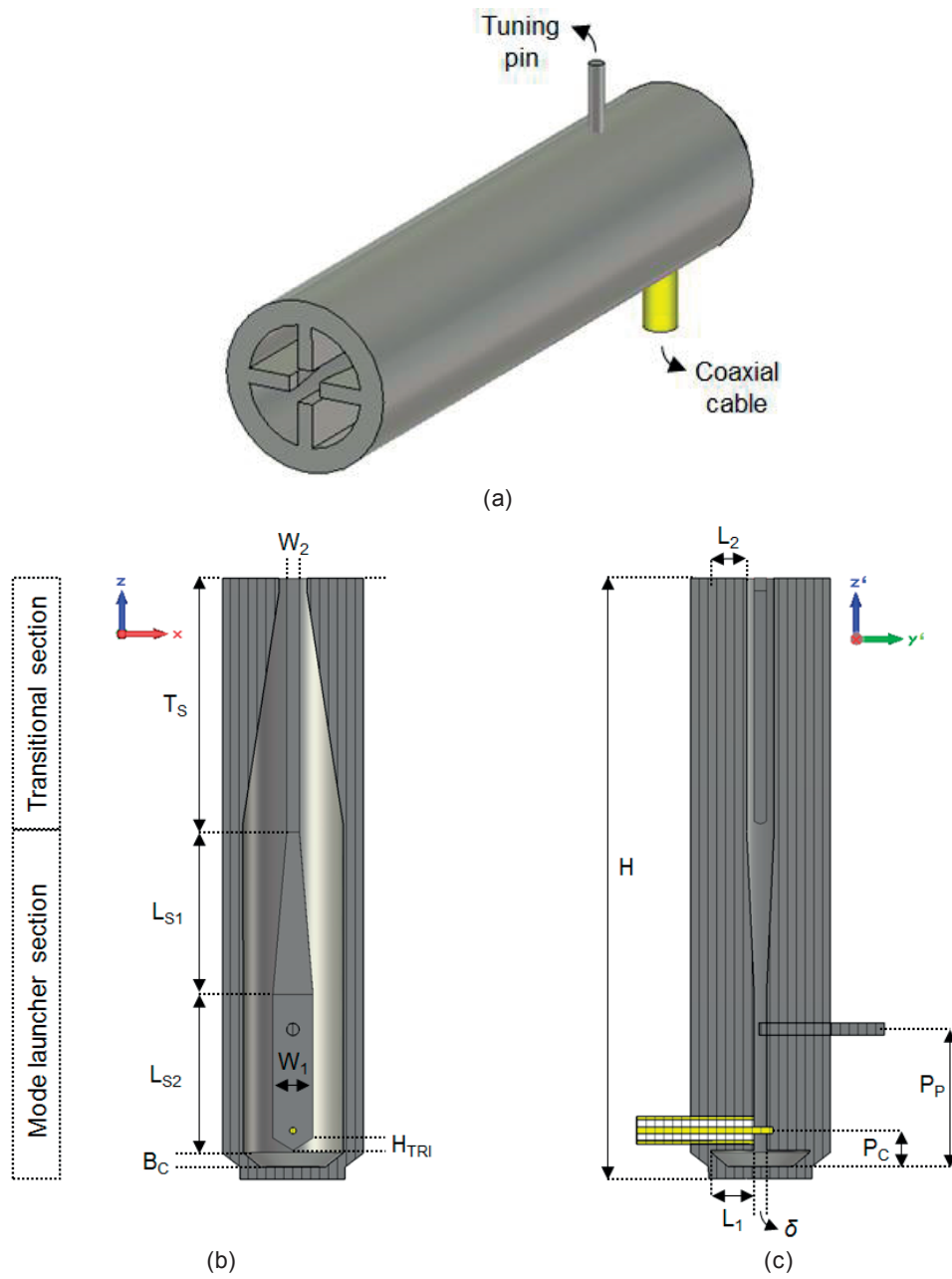
Fig. 3.9 – Coaxial-to-quad-ridged transition: (a) perspective view ; (b) XZ cutting plane; (c) YZ cutting plane (rotation of 90° in relation to the previous one). Dimensions in *mm*: H = 48.1; T_S = 20.3; L_{S1} = 13; L_{S2} = 11.5; B_C = 1.1; H_{TRI} = 1; P_C = 2.9; P_P = 11; δ = 1; W_1 = 3.2; L_1 = 3.5; W_2 = 1; H_2 = 2.9.
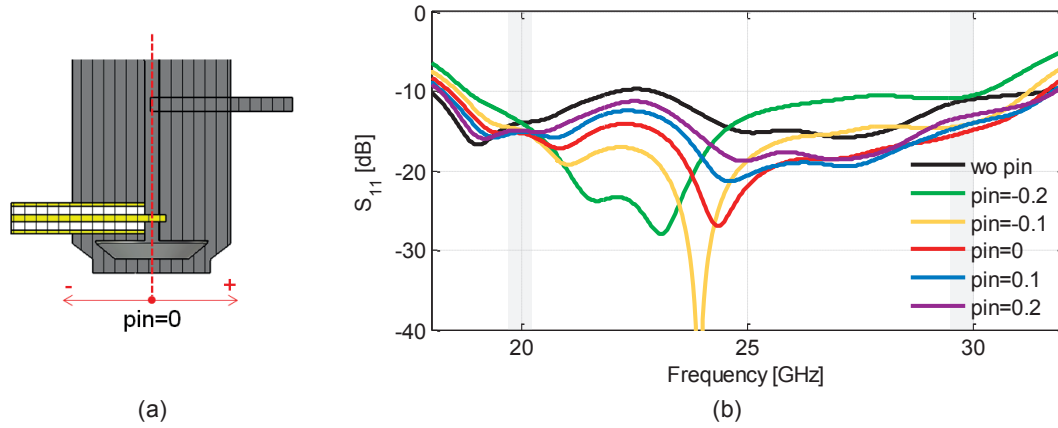
Fig. 3.10 – Influence of the tuning pin: (a) convention explanation; (b) simulated input reflection coefficients.

3.2.3 Complete feed system

The complete feed system is composed of both aforementioned structures, the horn antenna and the coaxial-to-waveguide transition. The fact of having only one coaxial cable in the transition restricts the system to LP. Nevertheless, the two-symmetry planes at the open-end of the transition allow feeding the horn with two orthogonal LPs by mounting the transition in 90° rotated positions with respect to the horn as shown in Fig. 3.11.

Fig. 3.12 presents the simulated input reflection coefficients of the two configurations presented in Fig. 3.11. The complete feed system presents a broadband behavior, allowing operation in the desired downlink and uplink Ka-bands. At the lower extreme of the downlink band, both curves present S_{11} values slightly above -10 dB. The worst cases of E_1 and E_2 are, respectively, S_{11} = -9.1 dB and S_{11} = -7.5 dB.

The LP radiation patterns at both frequencies are shown in Fig. 3.13. Thanks to a proper combination of these two orthogonal polarizations, it is possible to predict the CP response of the complete feed system by post-processing. Therefore, the combined CP radiation patterns are presented in Fig. 3.14. In addition, we added in the same figure the CP radiation patterns obtained only with the horn (previously shown in Fig. 3.5). This comparison shows we have achieved a good approximation through the post-processed intermediate step.

Fig. 3.11 – Two orthogonal LPs: (a) E-field in the symmetric plane of the horn (E_1); (b) E-field in the asymmetric plane of the horn (E_2).
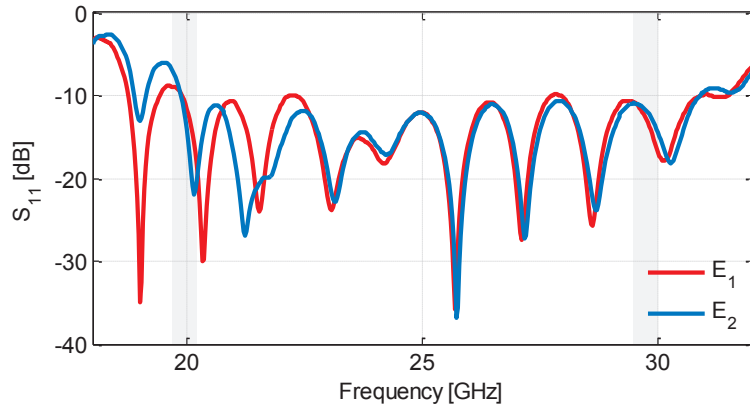
Fig. 3.12 – Simulated input reflection coefficients of the two configurations presented in Fig. 3.11.
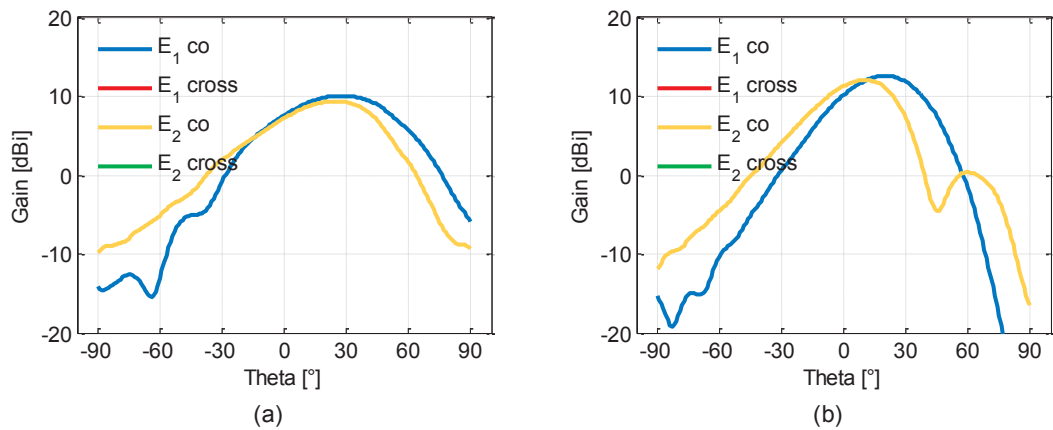
Fig. 3.13 – Simulated LP radiation patterns of the complete feed system: (a) at 20 GHz; (b) at 30 GHz.

49
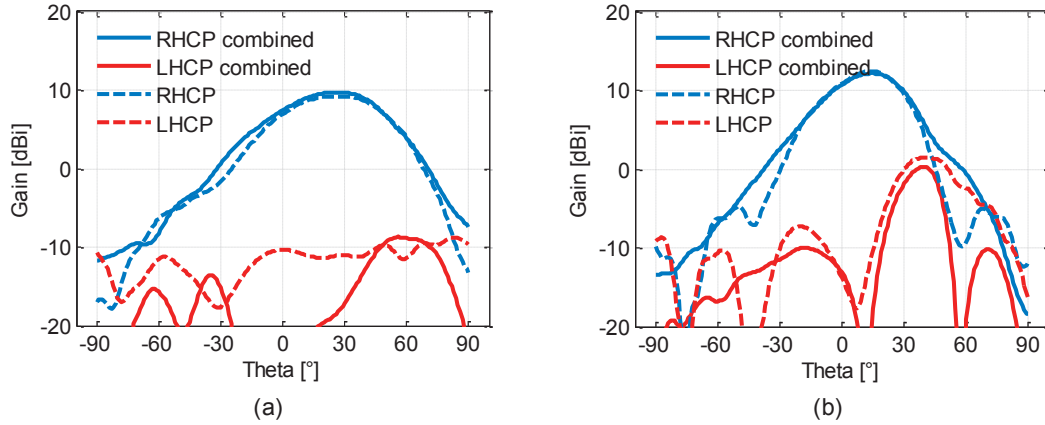
Fig. 3.14 – Simulated CP radiation patterns of the complete feed system: (a) at 20 GHz; (b) at 30 GHz.

3.3 Lens-based antenna system

As mentioned in the introduction of this chapter, Ka-band characteristics have greatly increased the interest in SOTM applications. The concept behind this application is to ensure a steady link between a ground moving platform and a satellite. This thesis aims to propose solutions for the ground terminal; thus, the antenna system that we are looking for, in addition to have to cope with both Ka frequency bands, needs to steer the beam in order to keep the connection link with space.

Therefore, the idea here presented is to combine the previous feed system with a lens antenna that will be responsible to increase the gain and to control the beam steering. The lens design here used was developed in IT-Lisbon and firstly introduced in [96] for operation at 60 GHz. However, in this specific context, we will work with its equivalent Ka-band scaled version that was previously presented in [97] and depicted in Fig. 3.15. The lens was scaled for the lowest frequency band (20 GHz), which ensures its operation at the highest one (30 GHz) as well. The selected material is polyethylene with ε_r = 2.35 and tan(δ) = 0.0004.

This design concept is different from most of the classical designs of scanning lenses. Normally the feed (or even a cluster of feeders) moves along the focal arc of the lens while the lens itself is stationary. When the target is a low-cost solution, an effort to keep the feed fixed should be done since this avoids the use of expensive rotary joints. In line with this, one possible solution could be moving the lens in a way that the phase center of the fixed feed is always aligned with the lens focal arc. However, as shown in [96], this approach limits the scanning range. Therefore, here the strategy was to focus on the focal point of the lens instead of its focal arc. We can enlarge the scanning range if we move the lens about its focal point because the output rays emerge parallel to the lens symmetry axis. Respecting this detail, the beam tilt angle is nearly the same as the lens tilt angle.

This new design concept allows to have more freedom for the optimization of the lens profile since there is no need to comply with a scanning beam condition. The lens design based on Geometrical Optics assumes that the feed is represented by its phase center. The lens has two shaped refracting surfaces that were optimized together to collimate the radiated beam while widening as much as possible the scanning angle interval. The distance from the lens focal point to its bottom surface is denoted by F and the lens total height by T; both dimensions and also the lens diameter are detailed in the caption of Fig. 3.15. The design involves the Snell law at the bottom lens surface and the usual path length condition defined by the following expression for beam collimation [96],

$$F + \sqrt{\varepsilon_r}T = r(\theta) + \sqrt{\varepsilon_r}l(\theta) + s(\theta).$$

Two refracting surfaces allow imposing an additional design condition which is used to favour wide beam scanning. For that, the otherwise arbitrary bottom lens surface r(θ) is written as a polynomial function where the coefficients are obtained by integration the above lens design equations with Genetic Algorithm optimization. Further details about the lens design are given in [96].
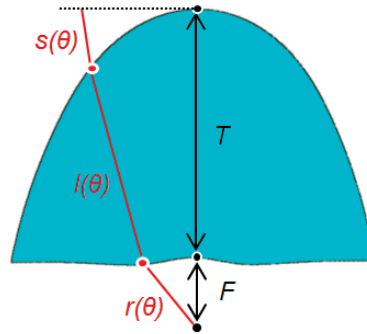
Fig. 3.15 – Lens antenna. Dimensions in *mm*: lens diameter = 87.5, T = 60 and F = 15.

The complete antenna composed of both lens and feed is presented in Fig. 3.16. For the sake of completeness, the movements of the lens in order to tilt the beam in both elevation and azimuth are illustrated in the same figure. The mechanical constraints of such system are here not discussed but a similar approach as shown in Fig. 3.16b could be an interesting solution. As previously explained, the lens focal point is placed in the feed phase center, and both remain always coincident for any tilted position of the lens. In this case, as we want the system to operate at two different frequencies, we consider the average of both phase center positions (shown in Fig. 3.6) as the final value.
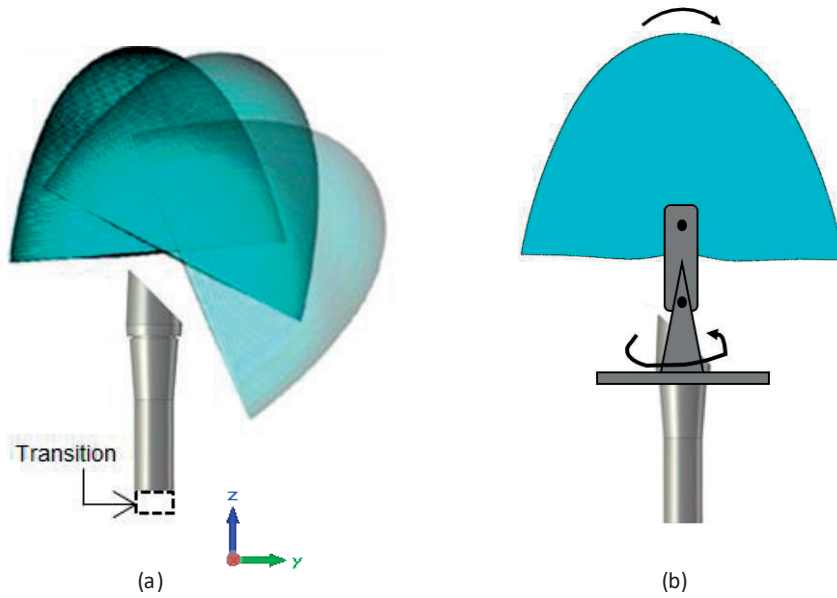
Fig. 3.16 – Lens-based antenna fed by the horn, scanning capabilities: (a) in elevation; (b) in both elevation and azimuth.

As previously discussed, we can obtain the results for two orthogonal LPs by applying a 90° rotation to the coaxial-to-waveguide transition with respect to the horn (Fig. 3.11). Both downlink and uplink radiation patterns associated to each LP for a specific lens tilt position, $\alpha = 20°$, are presented in Fig. 3.17. The beam followed the movement of the lens, pointing at approximately 20° at both frequencies and polarizations, with comparable gain values. Similar results were observed for other lens tilt angles, thus validating the theoretical concept.

A combination of these two LPs (as also done with the horn results, Fig. 3.14) allows achieving a good approximation of the CP response of the entire system. These results are shown in Fig. 3.18 for different lens tilt angles in the $0° < \alpha < 70°$ interval with 10° steps.
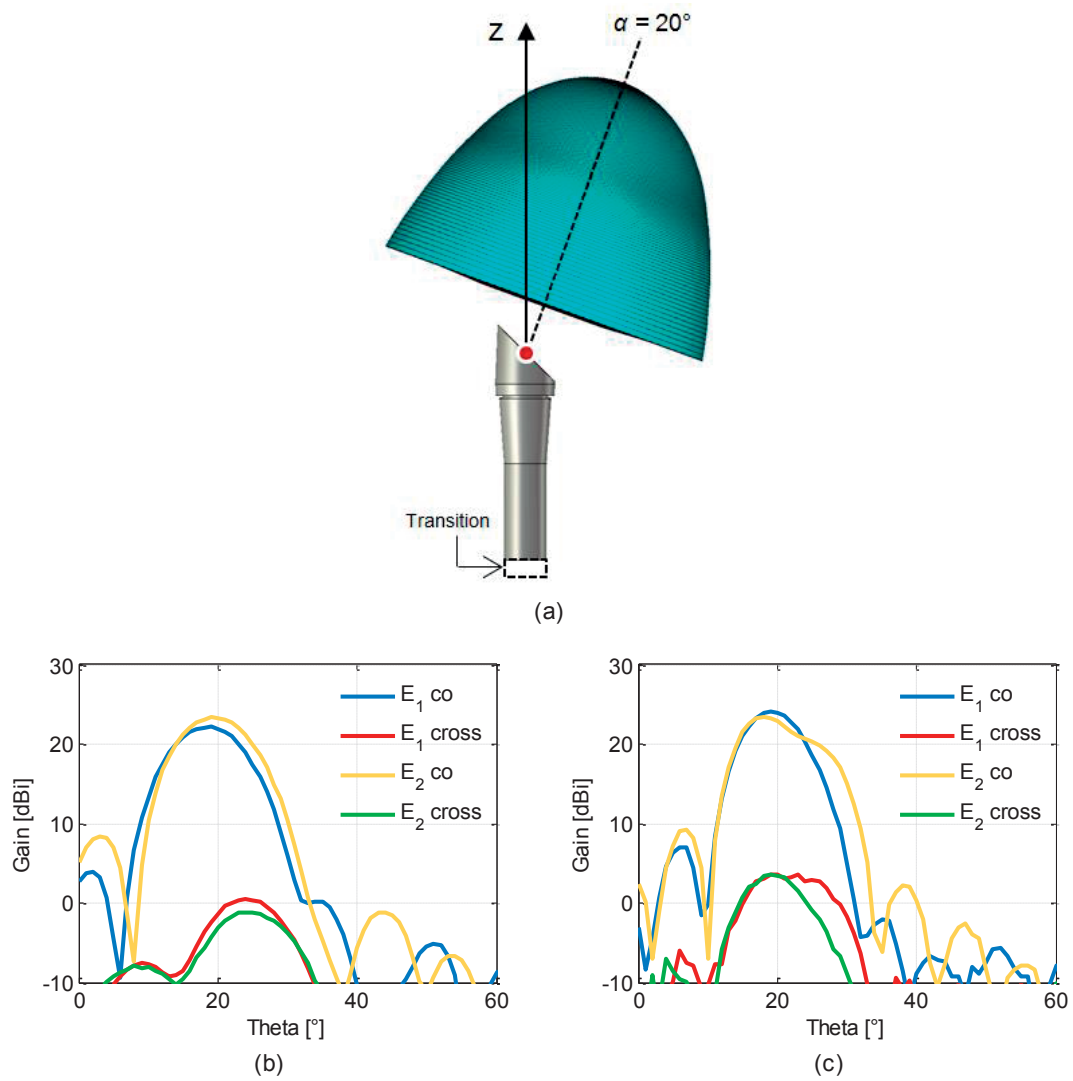
Fig. 3.17 – LP radiation patterns for one lens tilt position, α=20°: (a) system scheme at α=20°; (b) at 20 GHz; (c) at 30 GHz.
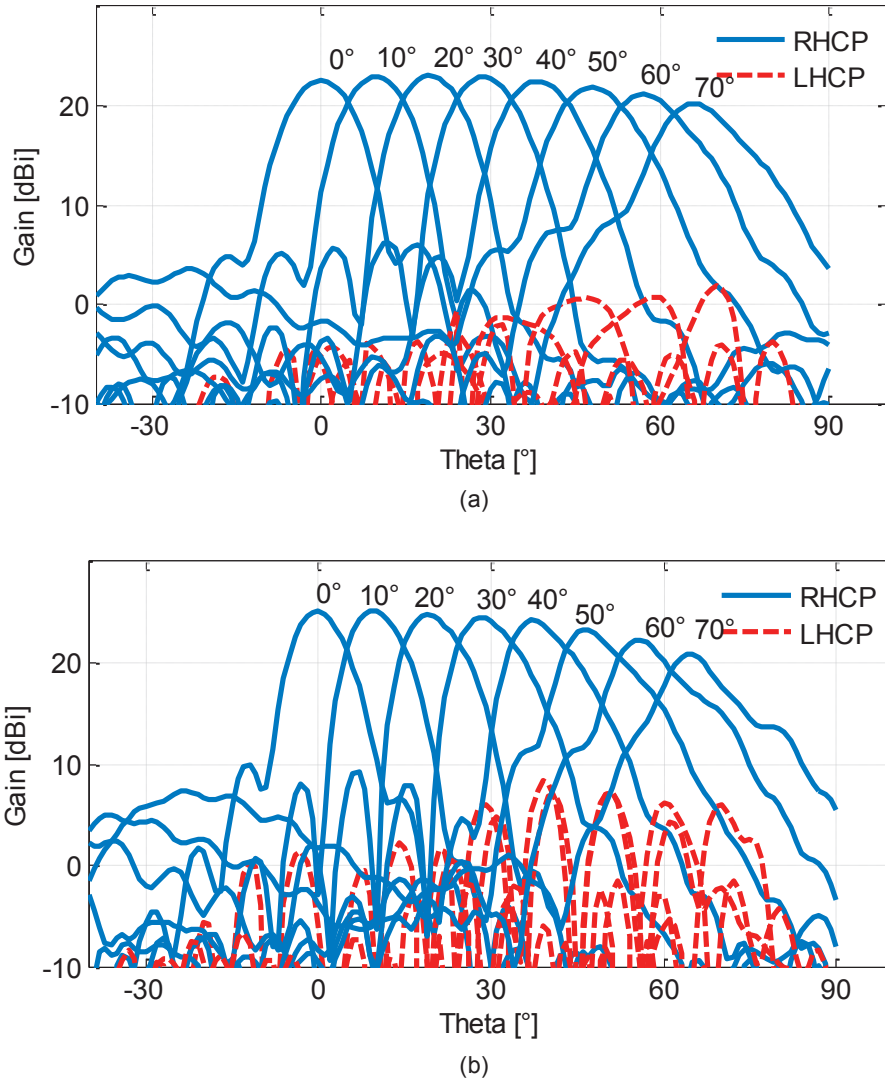
Fig. 3.18 – CP radiation patterns for different lens tilt angles ($0° < α < 70°$): (a) at 20 GHz; (b) at 30 GHz.

By observing Fig. 3.18 it is possible to see that the beam shape is well preserved within the wide scanning interval, especially at 20 GHz. It is also visible that the gain is higher at 30 GHz. Regarding the scan loss, it is higher at 30 GHz which was already expected due to the contribution of the horn ($α_{beam}$ = 27° at 20 GHz and $α_{beam}$ = 14° at 30 GHz, as shown in Fig. 3.5).

Table 3.II summarizes these performance indicators for both frequencies, where $α$ is the lens tilt angle, $α_{beam}$ is the beam tilt angle, G is the gain, $ΔG$ is the scan loss and $Δα_{beam}$ is half of the beam pointing difference between the two frequencies.

Table 3.II – Simulated performance indicators of the complete antenna system.

α [°]	20 GHz			30 GHz			Δα_beam [°]
	α_{beam} [°]	G [dBi]	ΔG [dB]	α_{beam} [°]	G [dBi]	ΔG [dB]	
0	0	22.5	0.5	0	25.1	0	0
10	10	22.9	0.1	9	25.1	0	0.5
20	19	23	0	19	24.7	0.4	0
30	29	22.9	0.1	28	24.4	0.7	0.5
40	38	22.4	0.6	37	24.2	0.9	0.5
50	48	21.8	1.2	46	23.3	1.8	1
60	57	21.1	1.9	56	22.3	2.8	0.5
70	66	20.2	2.8	65	20.9	4.2	0.5

This lens design has its limits, but these exceed those of the traditional scanning lenses. Excessive lens tilt has consequences in the achieved gain values because the feed radiation starts to illuminate a smaller area of the lens. But the second advantage of the proposed lens antenna is that the usually accepted 3 dB gain scan loss occurs for a much wider scan angle than in the best designs of the traditional scanning lenses (e.g. 20° in [147]). Our antenna configuration more than doubles this 3 dB angle, achieving 70° at 20 GHz band and 55° at 30 GHz. This is a major challenge solved, because furthermore it is achieved in two widely separated bands by a single antenna. Moreover, it is important to highlight another great achievement of this lens design which is a very small beam pointing error between the two frequencies. As the Table 3.II shows, this error is 1° in the worst case (α=50°). These results are achieved thanks to the lens design since the output radiation emerges in the same direction as the lens symmetry axis. This lens is then able to compensate the 13° of difference in the direction of the radiation that comes from the feed at both 20 GHz (α_{beam} = 27°) and 30 GHz (α_{beam}= 14°).

3.4   Prototypes and measurements

The simulated results encouraged the fabrication of the corresponding prototypes, here described in detail.

3.4.1   Lens antenna

The polyethylene lens was fabricated using a CNC milling machine with 50 µm precision available in IT-Lisbon. A simple mechanical support was developed to allow the movement of the

lens maintining proper feed alignment. It was fabricated using brass and aluminum, resorting to the same CNC machine. The complete prototype is shown in Fig. 3.19.

<div align="center">(a)   (b)</div>

Fig. 3.19 – Lens antenna prototype and its dedicated support: (a) α = 0°; (b) tilted position.

3.4.2 Antenna system with CNC feed horn

The quad-ridged horn and its dedicated coaxial-to-quad-ridged waveguide transition were fabricated in brass using the same CNC milling machine with 50 μm precision. The complexity of the structure does not allow its fabrication as a single block which imposes the planning of a split-block model. Following this strategy, the final feed system comprises nine different pieces as depicted in Fig. 3.20. It is important to refer here that this number of pieces allows having two independent structures (feed and transition), which is necessary to be able to measure the two orthogonal LPs previously mentioned in this document. The manufactured quad-ridged horn antenna comprises four pieces: two-half parts of the horn that already include one pair of ridges and two more independent ridges. In this prototype the movable part of the horn is actually fixed in order to simplify the manufacturing process. For the same reason, but also to avoid increasing the lead time and cost associated to the prototype, its external part has a parallelepiped form instead of being conformal with the interior. Neither of these simplifications affects the horn performance or the elevation scanning demonstration that is the main goal. The same approach was used to fabricate the coaxial-to-waveguide transition that comprises the other five pieces; the additional fifth piece was required to form the back cavity. All these sub-blocks are assembled with screws and alignment pins. Photographs of the feed prototype are shown in Fig. 3.21. The complete prototype is shown in Fig. 3.22.
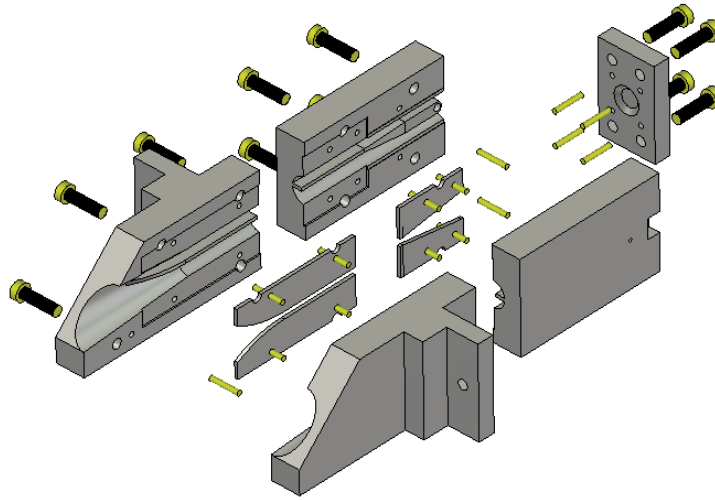
Fig. 3.20 – Split-block model of the feed prototype.
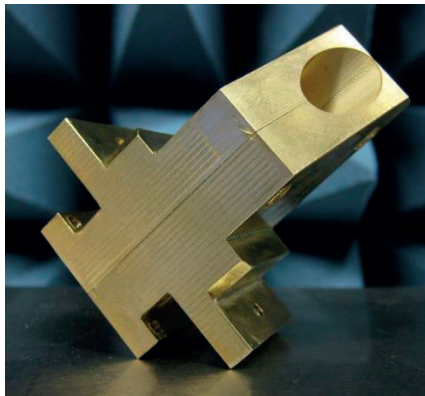
(a)
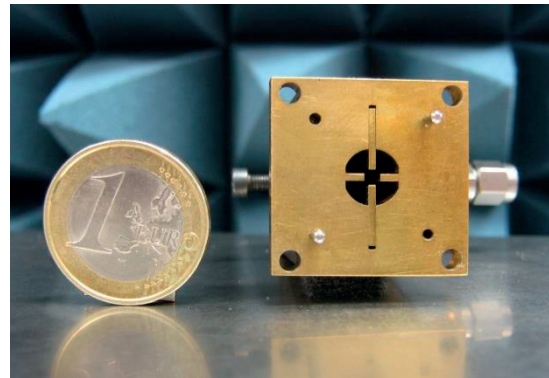
(b)

(c)

Fig. 3.21 – Feed prototype: (a) horn; (b) coaxial-to-waveguide transition; (c) inside view of the transition.

Fig. 3.22 – Complete antenna prototype.

The measured input reflection coefficients for the two orthogonal LPs are presented in Fig. 3.23. As shown, the reflection coefficient for the frequency bands of interest is acceptable with respect to the requirements. However, there is a disagreement between the overall shape of the return losses for the complete frequency range between simulations and measurements. Due to the use of split-block technology, the most probable causes for this disagreement are the air gaps and misalignments that can occur during the assembling process. Indeed, these causes affect the original accuracy of the CNC milling machine.
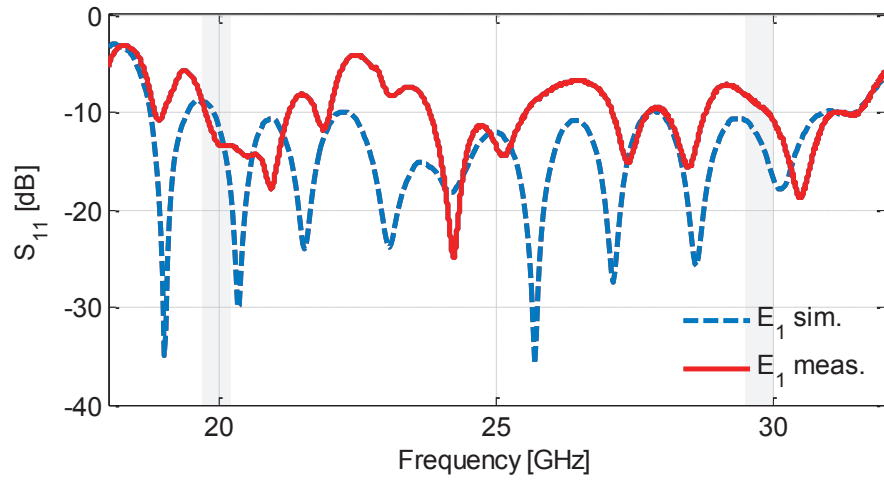
(a)
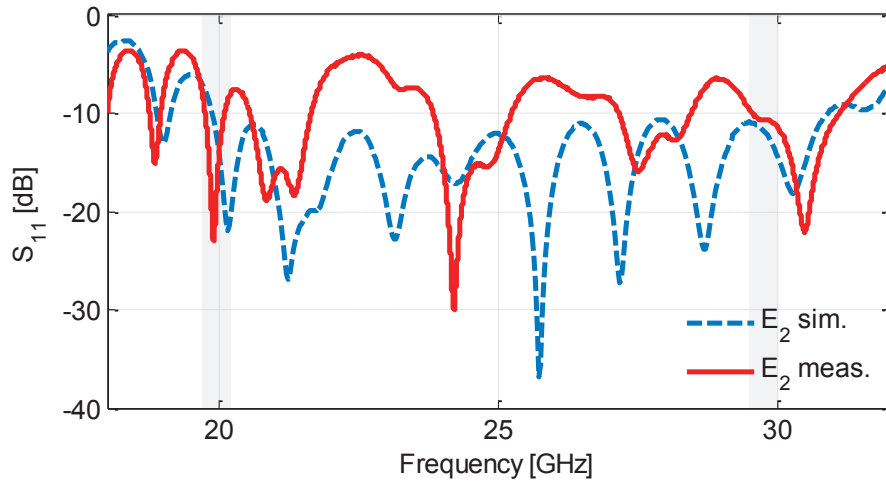
(b)

Fig. 3.23 – Simulated (dashed lines) and measured (solid lines) input reflection coefficient: (a) E₁ polarization; (b) E₂ polarization.

In order to verify that these measured results are due to manufacturing and assembling errors and inaccuracies, a new feed prototype has been manufactured using an additive technique; and it will be discussed in the next sub-section. Nevertheless, as aforementioned, the matching in the frequency bands of interest is acceptable, and for this reason we proceeded with radiation measurements at 20 GHz and 30 GHz. Regarding the radiation measurements, both E1 and E2 LPs were measured and afterwards combined by post-processing (as done with the simulated results). Fig. 3.24 compares both simulated and measured post-processed CP radiation patterns

for one lens tilt angle, α = 20°, and as shown, an excellent agreement is obtained. Similar agreements were observed for the other angles. Fig. 3.25 shows only measured CP radiation patterns for several lens tilt angle in the 0° < α < 70° interval with 10° steps. The corresponding measured performance indicators are detailed in Table 3.III. If we compare this values with the ones of Table 3.II, we can conclude that the agreement is very good.
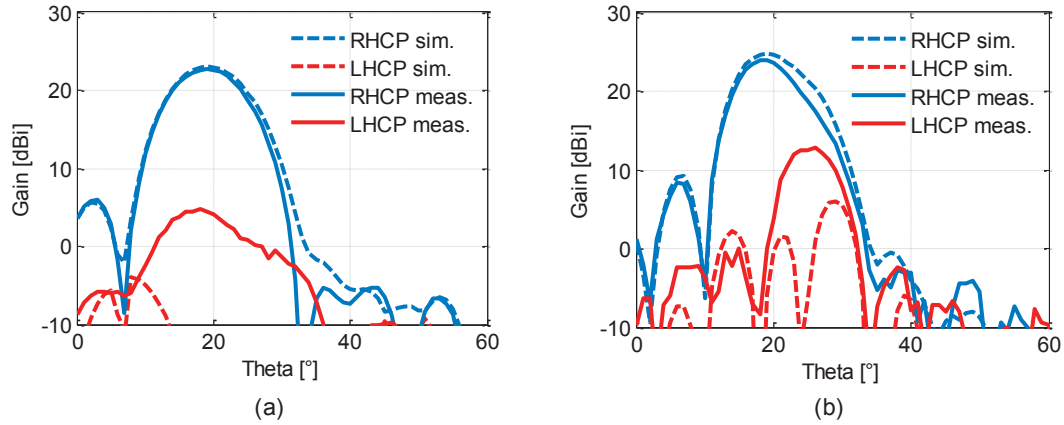
Fig. 3.24 – Simulated (dashed lines) and measured (solid lines) CP radiation patterns for one lens tilt position, α=20°: (a) at 20 GHz; (b) at 30 GHz.
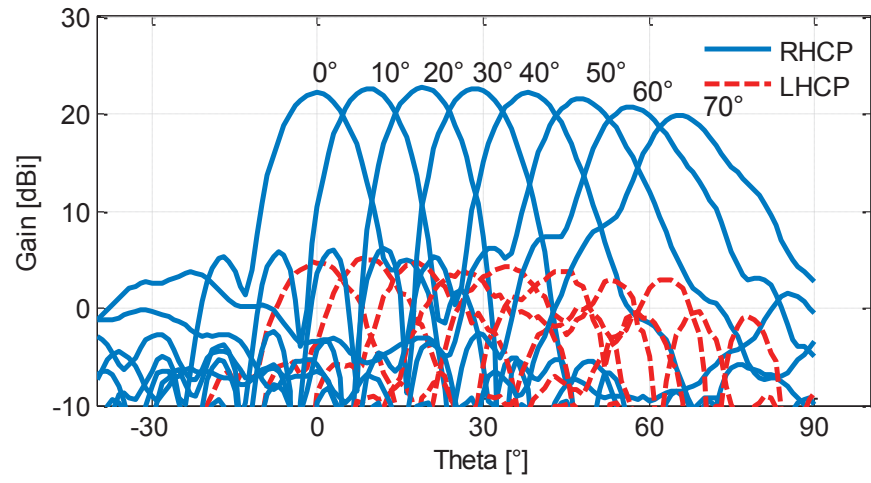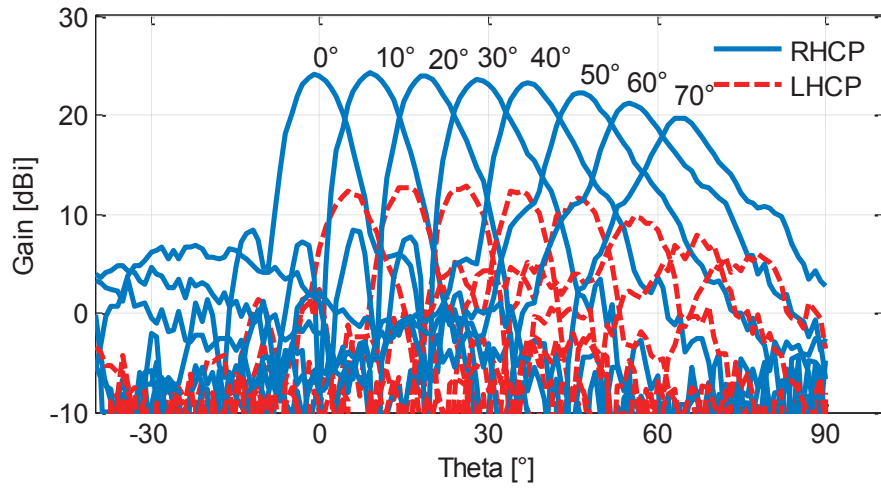
Fig. 3.25 – Measured CP radiation patterns for different lens tilt angles (0° < α < 70°): (a) at 20 GHz; (b) at 30 GHz.

Table 3.III – Measured performance indicators of the complete antenna system.

α [°]	20 GHz			30 GHz			$\Delta\alpha_{beam}$ [°]
	α_{beam} [°]	G [dBi]	ΔG [dB]	α_{beam} [°]	G [dBi]	ΔG [dB]	
0	0	22.2	0.5	0	24.1	0.1	0
10	9	22.6	0.1	9	24.2	0	0
20	19	22.7	0	19	23.9	0.3	0
30	28	22.6	0.1	28	23.6	0.6	0
40	38	22.1	0.6	37	23.2	1.0	0.5
50	48	21.5	1.2	47	22.3	2.0	0.5
60	57	20.7	2.0	55	21.2	3.0	1
70	66	19.9	2.8	64	19.7	4.5	1

3.4.3   Antenna system with AM feed horn

As explained and documented in the previous sub-section, the simulated and measured S-parameters obtained with the CNC feed prototype were not coherent within the all band. The targeted application drove the strategy of the CNC prototype towards CP, requiring nine sub-blocks; however, the assembling of all these might cause air gaps and misalignments, thus having a negative influence in the input reflection coefficient. In order to prove that the measured results are only linked to fabrication inaccuracies, we had changed our strategy by planning a new prototype with a reduced number of pieces. Following this direction and using the same manufacturing technique, we could reduce from nine to five pieces by limiting the prototype to a single LP. The equivalent model is presented in Fig. 3.26. Nevertheless, the air gaps and misalignments between the five different pieces could still have a strong influence in the results.
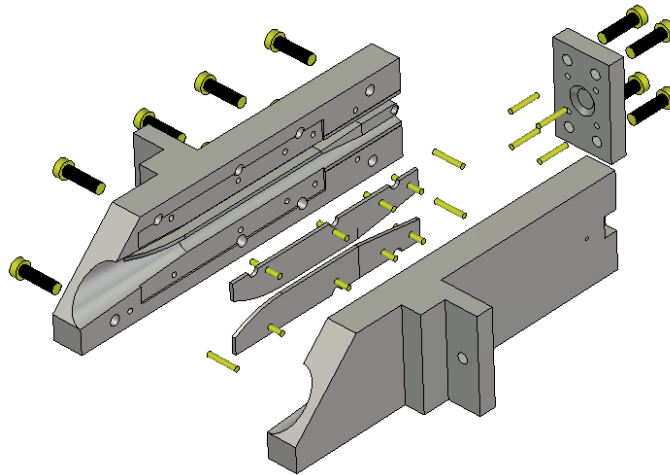
Fig. 3.26 – Model of the CNC feed prototype with five pieces, allowing only one LP.

This doubt made us look for other fabrication techniques aiming to save time and money. The Stereolithography (SLA) appeared here as an enabling AM technique providing a bunch of advantages. One of the most attractive was the possibility to fabricate a monolithic device. Then, in order to fabricate the feed antenna we would need a single piece instead of five which means we would eliminate completely the negative influence of the assembling process.

The SLA prototype was manufactured in collaboration with the Swiss company, SWISSto12, and it is shown in Fig. 3.27. They are specialized in a SLA technique that offers a local precision of 25 μm with a maximum tolerance of ±200 μm on large dimensions. Their current setup is able to produce devices with volumes of approximately 300 x 300 x 350 mm; therefore, the overall volume of the feed system is sufficiently small to be manufactured in a single piece.

The first fabrication step was to 3D-print the device. After printing and cleaning the polymer body, there was a preparation step, where the polymer surfaces were treated by chemical products. Afterwards, a uniform metallization of the entire device, including their complex inner shapes, was done through a chemical electroless process. The metal used was copper and it was deposited a layer of more than 3 μm thick, which is enough to ensure full RF conductivity at Ka band. Additionally, in this prototype, a very thin (100 nm) gold layer was added for passivation.

(a)

(b)
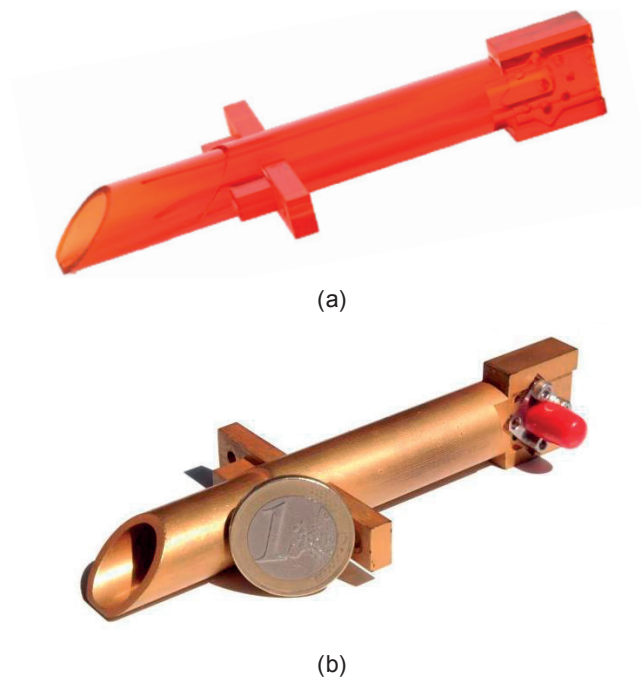
Fig. 3.27 – SLA feed prototype: (a) before metal coating; (b) after metal coating.

The simulated and measured input reflection coefficients of this prototype are presented in Fig. 3.28 and a good agreement between both curves is observed. This LP prototype corresponds to the E_2 version of the CNC prototype (Fig. 3.11b). Please note that the differences in the simulated curves of these two equivalent prototypes are justified by the adoption of different connectors. In the CNC version we used a semi-ridged EZ-86 coaxial cable, while here we used a SMA connector.
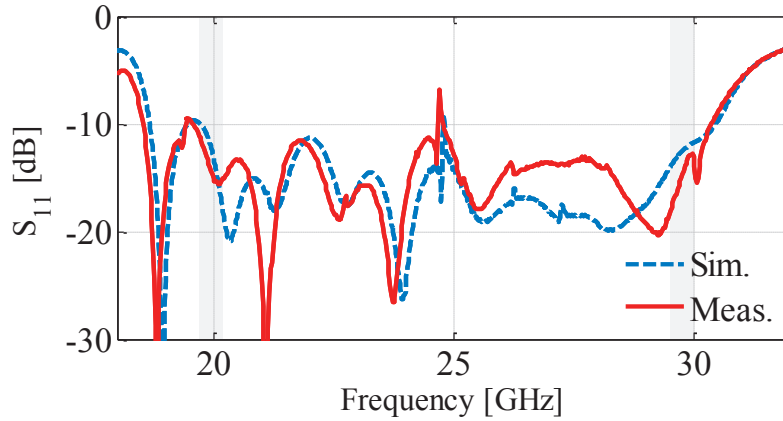
Fig. 3.28 – Simulated (dashed line) and measured (solid line) input reflection coefficients of the SLA feed prototype.

While using SLA neatly improves the matching characteristics of the horn, it does not alter the radiation characteristics within the desired sub-Ka bands, thus both prototypes have identical patterns as presented in Fig. 3.29.

(a)   (b)
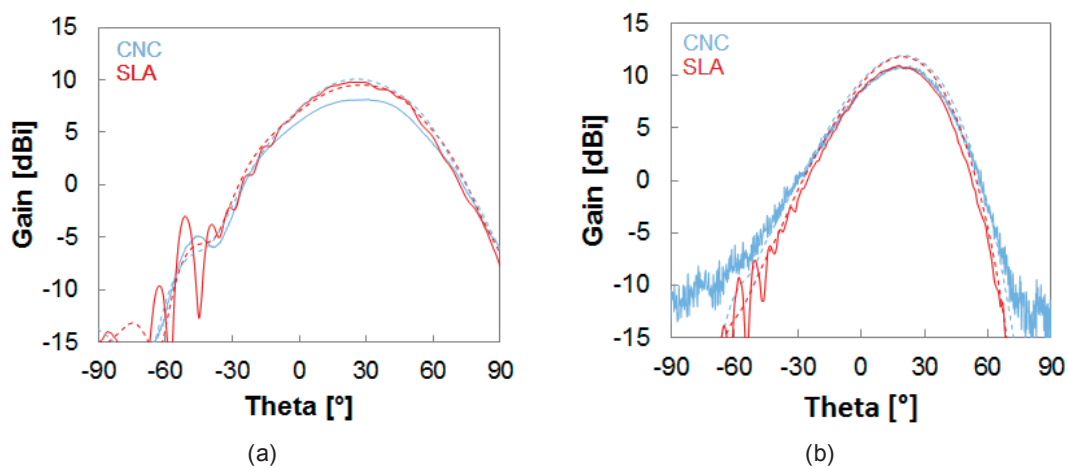
Fig. 3.29 - Simulated (dashed lines) and measured (solid lines) LP radiation patterns of both feed prototypes: (a) at 20 GHz; (b) at 30 GHz.

64

Hence, the SLA horn can be used instead of the CNC horn to feed the dielectric lens and the final resulting radiation patterns are not affected by this replacement. Please note that with this configuration, we can only obtain LP results. To verify this, the SLA horn prototype was integrated with the same lens already used with the CNC horn in the SOTM system as shown in Fig. 3.30. This new hybrid system is a good example of combination of different manufacturing techniques, exploiting the best possibilities of each one.

In Fig. 3.31, simulated and measured LP radiation patterns are compared for a specific lens tilt angle, α=20°, at both operating frequencies of 20 GHz and 30 GHz. At 20 GHz (Fig. 3.31a), the measured cross-pol curve seems to have acquired the shape of the co-pol which most probably means that we had a slight misalignment in the setup. Nevertheless, we can say that the results show reasonable agreement. Similar agreements were obtained for all the angles. Fig. 3.32 shows the measured LP radiation patterns for different lens tilt angles from 0° to 70° with 10° steps at both frequency bands. The maximum radiated power changes a little with the tilt angle, but the radiation remains with acceptable beam width up to α = 70° at both frequencies. The difference between maximum powers at the best and worst angles within the intended scanning range is called the scan loss and this is a relevant figure to qualify beam steering systems. In this case, the scan loss from 0° to 70° is only 2.5 dB at 20 GHz and 4.2 dB at 30 GHz, which are good achievements regarding the wide range.

Fig. 3.30 – Complete antenna prototype with the SLA feed.
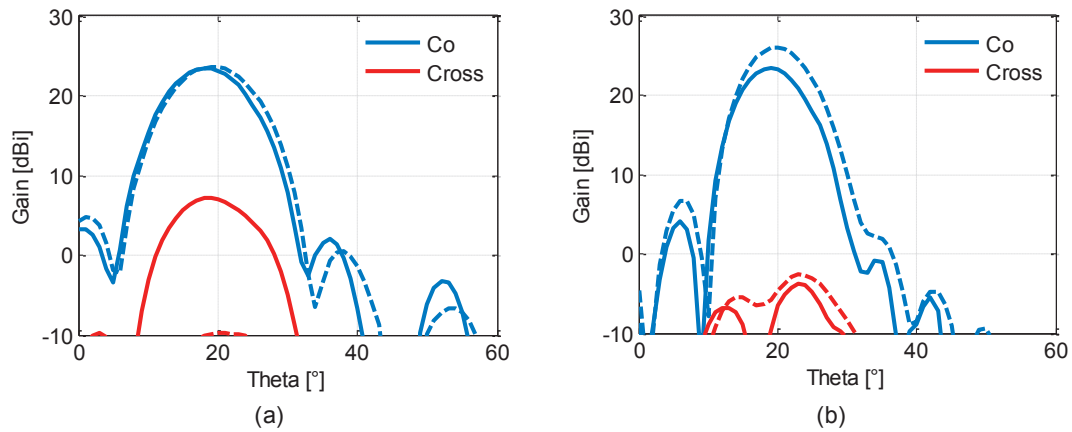
Fig. 3.31 – Simulated (dashed lines) and measured (solid lines) LP radiation patterns of the lens antenna fed by the SLA horn for one lens tilt position, α=20°: (a) at 20 GHz; (b) at 30 GHz.
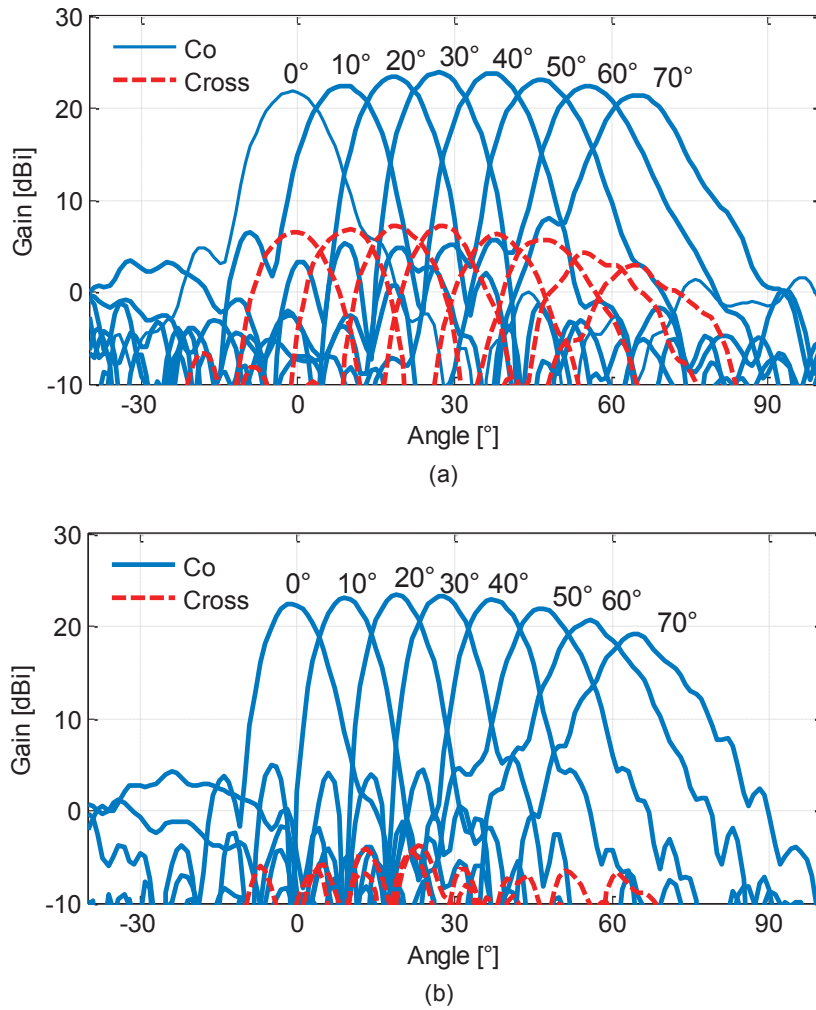
Fig. 3.32 - Measured LP radiation patterns for different lens tilt angles (0° < α < 70°): (a) at 20 GHz; (b) at 30 GHz.

3.5   Conclusions

The work presented in this chapter addressed the design and manufacturing of a horn feed system able to cope with downlink and uplink Ka-bands with CP and simultaneously fully compatible with an existing lens, which results in an antenna system to achieve large scanning angles. The feed antenna is composed by a quad-ridged horn and its dedicated coaxial-to-waveguide transition. The ridges enlarge the bandwidth, thus covering both Ka-band while keeping the CP features. A specially tailored coaxial-to-waveguide transition is also needed. In fact, to achieve CP the waveguide should include two coaxial cables orthogonally located. Nevertheless, this type of transition has two symmetry planes at its open-end, which allows a 90° rotation with respect to the horn. Therefore, it is possible to obtain the results for two orthogonal LPs and then get the CP response of the device by a proper post-processing combining both LP results.

Since the final goal is to combine this feed antenna with a lens and propose a system for Ka-band SOTM applications, an optimization was successfully performed on the horn aperture to help the lens to extend its original scanning performances. The design of the lens antenna used in this system was out of the scope of this thesis and was only briefly mentioned here for the sake of completeness.

Good simulated results for both the standalone feed and the complete antenna system encouraged the fabrication of the corresponding prototypes. First, the feed subsystem was manufactured using a CNC milling technique; however the measured results of this prototype in terms of matching in the whole band were not at all as expected. Nevertheless, thanks to the fact that at 20 GHz and 30 GHz we obtained a satisfactory matching we could still perform radiation measurements at these bands and a very good agreement with simulations.

In order to recover the expected behavior of the feeder over the full band, another prototype was manufactured but this time using a SLA technique. In addition of being more accurate than the previous one, we could fabricate a monolithic device which reduces dramatically the assembling errors. The advantages of SLA allowed us to obtain good matching results, validating the design of the antenna. Both prototypes were measured together with the lens and excellent agreements between simulated and measured results were obtained.

The combination of a 3D lens and a waveguide horn feeder behaves as theoretically predicted and show reasonable performances. But obviously, there is still space for further improvements, especially in terms of size. In the context of the feed, a planar design could dramatically reduce the length of the antenna, while offering supplementary possibilities for a direct implementation of CP excitation. Concurrently, a planar lens antenna or an equivalent device should also be considered to replace the bulky 3D lens. In addition to contribute to a much smaller final structure, the required lens rotation could be replaced by a relative translation between lens and feeder. This could result in a more compact and easy design. In the next chapter we aim to tackle these issues.

Chapter 4   Dual patch antenna

Sou frágil nas pequenas coisas,
Mas forte nas grandes.

Amália Rodrigues

This chapter contains the second feed antenna proposed in this thesis, a rather compact element when compared with the horn shown in the previous chapter. First, a brief introduction is presented in order to explain the motivation of this design. Then, the new antenna is presented, followed by a comparison between this design and the horn antenna, with and without the previously introduced dielectric 3D lens. Finally, a compact feeder would logically call for a more compact focusing device. With this idea in mind, a preliminary test combining both this feed antenna and a planar lens is shown. The chapter ends with some comments about the usefulness of these solutions.

4.1   Introduction

The horn antenna presented in the previous chapter was designed to work simultaneously at both downlink and uplink Ka-bands with CP. Moreover, another specific goal was to help the lens to reduce its scan loss over an elevation tilt range from 0° to 60°. These goals were achieved, although, as explained, CP operation was never actually implemented. The expected CP performances were estimated by post-processing on theoretical and measured results obtained for two orthogonal LP.

Now, an obvious improvement to consider refers to the total height of antenna system composed by the combination of feeder and lens. As already mentioned, this thesis focuses on feed antennas and therefore, the first challenge to tackle is the analysis and eventual realization of a more compact feeder.

As explained in the Chapter 2, planar printed antennas, usually including dielectric substrates, are very interesting compact solutions. Although the use of dielectrics makes these antennas not so attractive for space applications when compared to the metal-based solutions, they can be a good compromise in terms of performance and size for ground applications. It is this trade-off that we aim to study here. The new planar feed must be compared with the horn feeder, first when both feed antennas work standalone and then when combined with the same mechanical lens-based mechanically steerable subsystem discussed in the previous chapter. In particular, performances in terms of size, gain and phase center stability should be carefully compared.

In order to achieve a fully planar antenna system, in addition to replace the feed antenna, it is obvious that we should also replace the dielectric lens for a planar gain enhancement structure. In this case the relative movement between feeder and gain enhancer needed to tilt the beam would be translational instead of rotational, which should be simpler to implement. In this case, the maximum beam direction should be pointing at broadside and the feed antenna here discussed was designed to be in line with this requirement. Under this situation, we can already expect that the combination of this feed antenna with the lens will produce a bigger scan loss than the system where the same lens is fed by the horn. This detail is already highlighted here because it could drive to an unfair comparison at a first glance; indeed, it will be addressed again in the corresponding sub-section.

Finally, we were able to perform a preliminary test of the planar feed antenna presented in this chapter with a planar lens developed at IT-Lisbon. This planar lens is a single-band design working only at the uplink Ka-band. The obtained results at this frequency band were satisfactory and they paved the way for obtaining the sought-after dual-band behavior.

4.2   Review on planar antennas

As mentioned in the Chapter 2, planar printed antennas are well-known and widespread solutions nowadays, especially thanks to their low profile, light weight and ease of fabrication. The first publications about this technology date from early 1950s [148], [149]. From that time, many methods to analyse this type of antennas started to appear. Among all of them, the most popular ones are the transmission line, cavity and full-wave methods [68]. The transmission line method is considered as the easiest one and although it provides good physical insight, it is less accurate than the cavity model. On the other side, the price to pay for this improved accuracy is the higher complexity of the cavity model when compared with the transmission line model. These two methods are extensively explained in [68]. The full-wave started to receive more and more attention thanks to both the investment in softwares based on numerical methods and the larger access to powerful computers. At the same time, the research on planar antennas resulted in more demanding and sophisticated designs that would be much easier and faster analyzed by using these softwares. Currently, the full-wave methods are the most popular because in addition to be very accurate and robust, they are usually versatile and allow the easy implementation

of parameter sweep capabilities. Another attractive characteristic of the recent commercial full-wave softwares is the intuitive and user-friendly 3D modelling interface.

There are several pertinent aspects to keep in mind in order to start designing printed planar antennas. For instance, the permittivity of the substrate is an important decision. Normally, the dielectric constants (ε_r) range from 2.2 to 12. A lower permittivity allows better efficiency, larger bandwidth and wider fringing fields that consequently result in better radiation. However, these characteristics are obtained at the cost of larger element size. On the other hand, increasing the permittivity is equivalent to say that the electric length of the waves in the substrate is decreasing. Therefore, substrates with higher permittivity values are usually used to miniaturize the patch antenna. Here there is another relevant trade off since the excitation of surface waves is promoted by increasing either the thickness or the permittivity of the substrate. This fact can lead to greater losses and mutual coupling between elements. One of the solutions for eliminating these surface waves, especially when large bandwidths are desired, is to use a cavity. When aiming large bandwidths or an increased gain, the use of stacked patches is another common solution.

Stacked patch antennas is the name given to a design that places two or more electromagnetically coupled patches on top of each other. The sizes of the patches are normally different either to increase the bandwidth or to achieve dual-band behaviour. Two patches are used in most of the examples available in the literature which is equivalent to say that two resonances are usually considered. In these cases, the lower patch is fed by, for instance, transmission line, coaxial or slot techniques, and the upper patch is commonly parasitically coupled. The analysis of stacked patches is more complex than the single patch once there are a larger number of parameters to deal with.

As previously mentioned, the solution of integrating the patches inside a metallic cavity is commonly used. They are usually known as patch-excited cups (PECs) and the antenna presented in [86] by RUAG Space serves here as an example. Actually, RUAG Space has a large experience on this type of antennas for Global Navigation Satellite Systems (GNSS) applications since they are broadband and well-suited for CP. Shortly, the patches have different roles: while the upper patch aims to enhance the directivity, the lower ones (normally two) are used to tune the bandwidth. These antennas are normally excited through four feed points (with equal magnitude and 90° phase shift between each of them) that are coming from the bottom of the cavity until the first patch. Metal contacts can be prejudicial for some industrial applications with strict requirements, especially regarding Passive Intermodulation (PIM) and therefore, the antennas are excited with non-contacting probes through a capacitive coupling as discussed in [160].

4.3   Patch antenna design

The antenna proposed in this chapter consists of a stacked patch antenna (counting with two circular patches). A circular backed-cavity was adopted to improve the performance of the antenna. Four coaxial cables are inserted in the back part of the antenna and connected to the lower layer. In order to achieve good quality CP, these four coaxial cables are fed in sequential rotation. This means that all the four cables present equal voltage while having phase differences of 90° between them. Note that a feeding network should be designed in order to divide the power and to provide these phase shifts; however, in this chapter, we will assume ideal ports at each coaxial cable. The antenna design is explained in Fig. 4.1.

(a)	(b)	(c)	(d)
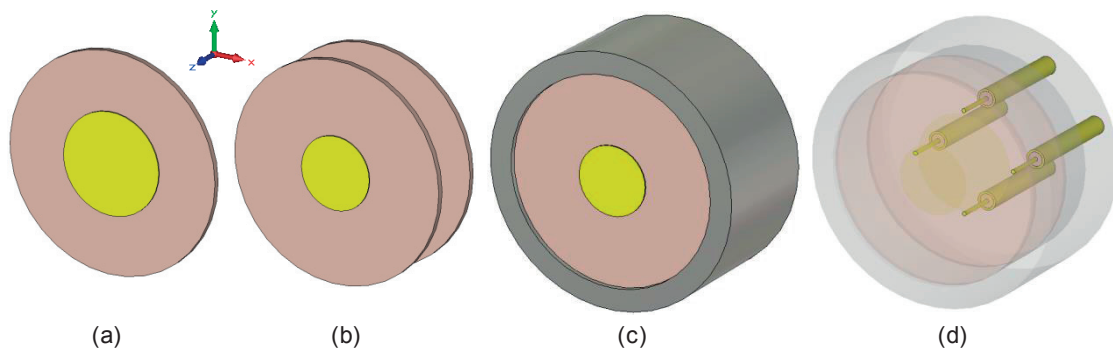
Fig. 4.1 – Design explanation: (a) lower patch; (b) upper patch added; (c) integration of both patches inside the metallic cavity; (d) sequential rotation feeding through four coaxial cables.

The process starts by modelling the stacked patch antenna in the commercial full-wave software, excited by the four coaxial cables. The optimization of the antenna design is guided by two following families of parameters:

o   Substrate parameters meaning their permittivity and thickness;
o   Geometrical parameters of the antenna meaning the diameter of both patches, the height between the two layers, the size of the cavity and the position of the pins.

Regarding the substrate, we preferentially aim one with low thickness because, in this case, the substrate is just to accomodate the patches. A pragmatic approach trying to respect it but also based on the ease of manufacturing, availability in the laboratory and popularity in the world of antenna design was used to choose the substrate. In the end, we used the 0.254 mm thick Rogers Duroid RT5870 with permittivity ε_r = 2.33 and loss tangent tan(δ) = 0.0012.

The patches, as shown in Fig. 4.1, have been chosen to be circular. The symmetry and simplicity of this shape are two relevant reasons to justify why it is seen as a popular and classical choice. At first, the diameter of the patches were set to be a half-wavelength at 20 GHz and 30 GHz which corresponds to $\lambda/2$ = 7.5 mm and $\lambda/2$ = 5 mm, respectively. Nevertheless, the final patch

diameters as well as the distance between both of them and the position of the coaxial cables result from a parametric sweep optimization performed to tune the resonances according to the downlink and uplink Ka-bands. As the parameters were optimized at the same time, it is indeed difficult to clearly associate the effects to each parameter; however we can extract the following conclusions:

- o The diameters of the patches have a direct influence on the resonanting frequencies. The lower (and bigger) patch has greater influence in the downlink band while the influence of the upper (and smaller) patch is higher in the uplink band;
- o The distance between both patches have an influence on their mutual coupling;
- o The position of the coaxial cables have also an influence on the resonances;
- o They all have an influence in the input impedance.

At the end of this process, the best solutions were still refined until we have achieved the final one which is presented in Fig. 4.2. The final dimensions are detailed in its caption. One particular characteristic of this design is that the inner conductors of the coaxial cables are not connected to the lower patch as it is commonly seen. In contrary, they are placed very close to it prosecuting a horizontal coupling which was beneficial in this case. The coaxial cable model used in this design is the EZ34 and all the four cables are placed 2.35 mm away from the center of the cavity. This EZ34 cable has the following dimensions (diameters): inner conductor = 0.2 mm; dielectric = 0.66 mm; and outer conductor = 0.86 mm.

(a)

(b)
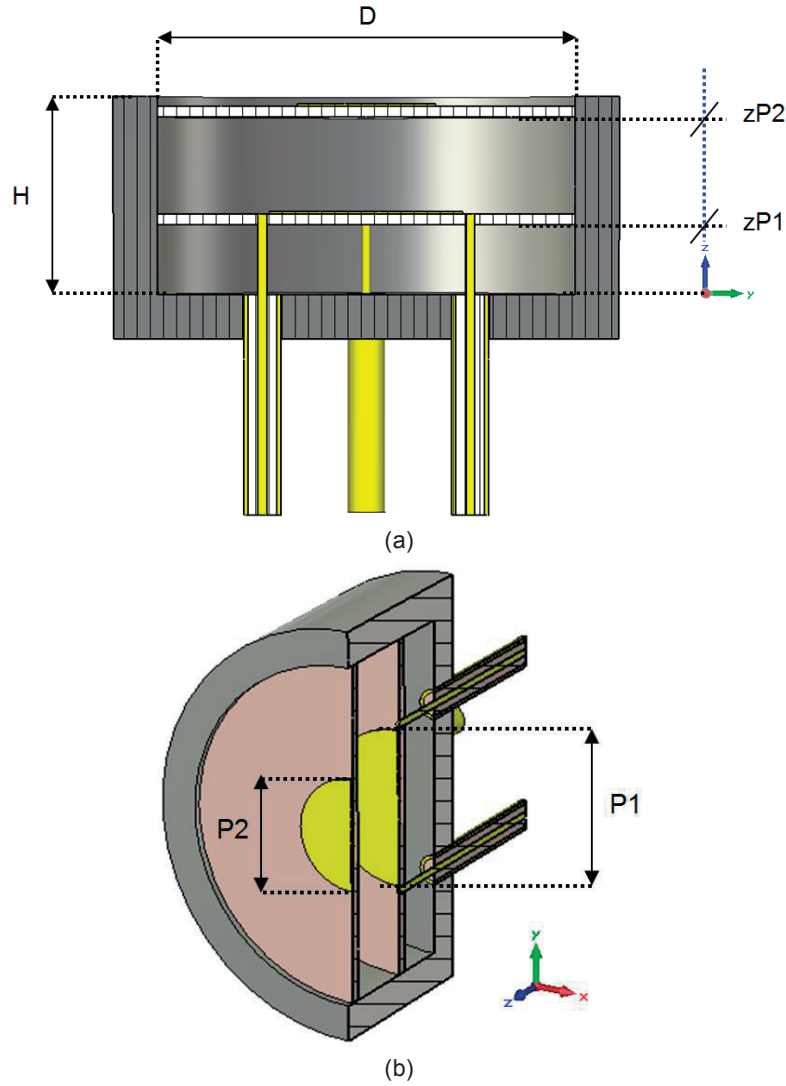
Fig. 4.2 – Final antenna design: (a) YZ cutting plane, side view; (b) YZ cutting plane, perspective view. Dimensions in *mm*: height of the cavity, H = 4.5; diameter of the cavity, D = 9.48; diameter of the lower patch, P1 = 4.4; diameter of the upper patch, P2 = 3.14; z-position of the inferior surface of the lower substrate, zP1 = 1.58; z-position of the inferior surface of the upper substrate, zP1 = 4.02. EZ34 coaxial cables are placed 2.35 mm away from the center of the cavity. EZ34 diameters in *mm*: inner conductor = 0.2; dielectric = 0.66; outer conductor = 0.86. Wall thickness of the cavity is 1 mm.

The antenna is a symmetric multi-port device as depicted in Fig. 4.1. Thanks to its four-fold symmetry and four accesses, this antenna is ready for producing CP through sequential rotation. According to this feeding technique, the four coaxial cables should be simultaneously excited and then the active S-parameters should be construed for performance assessment. Under a premise of the ideal 90° phase shift, the active input reflection coefficient at the port 1 can be formulated as following:

$$S_{11}^{Active} = S_{11} + \frac{v_2}{v_1}S_{21} + \frac{v_3}{v_1}S_{31} + \frac{v_4}{v_1}S_{41} = S_{11} + jS_{21} - S_{31} - jS_{41} = S_{11} - S_{31}.$$

It has been considered that the antenna is fully symmetrical and therefore $S_{21} = S_{41}$. Moreover, owing to the structure symmetry, the active input reflection coefficients of all the ports are equal.

As Fig. 4.3 shows the S_{11} active is below -15 dB in both desired Ka-bands: downlink, 19.7 to 20.2 GHz; and uplink, 29.5 to 30 GHz.
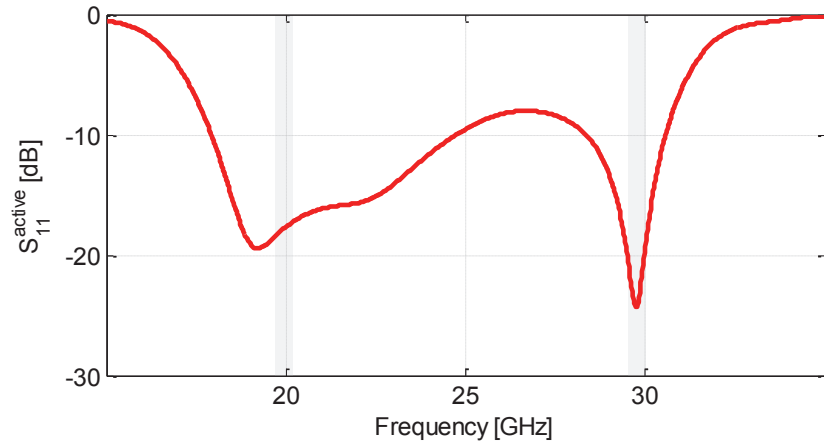
Fig. 4.3 – S11 active of the antenna.

The CP radiation patterns at 20 GHz and 30 GHz are presented in Fig. 4.4. It is clear that the gain is higher in uplink than in downlink. The maximum gain values at 20 GHz and 30 GHz are 7.7 dBi and 9.3 dBi, respectively. The gain does not vary significantly in the desired Ka-bands. This can be observed in Fig. 4.5 for both downlink and uplink Ka-bands.
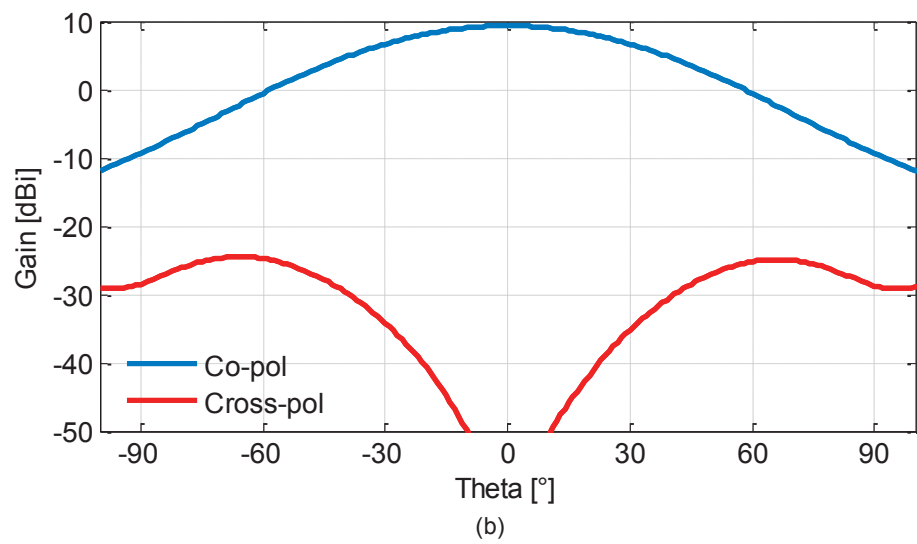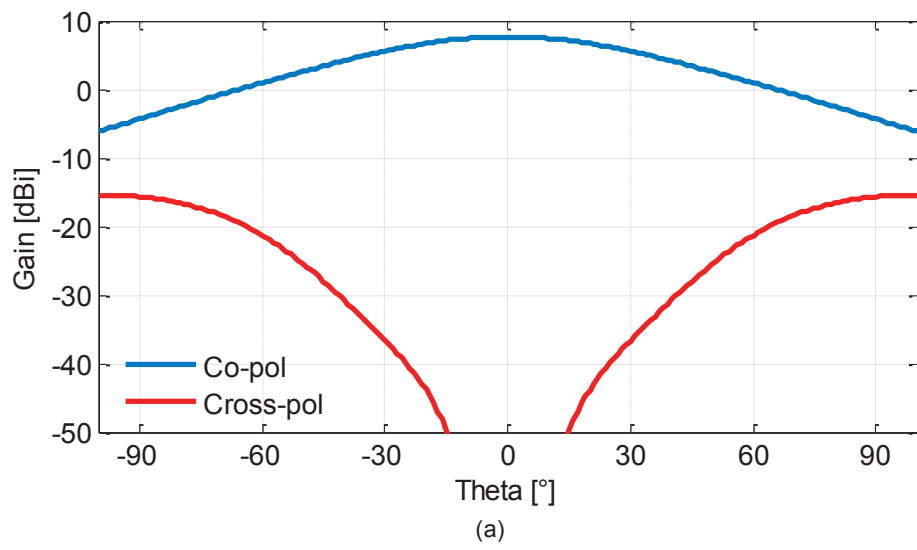
Fig. 4.4 – CP radiation pattern: (a) at 20 GHz; (b) at 30 GHz.
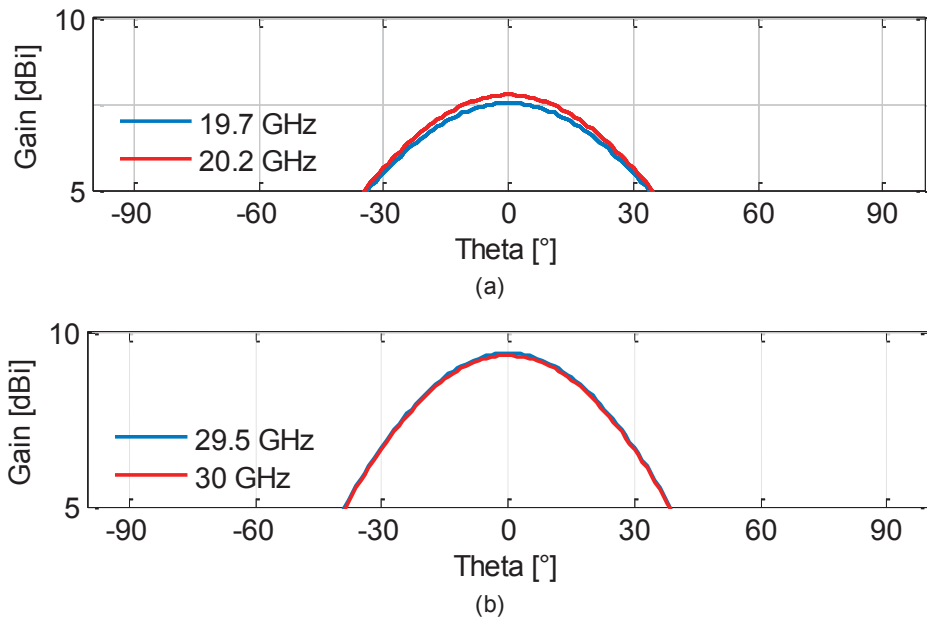
Fig. 4.5 – Gain variation (co-pol.): (a) at downlink; (b) at uplink.

The axial ratio for phi=0 at 20 GHz and 30 GHz are shown in Fig. 4.6. Considering this last figure, it is possible to conclude that the <3 dB region is 77° at 20 GHz and 105° at 30 GHz. The axial ration variation over both bands is also not significant as it can be seen in Fig. 4.7. The worst cases are the higher frequencies at both bands, 20.2 and 30 GHz. Fig. 4.8 shows the axial ratio for these specific frequencies, respectively, for the following four different phi values: 0°, 30°, 60° and 90°. As it is possible to see, the results are more stable at downlink Ka-band.
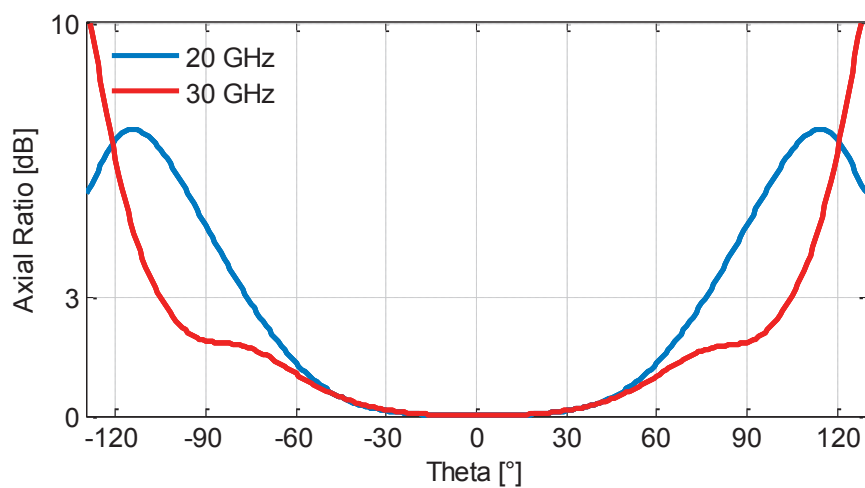
Fig. 4.6 – Axial ratio at both 20 GHz and 30 GHz.
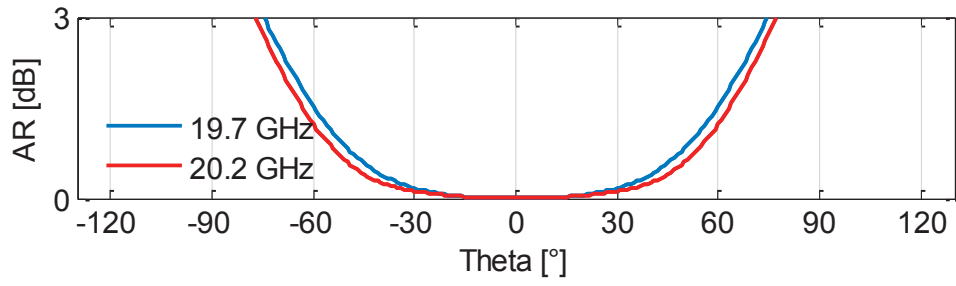
(a)
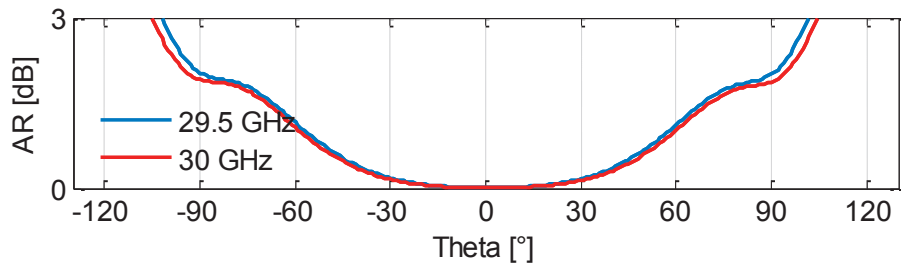
(b)

Fig. 4.7– Axial ratio variation: (a) at downlink; (b) at uplink.
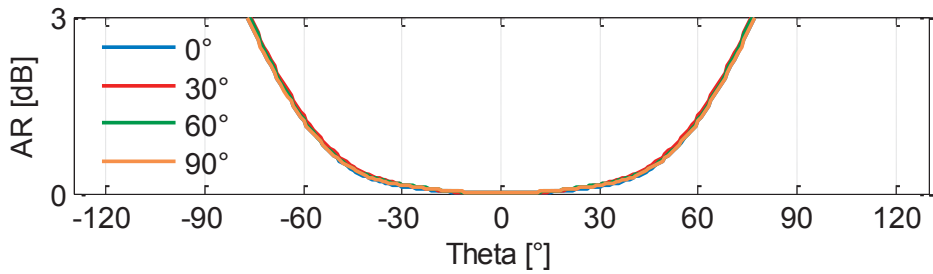
(a)
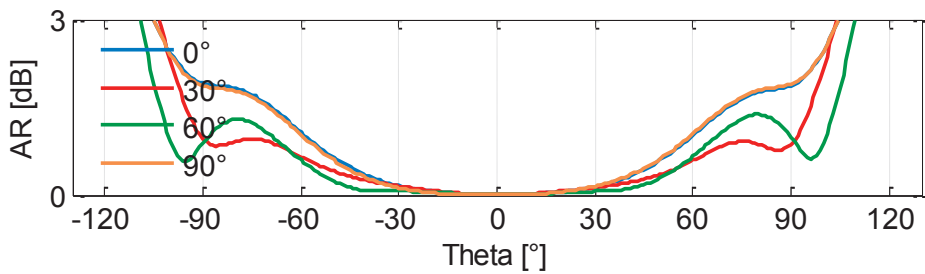
(b)

Fig. 4.8 – Axial ratio for different phi values: (a) at 20.2 GHz; (b) at 30 GHz.

78

4.4   Trade off: horn vs planar printed feed

The planar printed antenna described in the previous section was designed to replace the horn antenna presented in Chapter 3. One of the evident advantages of this design is the dramatic size reduction in relation to the horn. Here, in order to do a fair comparison, we will consider just the horn alone (discarding the coaxial to waveguide transition), once a feeding network for the patch antenna is out of the scope of this chapter. As detailed in the Chapter 3, the height of the horn is 61.15 mm which is aproximately equivalent to 6.12λ at 20 GHz and 4.08λ at 30 GHz. Regarding the patch antenna, its internal height is 4.5 mm. The 1 mm wall thickness turns its external height to 5.5 mm which corresponds to 0.55λ at 20 GHz and 0.37λ at 30 GHz. Therefore, a reduction of 91% in height was achieved thanks to the new antenna design. Fig. 4.9 aims to demonstrate this difference. Moreover, this figure also helps to point out another difference between both designs: the maximum gain direction. Thanks to the 45°-slant aperture, the horn tilts the beam by 27° at downlink and by 14° at uplink while the patch antenna points always at broadside. Due to its aperture asymmetry, the horn (or part of it) must rotate synchronously with the lens to achieve a full scan in azimuth. This fact increases the complexity of the system and also its cost in comparison to the planar printed feed that remains fixed.
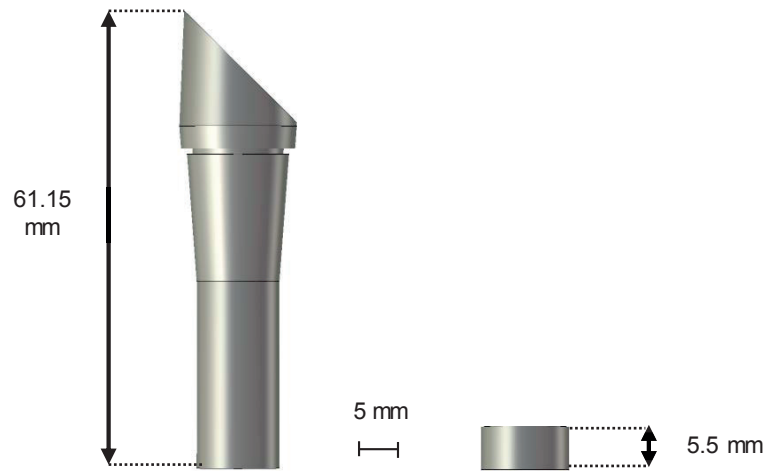
Fig. 4.9 – Size comparison between the horn and patch antennas.

Another important feature is the gain. It is known that horn antennas present, in general, higher gain when compared with planar printed antennas. There is no exception in this case; however this reduction in gain can be seen as the price to pay for the aforementioned great reduction in size. The gain values offered by both feeders for both Ka-bands are detailed in Table 4.I and Table 4.II. Fig. 4.10 aims to illustrate the gain difference.

Table 4.I – Gain comparison: downlink Ka-band.

Downlink Ka-band		
Freq. [GHz]	G_{Horn} [dBi]	G_{Cavity} [dBi]
19.7	9.58	7.53
19.8	9.55	7.58
19.9	9.51	7.62
20	9.48	7.67
20.1	9.45	7.72
20.2	9.43	7.76

Table 4.II – Gain comparison: uplink Ka-band.

Uplink Ka-band		
Freq. [GHz]	G_{Horn} [dBi]	G_{Cavity} [dBi]
29.5	12.43	9.41
29.6	12.43	9.40
29.7	12.43	9.38
29.8	12.43	9.37
29.9	12.45	9.35
30	12.46	9.34
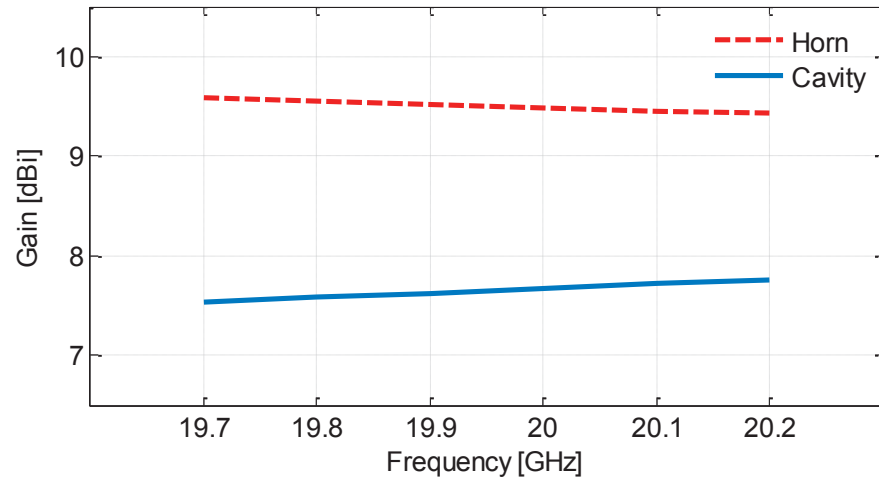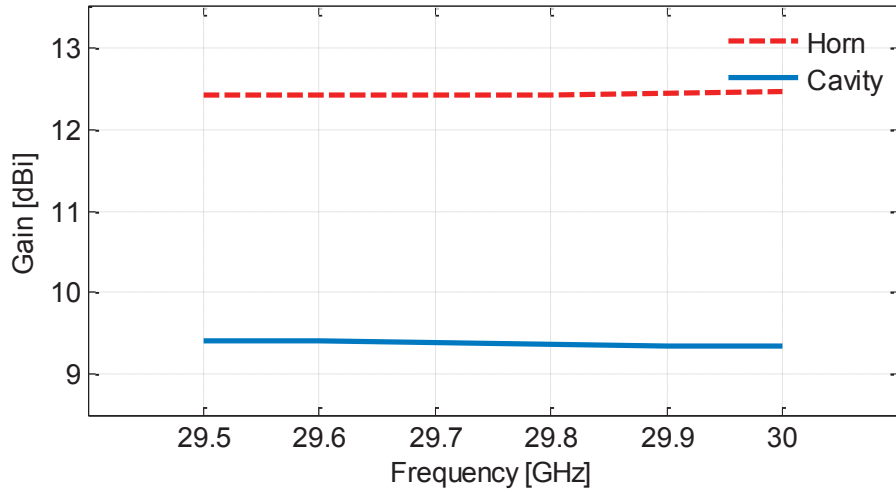
Fig. 4.10 – Gain comparison: (a) at dow nlink; (b) at uplink.

As mentioned in the Introduction, the phase center is an important characteristic to analyze when the antenna is intended to feed a gain enhancement structure. Therefore we decided to compare the phase center stability of both antennas over the desired Ka-bands. The horn antennas are well known to have a very stable phase center which contributes to their choice as feeders and the ridged one here presented is not an exception to this rule. Nevertheless, the proposed patch antenna is even providing a slightly better result in both bands. This comparison is shown in Fig. 4.11. First, we mark with a red circle the place of the phase center of each antenna (see Fig. 4.11a - Fig. 4.11c) and afterwards, we show the corresponding zoom-in picture for downlink (see Fig. 4.11d - Fig. 4.11f) and uplink (see Fig. 4.11g - Fig. 4.11i). Due to the asymmetry in the

horn's aperture, its phase center variation is not just along the z-axis. Thus, this effect is obviously not seen in the patch antenna exactly because it is completely symmetric. For this reason, we are presenting the phase center variation in the XZ and YZ planes for the horn; while for the patch we present only one case once they are equivalent. Please note that the same scale is used in all the zoom-in pictures and it is highlighted in the first one, Fig. 4.11d.

Considering that both antennas have a stable and well-defined phase center, we can say that the trade-off is between the size and the gain. At this point, it is also interesting to compare the feeders when integrated in the lens-based antenna system introduced in the previous chapter. As previously explained, the dielectric lens is intended to increase the directivity and to achieve beam steering. In line with this, it is indispensable to highlight again that each feeder has different maximum gain directions. This difference will have an influence in the scan loss and thus a higher value is expected when combining the patch antenna with the lens.

The full-wave results of the two complete systems have been obtained at 20 GHz and 30 GHz by tilting the lens from 0° to 60° with 10° steps. Since these results for the horn-lens combination were documented in Chapter 3 (see Fig. 3.18), here we just present the ones associated to the planar printed antenna's case (see Fig. 4.12). The radiation patterns show us that the gain is higher at 30 GHz than at 20 GHz, but in both frequencies the shape of the pattern is not being much deformed over the tilt range which demonstrates the solidity of the system.

The gain values offered by each feeder together with the same dielectric lens for both Ka-bands are detailed in Table 4.III and Table 4.IV where the maximum values are marked in bold. As it can be seen, and as it was expected, the maximum gain obtained when the lens is fed by the patch antenna corresponds to the lens tilt angle $\alpha = 0°$ (which is equivalent to say that the gain is maximum at broadside). Regarding the horn's case, the maximum gain of the system is obtained when the lens is tilted by an angle that is close to the maximum gain direction of the horn standalone. Fig. 4.13 aims to illustrate the gain scan loss of both systems at 20 GHz and 30 GHz.
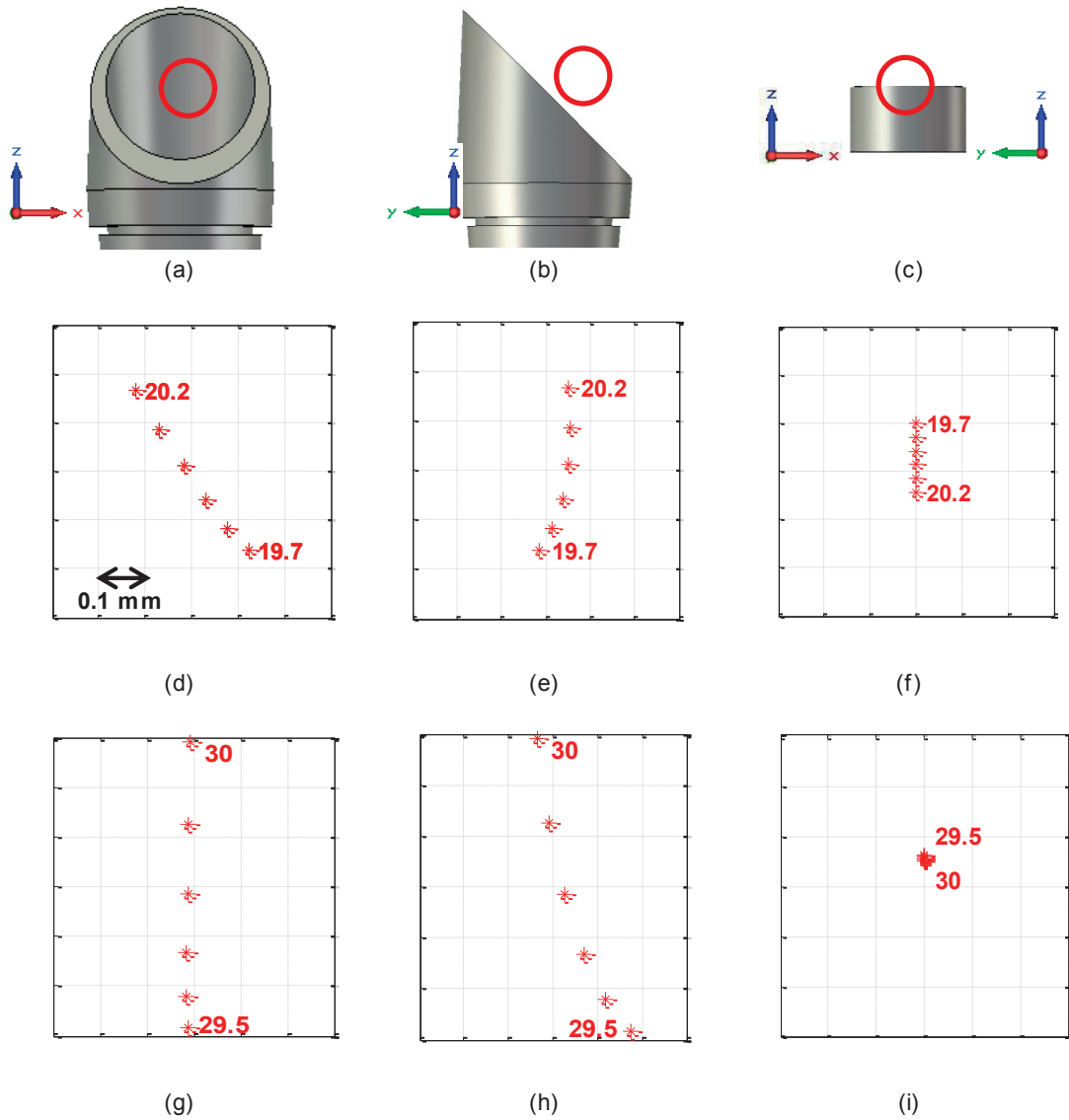
Fig. 4.11 – Phase center comparison. Phase center area: (a) horn, XZ-plane; (b) horn, YZ-plane; (c) patch. Phase center variation at dow nlink: (d) (d) horn, XZ-plane; (e) horn, YZ-plane; (f) patch. Phase center variation at uplink: (g) horn, XZ-plane; (h) horn, YZ-plane; (i) patch. The same scale is used in all the pictures regarding the phase center variation and it is highlighted in (d).
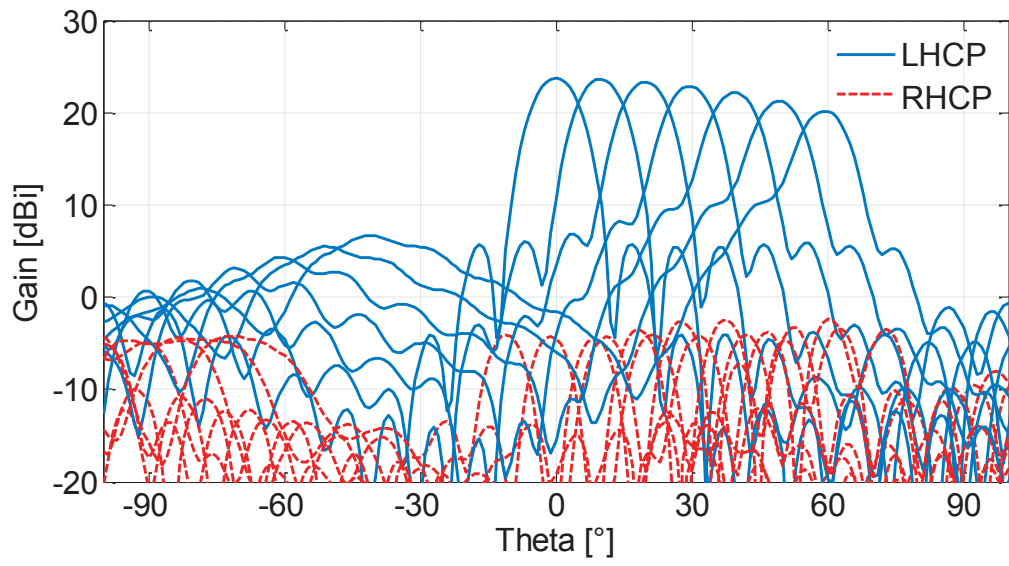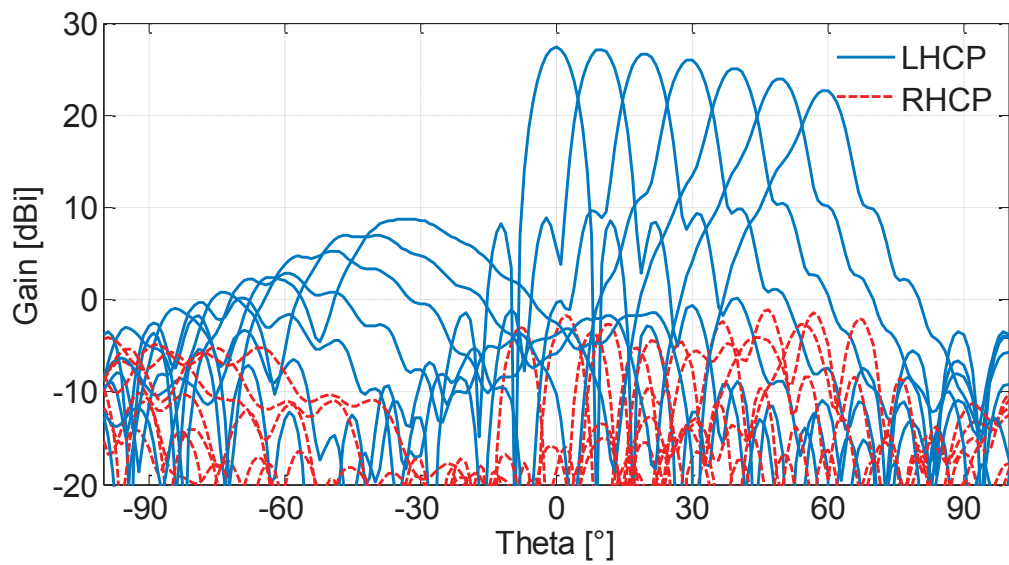
Fig. 4.12 – CP radiation patterns of the antenna system using the patch as feeder: (a) at 20 GHz; (b) at 30 GHz.

Table 4.III – Gain comparison of both lens-based antenna systems at 20 GHz.

20 GHz		
Lens tilt angle, α [°]	$G_{Lens+Horn}$ [dBi]	$G_{Lens+Patch}$ [dBi]
0	22.2	**23.3**
10	22.6	23.2
20	**22.7**	22.8
30	22.6	22.3
40	22.1	21.5
50	21.5	20.5
60	20.7	19.3

Table 4.IV – Gain comparison of both lens-based antenna systems at 30 GHz.

30 GHz		
Lens tilt angle, α [°]	$G_{Lens+Horn}$ [dBi]	$G_{Lens+Patch}$ [dBi]
0	24.1	**26.1**
10	**24.2**	26.0
20	23.9	25.6
30	23.6	24.9
40	23.2	24.2
50	22.2	23.3
60	21.2	22.4
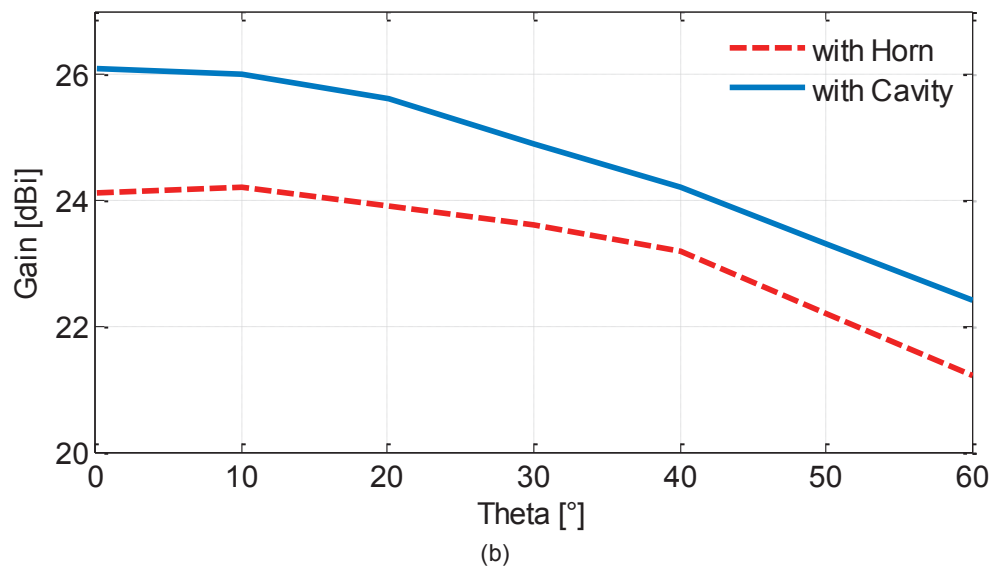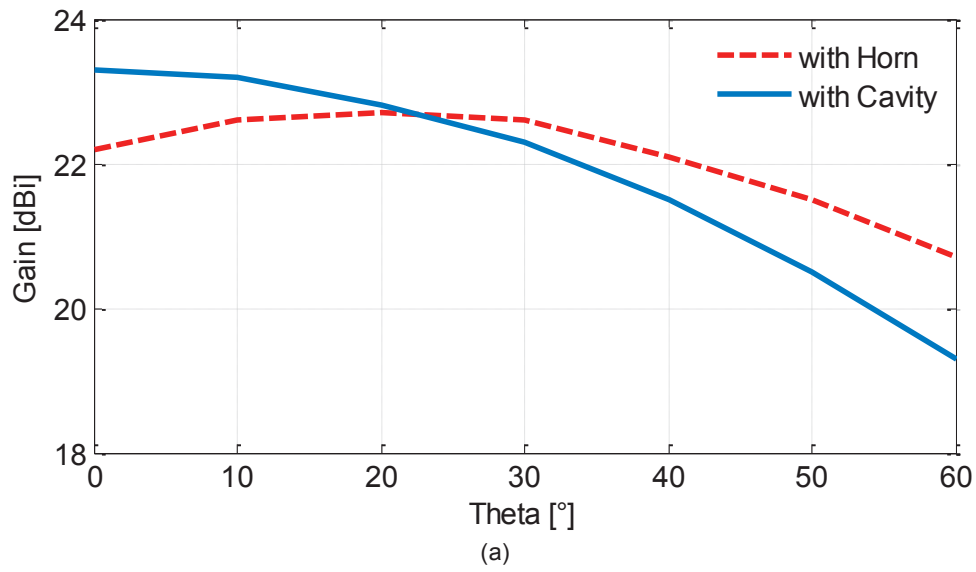
Fig. 4.13 – Scan loss: (a) at 20 GHz; (b) at 30 GHz.

Despite the horn antenna has higher gain than the patch (see Fig. 4.10), the same can not be extended to the lens-based system. By observing Fig. 4.13, it is possible to see that the highest gain is produced by combining the patch antenna with the lens in both bands. On the other hand, this system presents a higher scan loss in the range 0° < α < 60°. However, it is not fair neither rigorous to compare the scan loss of both systems without taking into account the influence of the 45°-slant horn aperture. For instance, at 20 GHz, the maximum gain of the horn-lens system is 22.7 dBi and it is obtained when the lens is tilted by 20° (α = 20°). The lower gain value is 20.7

86

dBi and corresponds to α = 60°. Then, the scan loss in this case is 2 dBi. In order to compare this value to the one produced by the patch-lens system, we should consider the same number of steps in the tilting which in this case are four (20° < α < 60°). Following this idea, at 20 GHz, the scan loss of the patch-lens configuration is 1.8 dBi, being 0° < α < 40° the considered interval. Applying the same strategy at 30 GHz, the scan loss of the horn-lens system is 3 dBi while the equivalent value of the patch-lens system is 2.8 dBi.

At a first glance, the gain results of both lens-based systems can be intriguing. But if we carefully analyze the system conditions, they make sense indeed. First, it is important to reveal that the lens was not optimized for any specific feed, but considering an ideal low-directive point source. Thus, as the patch antenna illuminates a bigger portion of the lens bottom surface, the output is a higher gain. Then, the lower gain produced by the horn-lens system can by justified by narrower beam of the horn (once it is more directive) together with its slanted aperture. However, the slanted horn aperture turns to be an advantage regarding the beam tilting, especially in the extreme positions, because the spill over is lower in this case. And this fact contributes to have a more stable gain over the entire lens scan range. Fig. 4.14 and Fig. 4.15 aim to illustrate this analysis.

It is important to highlight all these differences in order to decide between both systems according to the requirements of the application. The results presented in this chapter show that planar feed antennas are good alternative solutions, especially in cases where compactness are important requirements.

(a)   (b)

Fig. 4.14 – Horn-lens system: (a) α = 0°; (b) α = 60°.

(a)   (b)

Fig. 4.15 – Patch-lens system: (a) α = 0°; (b) α = 60°.

4.5 Combined feed system: planar intermediate lens fed by the patch antenna

The reduction of 91% in height allowed by this feed antenna was already a great achievement. However, it would be very interesting use this antenna together with a planar lens in order to reduce even more the height of the total system. A first step towards this direction is here presented.

In order to discuss this first step, let us briefly introduce the final goal which is to achieve an equivalent planar system. Despite the reduced height, the scanning will be achieved by an in-plane lens translation instead of a tilt and rotational movement which simplifies the system. The first idea of the lens-based planar antenna system is depicted in Fig. 4.16. The main provides the scanning coverage and since we are aiming a high-gain solution, its diameter needs to be quite large. Consequently its focal point will be in a considerable distant from the lens bottom surface (see Fig. 4.16a). This fact can prevent the primary goal of having a smaller antenna system in terms of height. This concept is described in [100] where both lens' designs are explained. Here we will not enter in further explanations of the lens design, since the main focus and contribution of this thesis is the feeder. Our objective here is to re-use the intermediate lens design [100] in order to verify the performance together with the developed feed antenna.
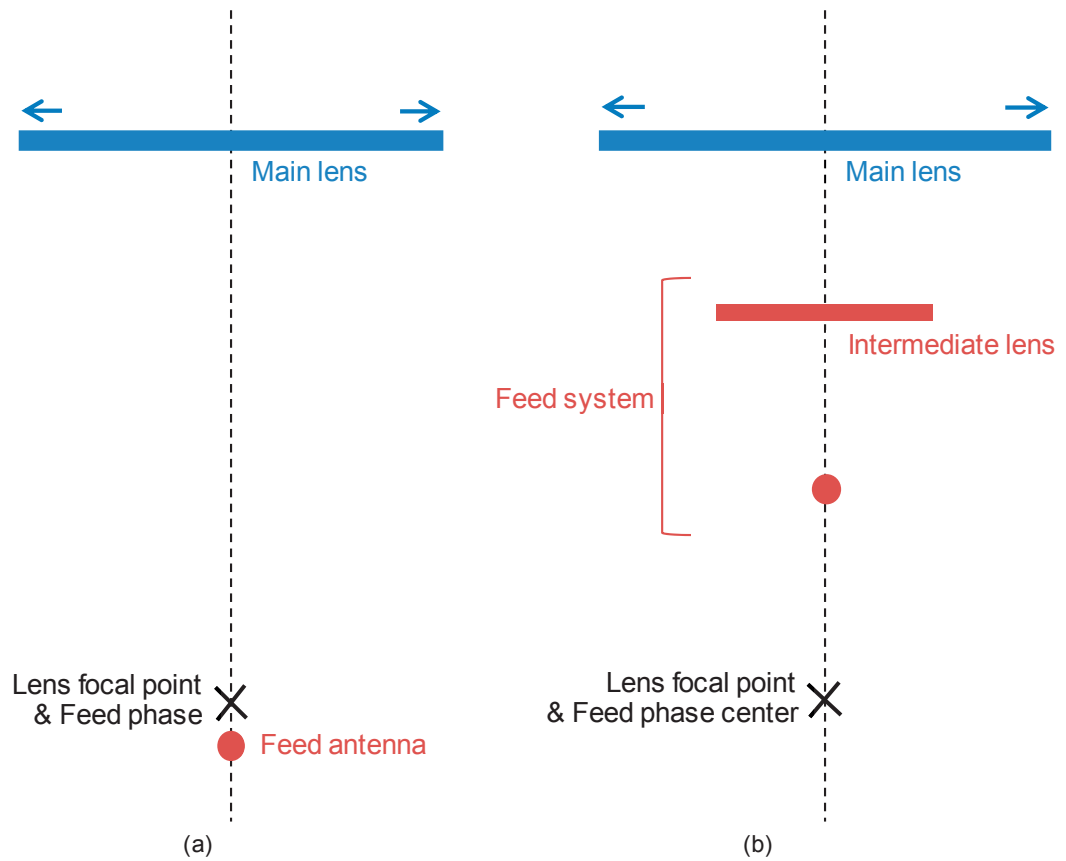
Fig. 4.16 – Planar antenna system: (a) without intermediate lens; (b) with intermediate lens.

In order to avoid this issue, we focus again in the feed side proposing here a combined feed system composed of the aforementioned patch antenna and an intermediate planar lens (see Fig. 4.16b). The intermediate lens is responsible for enhancing the directivity of the feed and also for pushing down (in the z-axis) its phase center position. By playing with the original phase center position, the feed antenna can be placed closer to the main lens reducing the effective total height of the system.

The lens design is out of the scope of this thesis and therefore, thanks to the expertise of IT-Lisbon in this topic, the study analysis could be performed. As mentioned above, further details about the lens are discussed in [100]. Their first approach to design these lenses in order to prove the concept was to target only the higher frequency band and also a lower gain. The phase center of the patch antenna should be placed 20 mm below the bottom surface of the intermediate lens according to the theoretical study of the global system performed by at IT-Lisbon (it corresponds to F_i in Fig. 4.17). Respecting this distance the combined feed should present around 14 dBi of directivity and it should push down the phase center around 20 mm (it corresponds to P_s in Fig. 4.17).

The S_{11} active of both combined feed system and patch antenna standalone are shown in Fig. 4.18. As it is possible to check, the intermediate lens does not deteriorate the good result obtained with the feeder. The CP radiation patterns for the uplink Ka-band are presented in Fig. 4.19. The maximum gain value obtained in the full-wave simulation was 12.34 dBi which is close to the predicted one. The axial ratio results for phi=0 are shown in Fig. 4.20. More results are shown in Table 4.V and it is clear that they are a very good approximation of the theoretical ones. The lower directivity value is 12.35 dBi which means less than 2 dBi from the theoretic target, 14 dBi. The phase center moved down 20.5 mm in the worst case. Note that in Table 4.V the phase center position is related to the original of the referential depicted in Fig. 4.17. Then the z-coordinate corresponds to the following sum, $F_f = F_i + P_s$.
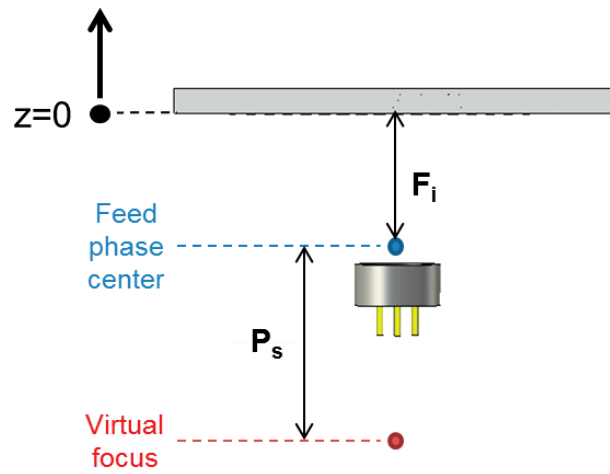
Fig. 4.17 – Combined feed system: intermediate lens fed by a patch antenna.
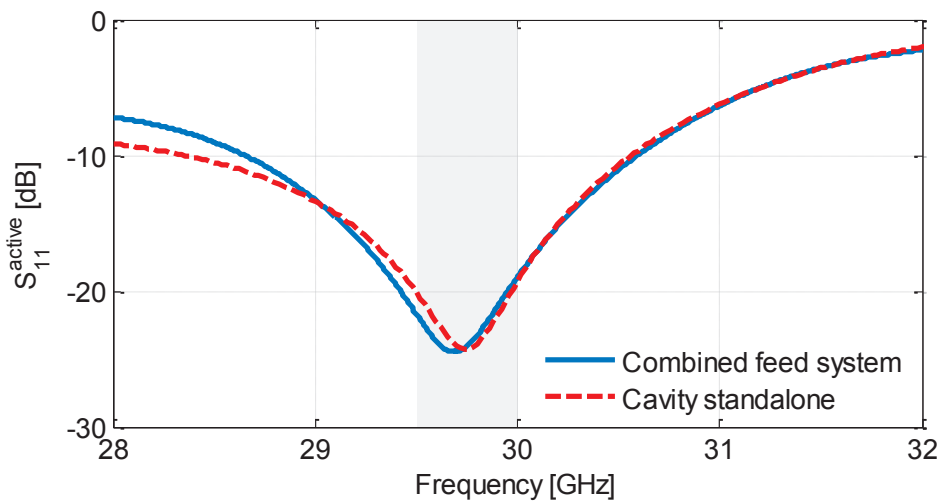
Fig. 4.18 – S11 active of both combined feed system and patch antenna standalone.
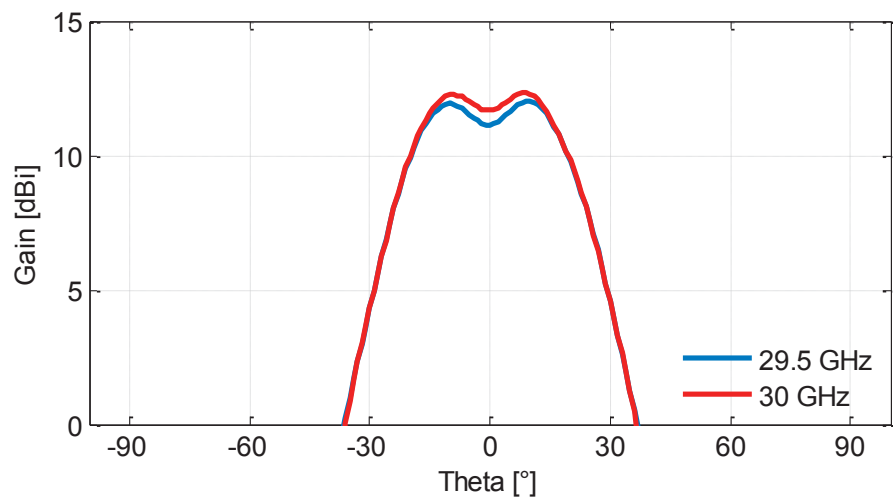
Fig. 4.19 – CP radiation patterns of the combined feed system at uplink Ka-band.
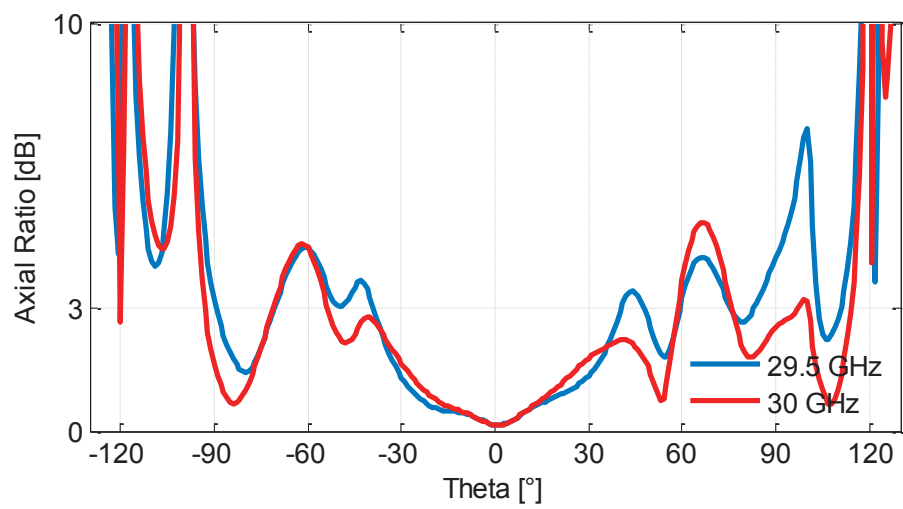
Fig. 4.20 – Axial ratio of the combined feed system.

Table 4.V – Gain comparison: uplink Ka-band.

Uplink Ka-band			
Freq. [GHz]	G [dBi]	D [dB]	Phase Center (X,Y,Z) - Sigma
29.5	12.09	12.35	(0, 0, -40.498) – 1.691
29.6	12.19	12.42	(0, 0, -40.500) – 1.905
29.7	12.23	12.48	(0, 0, -40.534) – 2.097
29.8	12.28	12.53	(0, 0, -40.601) – 2.260
29.9	12.32	12.59	(0, 0, -40.698) – 2.392
30	12.34	12.64	(0, 0, -40.824) – 2.492

The study of this combined feed system aims to push down the phase center as much as possible while keeping the desired directivity. The first test was to move up and down the feed antenna while keeping the same lens as illustrated in Fig. 4.21. For both cases the distance used was λ/4 at 30 GHz. Table 4.VI and Table 4.VII summarize the results for both cases shown in Fig. 4.21a and Fig. 4.21b, respectively.
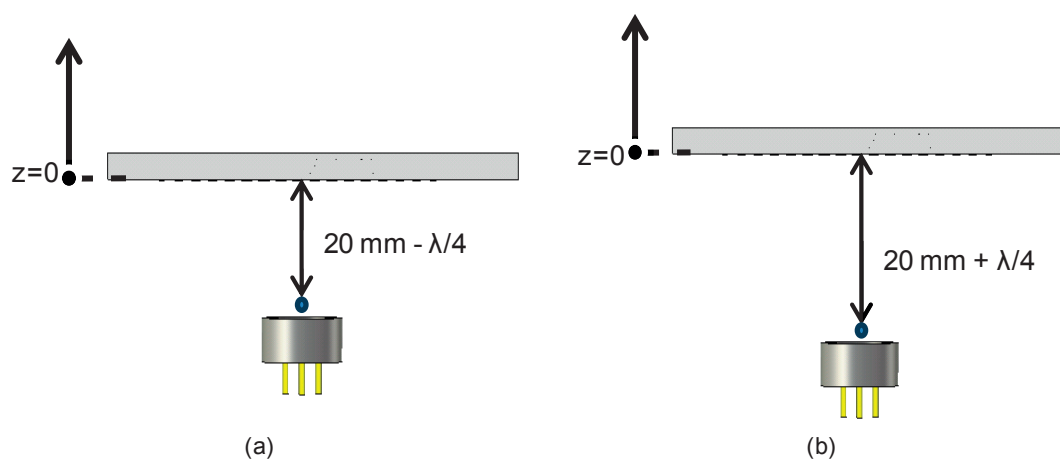
Fig. 4.21 – First test cases: (a) moving up the feed; (b) moving down the feed.

Table 4.VI – Simulated performance indicator values of the combined feed system when the feed was moved up (see Fig. 4.21a).

Uplink Ka-band			
Freq. [GHz]	G [dBi]	D [dB]	Phase Center (X,Y,Z) – Sigma
29.5	11.02	11.36	(0, 0, -30.541) – 4.626
29.6	11.13	11.44	(0, 0, -30.508) – 4.626
29.7	11.24	11.53	(0, 0, -30.493) – 4.619
29.8	11.33	11.61	(0, 0, -30.495) – 4.611
29.9	11.42	11.70	(0, 0, -30.514) – 4.606
30	11.49	11.79	(0, 0, -30.549) – 4.607

Table 4.VII – Simulated performance indicator values of the combined feed system when the feed was moved down (see Fig. 4.21b).

Uplink Ka-band			
Freq. [GHz]	G [dBi]	D [dB]	Phase Center (X,Y,Z) – Sigma
29.5	12.25	12.57	(0, 0, -48.428) – 5.567
29.6	12.35	12.64	(0, 0, -48.266) – 5.379
29.7	12.44	12.72	(0, 0, -48.118) – 5.202
29.8	12.52	12.80	(0, 0, -47.984) – 5.035
29.9	12.59	12.88	(0, 0, -47.866) – 4.875
30	12.66	12.97	(0, 0, -47.765) – 4.721

In order to perform an optimization study of this combined feed system it was developed a script to design the single band intermediate lens according to the following parameters: frequency, size, phase distribution and main lens virtual focus. This study aims to reach a directivity value as near as possible to the desired one, 14 dBi. Several lenses were designed using the script and then several combined feed systems analyzed. The first step was to change the distances previously defined as F_f and F_i, either increasing or decreasing them. The three different cases presented in Fig. 4.22 are summarized in the Table 4.VIII.
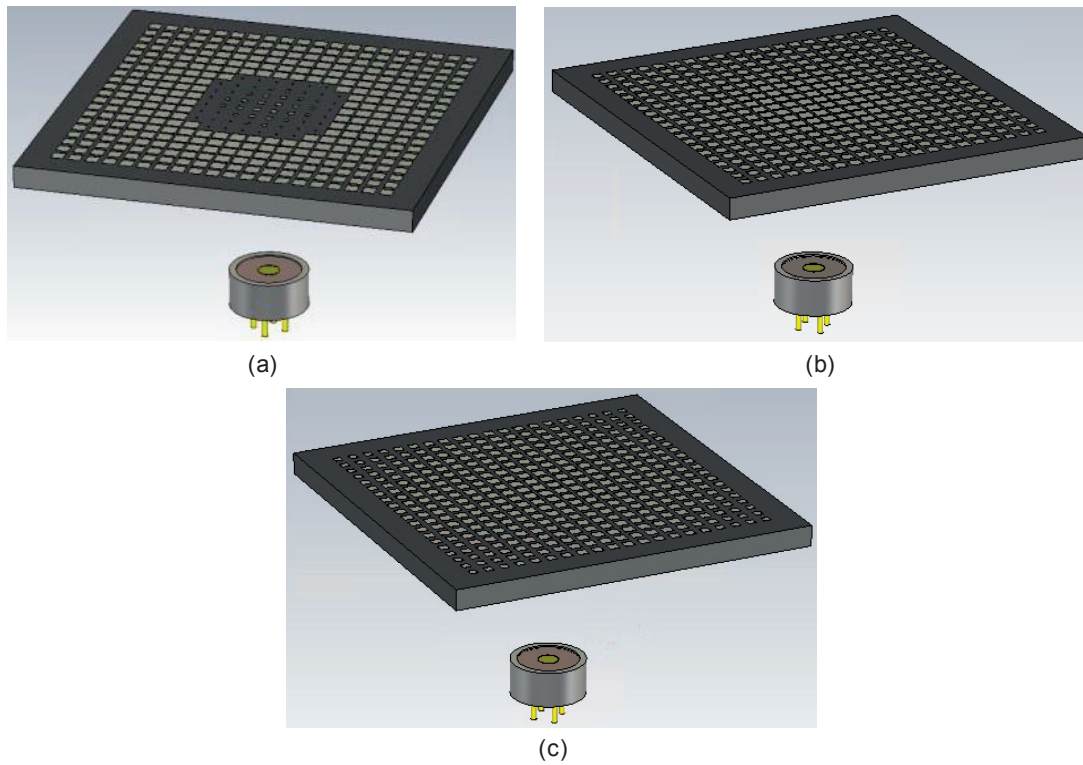
Fig. 4.22 - Three different combined feed systems (different intermediate lens fed by the same feed antenna): (a) case 1; (b) case 2; (c) case 3.

Table 4.VIII – Simulated performance indicator values resulting from the parametric study of the combined feed system at 30 GHz.

Case	Fi [mm]	Ff [mm]	D [dB]	Phase Center (X,Y,Z) - Sigma
1	22	42.5	14.16	(0, 0, -59.6986) – 35.925
2	22	40	14.44	(0, 0, -43.9756) – 12.822
3	24	40	13.89	(0, 0, -41.3594) – 4.778

This study allowed a better understanding about the behavior of the intermediate lens. The lens of the case 1 (Fig. 4.22a) has a visible abrupt discontinuity in the cells distribution that corresponds to a step in the phase. Another characteristic of this specific lens is the fact that the cells closer to the edges are bigger if we compare them with the same cells in the other two cases (Fig. 4.22b and Fig. 4.22c). The study allowed us to conclude that these two characteristics together are not beneficial to get a well-defined phase center. As we can see in Table 4.VIII, the first case shows a really high sigma value. Please note that for the sigma definition we have considered the one of CST Microwave Studio [144] since it was the software used for these

simulations. Considering the second and third cases, we can see that the main difference between both lenses is the cells distribution in the edges. Even if this detail is not influencing as much as the abrupt discontinuity noticed in the first case, it still contributes to have a more well-defined phase center.

The second step of the study was to change the reference phase of the central cell (parameter **h**) while keeping always the same values for F_f and F_i. The starting point was the first case of the previous step (Fig. 4.22a) and the goal was to play with the phase in order to avoid another abrupt discontinuity to support the conclusions taken after the first step. The three different cases presented in Fig. 4.23 are summarized in Table 4.IX.

(a)

(b)

(c)
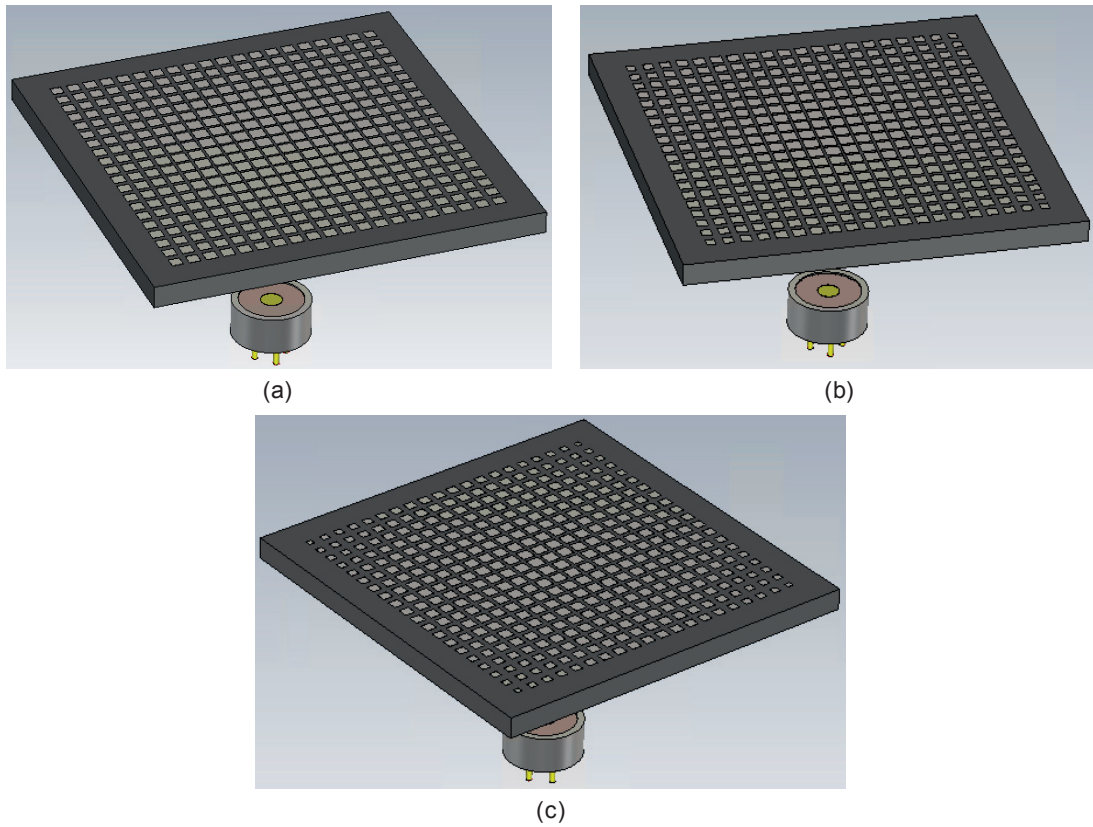
Fig. 4.23 - Three different combined feed systems (different intermediate lens fed by the same feed antenna): (a) case 1A; (b) case 1B; (c) case 1C.

Table 4.IX – Simulated performance indicator values resulting from the parametric study of the combined feed system at 30 GHz.

Case	Fi [mm]	Ff [mm]	h [°]	D [dB]	Phase Center (X,Y,Z) - Sigma
1A	22	42.5	45	14.30	(0, 0, -63.0764) – 23.028
1B	22	42.5	80	14.43	(0, 0, -50.3482) – 15.700
1C	22	42.5	130	14.19	(0, 0, -39.8852) – 4.751

Analyzing the three different lenses and their cells distribution (Fig. 4.23) together with the results shown in Table 4.IX, it is possible to conclude that the cells in the edges are also playing an important role respecting the phase center. The optimized combined feed system (case 1C) has the desired directivity of 14 dBi and the virtual focus moved down 18 mm approximately, which is a very good result according to the theoretical one.

In summa, this study proved the feasibility of a combined feed system composed by a planar feed antenna and a planar lens. The optimized solution (case 1C) has around 30.5 mm of height which corresponds to approximately half-size of the horn antenna (61.15 mm). Moreover, this solution also provides a slight improvement in the gain (in the order of 1.5 dBi). The only drawback in relation to the horn antenna is the fact of being two different devices instead of only one. But if we consider the weight, it should be even lower. Regarding the cost, as this system mainly uses printed elements, we can estimate it will also be lower.

4.6   Prototype discussion

Taking into account all these very satisfactory simulated results, the normal further step was the manufacturing. The patch antennas were fabricated using PCB technology while the cavity and the respective antenna support were made out of brass using a CNC machine. The final prototype is presented in Fig. 4.24. As previously mentioned, the inner diameter of the circular cavity is 9.48 mm which gives us the notion of the remaining dimensions. Thus, it is possible to understand that the prototype is really small and therefore, the accuracy needed to fabricate is high. Moreover, while looking at the back part of the antenna (see Fig. 2.24b), we can see that one of the hardest tasks is to accommodate and solder the four coaxial cables.

The feed antenna was manufactured using the same CNC milling machine as previously used for the horn antenna. In this case, we realized again that this CNC workshop had no possibility of manufacturing such antennas. As aforementioned, at this frequency band and also considering the inner details of both designs, the accuracy is a critical point. The 50 μm precision of the available CNC milling machine proved not to be enough and compatible with such challenges. Therefore, the measured results were not in good agreement with the simulated ones and after analysing the results , we are quite sure that the problem was some displacement in the position of the coaxial cables. Instead of being aside of the lower patch as presented, they should be in
96

contact with it which produces a negative effect in the electromagnetic performance of the antenna.

A possible solution to ease the manufacturing process could be to re-design the antenna in order to have the inner conductors of the coaxial cables in contact with the lower patch. However, in this moment of the thesis, we had two paths on top of the table, following the idea of small adjustments to ease the manufacturing and make a second tentative prototype; or learn with this antenna, profiting from all the conclusions we extract until here and concentrate in the design of a new fully metallic planar antenna. Considering the experience we acquired with this prototype and also with the horn prototypes (described in Chapter 3), and taking into account the CNC available equipment, we have decided that it is worthy to take the second path. The fully metallic planar antenna would allow us to use again the precise SLA technology to fabricate the prototype.. This new antenna is presented in the next chapter.

Nevertheless, taking into account our own experience with CST Microwave Studio [144], there is no reason to doubt about the simulated results and therefore the good performance of the feed antenna presented in this chapter. We believe that a successful prototype depends on using a CNC workshop with higher experience and precision.

(a)
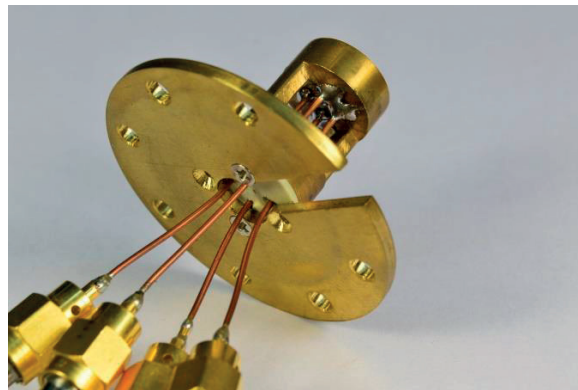
(b)

Fig. 4.24 – Planar antenna prototype: (a) front view ; (b) back view .

4.7 Conclusions

The work presented in this chapter addressed the design of new feeder in the form of a planar printed antenna. This antenna is composed by two circular patches that are placed inside a metallic circular cavity and the excitation is done through four coaxial cables inserted from the back part of the antenna. The motivations behind this feeder were to achieve a more compact design (especially in terms of height) and also to have a device where CP can be directly and physically implemented rather than estimated by numerical post-processing. In order to have the real CP performance, the 90° phase differences should be implemented and this question will be addressed in the next chapter.

While the horn antenna was a broadband design that covered not only the downlink and uplink Ka-bands but also all the intermediate frequencies, the planar printed antenna presented here is a true dual-band antenna. This feature could be of interest if undesirable strong signals are present between the downlink and uplink Ka-bands, since this antenna could filter them out and mitigate interferences.

As expected, the planar antenna gain is lower (approximately 2 dB at downlink and 3 dB at uplink) than the value obtained with the horn antenna previously shown in this thesis; however, this is a reasonable price to pay for a reduction of 91% in terms of height. The other feature analyzed was the phase center and we have arrived to the conclusion that it remains stable in both antennas over the desired frequency bands.

The study has continued with the integration of this planar feed antenna with the lens-based system introduced in Chapter 3. Surprising at first glance, the lower gain of the standalone antenna does not penalize its combination with the lens. But these results are coherent and can be easily explained. Due to its broader radiation pattern (consequence of its lower gain), the patch antenna illuminates a bigger portion of the lens bottom surface. For this reason, this configuration is able to achieve higher gain than the horn-based one. Regarding the scan loss, in the full range ($0° < \alpha < 60°$), results are slightly worse when the patch feeder is used. However, for a fair analysis we need to take into account that the maximum gain directions of both feeders are not the same. By doing that we were able to conclude that both systems present similar responses within equivalent intervals.

A compact feeder would logically call for a more compact focusing device than the 3D lens previously used and the real breakthrough would consist in using both a planar feeder and a planar lens. Following this idea, a preliminary test combining our planar antenna with a planar intermediate lens is presented. These two structures combined would yield a new feeding sub-system that could efficiently illuminate the final planar lens. The new feeder shows a higher gain than the patch antenna standalone (and even slightly higher than the horn's gain), but the height of this new combined feed system remains at half of the height of the horn. This promising solution turned out to be a very good alternative to consider when the size is a strict requirement.

Chapter 5 Ridged cavity-backed slot antenna

Cada nuevo amigo que ganamos en la carrera de la vida nos perfecciona y enriquece más aún por lo que de nosotros mismos nos descubre, que por lo que de él mismo nos da.

Miguel de Unamuno

This chapter refers to the third feed antenna proposed in this thesis. The chapter starts with a brief introduction in order to recall the work performed until this point and to clarify the further motivation and goals. Then, the design is put into context regarding previous research lines. Afterwards, the proposed antenna is introduced as well as its principle of operation. For the sake of completeness, a dedicated BFN is also presented. Finally, the potential of this antenna is shown in the context of a SOTM application. The theoretical predictions are confirmed by corresponding measurements.

5.1   Introduction

The motivation behind the dual patch antenna presented in the previous chapter was a reduction in terms of height, especially when compared with the horn antenna introduced in Chapter 3. This specific goal was achieved while the requirements regarding operation at both desired downlink and uplink Ka bands with CP were also fulfilled. Opposite to the broadband behavior of the horn, the patch antenna has a dual-band behavior and CP is directly achieved thanks to the implementation of a sequential rotation feeding. Still in line with the comparison of both antennas, despite of offering lower gain as a standalone device, the performance of the patch antenna when combined with the lens is satisfactory at broadside; however, the scan loss is higher as it should be expected.

As explained in the previous chapter, a successful prototype of our patch antenna could not be manufactured. This was due to the limitations in the technologies currently available in our laboratories, that prevented a convincing materialization of our design. Therefore, and thanks to the experience acquired in the horn's case, we have decided to concentrate on the design of a new feeder that could be 3D-printed, while retaining most features from our patch antenna design. Hence, we seek for a fully metallic antenna element in order to use the same SLA technology as before.

As mentioned in the Chapter 2, cavity antennas are very interesting solutions that are prone to favor low-profile design, and respect the material's restriction of SLA. Then, this type of antennas, together with the experience acquired with the previous proposed feeders, was the starting point of this chapter, as potential candidates for a monolithic, low-profile and low weight antenna very well suited for SOTM applications. The required CP will be achieved, as before, by using sequential rotation techniques. A dedicated BFN has been designed in collaboration with Dr. Tomislav Debogovic (former LEMA-EPFL currently at Swissto12) in order to provide the proper phase differences required for CP operation. This BFN is based on standard PCB technology and with the sole propose of allowing our new antenna to be measured. The design of a waveguide-based BFN for the same purpose that could be also 3D-printed is very interesting but also very challenging. Therefore, since the focus and main contribution of this thesis is the antenna element, this idea was not addressed here. Indeed the 3D-printed antenna and the associated BFN were successfully manufactured and the measurements were fully satisfying.

In line with the research performed until this point, this chapter also proposes a complete planar antenna system for SOTM, by combining our low-profile feeder with a planar gain enhancement device. The design of this second device (a transmitarray) is out of the scope of this work; however, it was possible to take advantage of parallel research being undertaken in our laboratories to build and test such a system.

5.2   Review on compact antennas

Cavity antennas can be seen as resonators made from a closed waveguide section, where the electric and magnetic energies are stored. These structures are usually hollow or filled with a dielectric material. The fields within the cavity can be excited following different strategies. Here we favor the use of metallic probes, and this should be considered in the overall analysis [150].

Usually, the cavity is combined with a primary or basic antenna (e.g. patch) to enhance its performances, thus obtaining a combined structure that becomes a new improved antenna. For instance, as done in the previous chapter, it is possible to control the undesired excitation of surface waves by placing patch antennas inside a cavity. Another intensively investigated configuration is the cavity-backed slot antenna, where the cavity is beneficial, for example in terms of bandwidth. A basic example of this type of antenna is shown in Fig. 5.1.

Back in the late 1940s, investigation regarding the radiation from slots cut in rectangular wave-guides was carried on [151], [152]. Some years later, studies on rectangular cavity-backed slots have been pursued; however, they can be considered as preliminary since neither the effects of the cavity nor the higher order modes on the field distribution in the slot aperture were taken into account [153], [154]. More complete and deeper analysis of these structures appeared afterwards [155], [156].
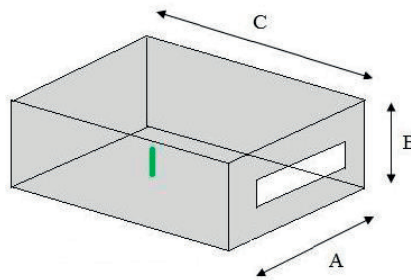
Fig. 5.1 – Basic example of a rectangular cavity-backed slot antenna [151].

In the context of cavity-backed slot antennas, the structure proposed in [84] served here as the starting point to design a fully metallic feeder. As shown in Fig. 5.2a, the antenna consists of a ridged squared cavity with a slot on its top aperture fed by four pins. The goal behind this design was to achieve a hemispherical-coverage antenna for an aircraft application operating in the 240-400 MHz frequency range. The authors explain that the adoption of ridges is responsible to enlarge the bandwidth as shown in Fig. 5.2b.

(a)   (b)
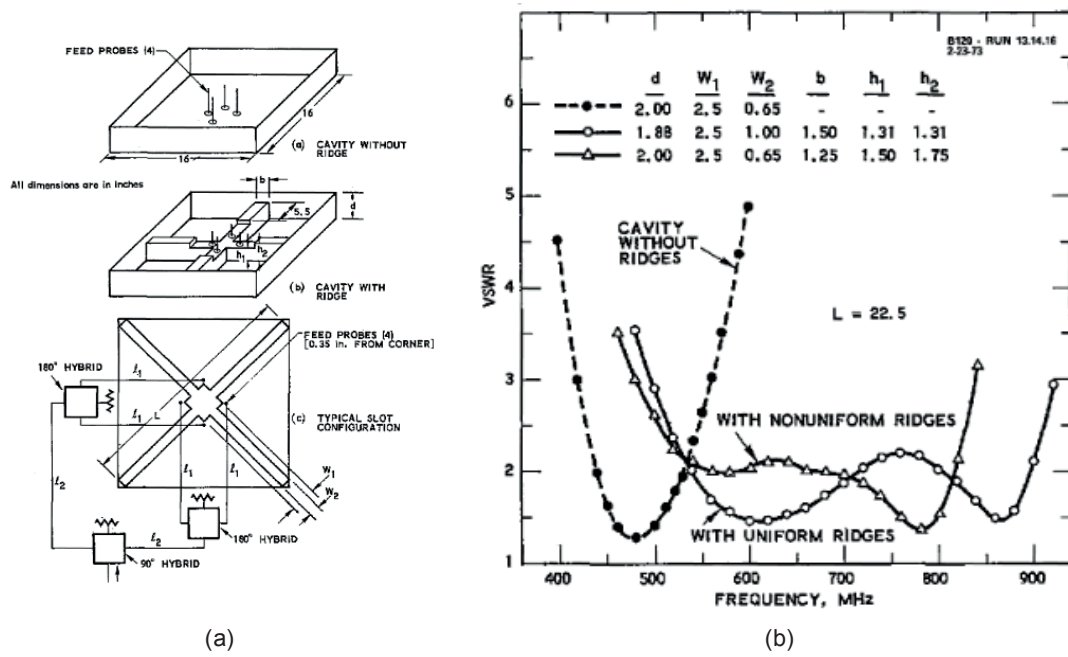
Fig. 5.2 – Squared ridged cavity proposed in [84]: (a) design; (b) voltage standing wave ratio (VSWR) bandwidth with and without ridges.

Here it should be noted that the bandwidth is expressed in terms of VSWR and the target fixed by the authors is VSWR < 2.5:1. By using the classical equivalences,

$$VSWR = \frac{1 + |\Gamma|}{1 - |\Gamma|} \; [\![: 1]\!]$$

$$|\Gamma| = 10^{-\frac{RL\,(dB)}{20}}$$

$$RL = 20 log_{10}\left(\frac{VSWR + 1}{VSWR - 1}\right)$$

it is possible to find the corresponding return loss (RL) value. Table 5.I shows exactly this correspondence and helps to understand that the authors have used a less restrictive requirement than the nowadays commonly accepted RL=10 dB.

102

Table 5.I – VSWR, RL and Γ conversions.

VSWR [[:1]]	RL [dB]	Γ
2.5	7.36	0.428
1.92	10	0.316

The compact fully metallic antenna proposed in [84] is very interesting, but unfortunately, no physical explanations regarding its behavior were given. This design was reconsidered in [157] by LEMA-EPFL for creating a square ridged cavity antenna operating in the DCS and UMTS frequency bands (ranging from 1.702 to 2.434 GHz). The antenna's performances were understood and optimized interpreting the design as two folded dipoles rather than two independent slots. The corresponding prototype and its near-field pattern are shown in Fig. 5.3.

(a)   (b)
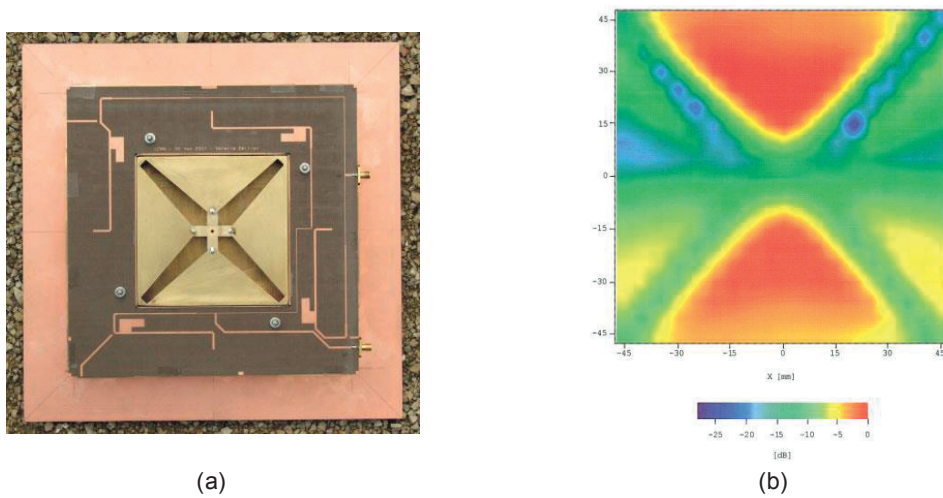
Fig. 5.3 – Squared ridged cavity used in [157]: (a) cavity integrated with other antenna for dual-band operation; (b) near-field of the cavity antenna.

These pioneer designs [84], [157] were indeed the starting point of a deeper research path on cavity-backed slot antennas carried on by LEMA-EPFL. This time the goal was the development of low-profile antennas for Global Navigation Satellite Systems (GNSS) in collaboration with the Swedish company, RUAG Space, in the frame of a project funded by Swiss Space Office [86]. The outcome of this project is shown in Fig. 5.4 and it consists of a **Ri**dged **C**avity-backed **S**lot **A**ntenna called GNSS-RiCSA. The antenna is also fed in sequential rotation through four coaxial cables.
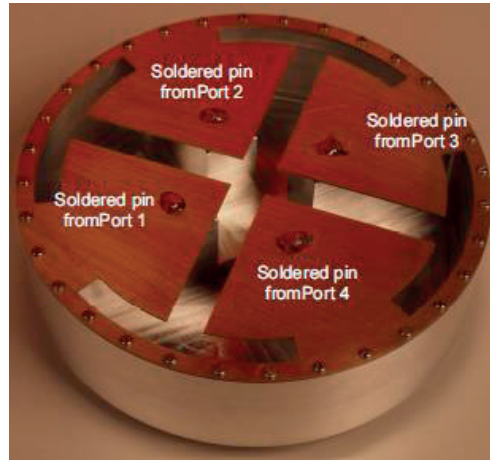
Fig. 5.4 – GNSS-RiCSA [86].

The antenna operation mechanism was in this case explained in terms of resonances in the ridged waveguide, and the corresponding eigenmode analysis. This understanding allowed to optimize the antenna behavior in order to fulfill the project requirements. For instance, the required broadband behavior was achieved by properly tuning two resonances of the cavity. It can be seen in Fig. 5.5 that the active S_{11} is below the threshold of -10 dB from 1.16 GHz to 1.61 GHz. Please note that the active input reflection coefficient is considered here, since this multi-port antenna also exhibits four-fold symmetry and four accesses, like the patch antenna introduced in the previous chapter. In addition to wider bandwidth, this antenna is also more compact than the one presented in [84].

(a)

(b)
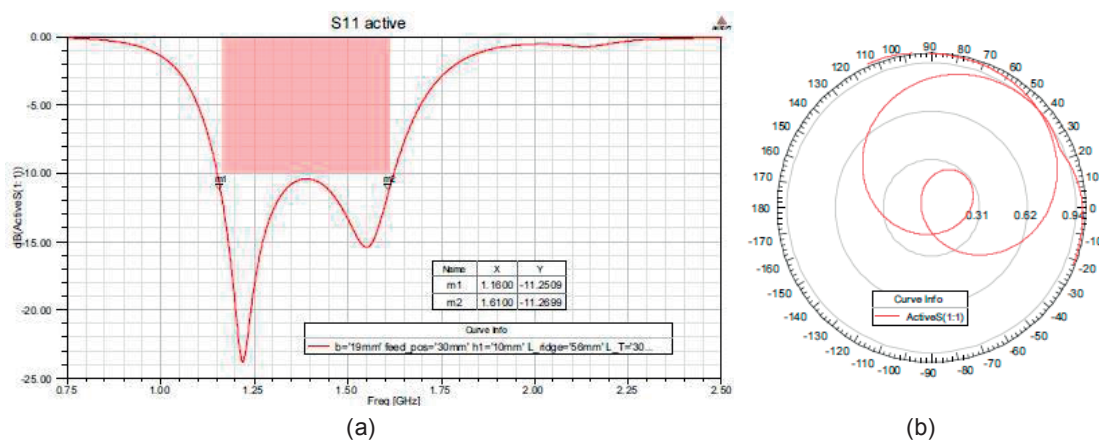
Fig. 5.5 – Broadband behavior by combining two resonances [86]: (a) active S_{11}; (b) polar representation of the active S_{11}.

Both previously discussed antennas are good candidates when aiming a compact fully metallic structure which is the case in this stage of the PhD dissertation. The obvious challenge to be solved is that the scalling to Ka-band will require globally a twenty-fold reduction on the antenna dimensions. This would put the resulting antenna as a great challenge for most current manufacturing techniques. Here, SLA technology will be used by the first time to successfully build such an antenna. Therefore, we will further develop the modal strategy to transform the previous designs and adapt them to the creation of a dual-band device at Ka-band, that will take full advantage from the operation mechanism and correlated benefits of this type of antennas.

5.3   Antenna structure and its principle of operation

The proposed feed in this chapter is again a **Ri**dged **C**avity-backed **S**lot **A**ntenna that we will call Ka-RiCSA from now on. It consists of a metallic cylindrical ridged cavity perforated on its top aperture with a crossed-slot. The final design is presented in Fig. 5.6. The ridges inserted inside the structure allow tuning the resonances of the cavity, and thus attaining the desired dual-band operation. In order to produce CP, as in the antenna described in the previous chapter and also the examples previously shown [84], [86], [157], this antenna is excited in sequential rotation through four coaxial cables that are symmetrically placed near the center of the cavity as depicted in Fig. 5.6. The inner conductor of each cable is then attached to the crossed-slot. Consequently, the signals fed by the coaxial cables have equal magnitude and successive 90° phase differences. Due to this fact, the active input reflection coefficient and impedance must be here considered once all the four ports are excited at the same time in the antenna. In order to divide the power and to provide these phase shifts, a dedicated proof-of-concept BFN has been designed as described in the next section.
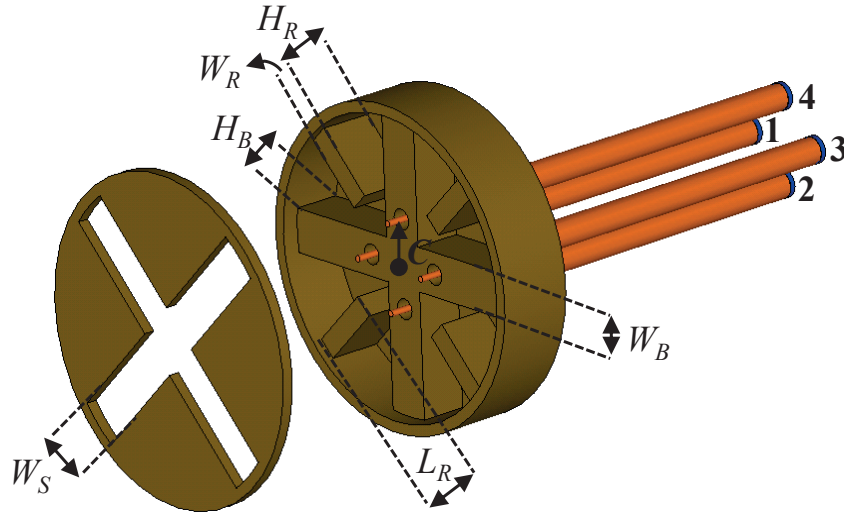
Fig. 5.6 – Ka-RiCSA. Dimensions in *mm*: outer diameter, *D*=14.6 (inner *D*=13.6), outer height, *H*=4 (inner *H*=3), W_B=2, H_B=2.3, W_R=1, H_R=2.8, L_R=3.5, W_S=2.1, *C*=3. Wall thickness is 0.5 mm.

The outer diameter of the antenna is 14.6 mm (which corresponds to 1.46λ at 30 GHz) and the outer height is 4 mm (which means 0.4λ at 30 GHz). These dimensions and also the remaining ones are detailed in the caption of Fig. 5.6. The optimization of these dimensions is carried out aiming at dual-band operation, covering the entire downlink and uplink Ka-bands. The active input reflection coefficient obtained after the optimization is shown in Fig. 5.7, where the achieved −10 dB bandwidth in relation to the middle frequency is 22.8% at downlink and 12.6% at uplink. Furthermore, by observing Fig. 5.7, it is possible to conclude that the antenna is acting almost as a notch filter in the middle of both desired bands, which is an interesting feature.
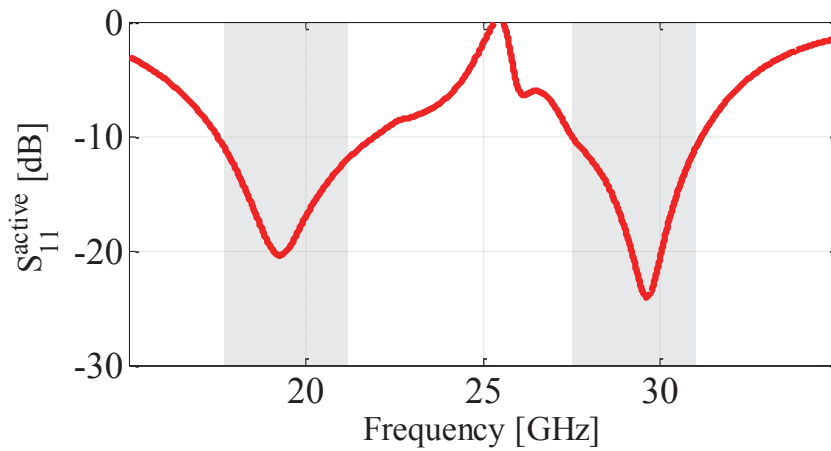
Fig. 5.7 – Active input reflection coefficient of Ka-RiCSA.

The operation of Ka-RiCSA is based in the resonances of the ridged cavity perturbed by the top crossed slot. In order to understand it, we have analyzed the modal solutions that are excited in this complex cavity using a full wave commercial software [161]. Following this approach, we will first start considering the modal solutions of an empty circular cavity with the same height and diameter as the final design shown in Fig. 5.6 (in this case, the inner dimensions). Later, we will progressively include the effect of the feeding pins, the ridges and the interaction of both cavity and slot.

1. Firstly, we analyze the modes of an empty cavity. The five first eigenmodal solutions of an empty circular cavity are illustrated in Table 5.II, they have been obtained using the eigenmodal tool of HFSS [158]. It is possible to see that they correspond to the well-known modal solutions of a circular resonator, the Transverse Magnetic (TM) modes: TM_{100}, TM_{110}, TM_{120}, TM_{200} and TM_{130}. The subscript notation of the modes is the following: radial, azimuthal and longitudinal mode numbers. Note that the first modes to be excited are TM (the electric field is polarized along z), due to the fact that the height of

106

the cavity is smaller than λ/2, and no Transverse Electric (TE) mode will resonate in this cavity if it does not allow variations along z.

Table 5.II – Eigenmode analysis of an empty cavity with same height and diameter of the final design shown in Fig. 5.6.

Mag_E				
Vector_E				
Vector_H				
Frequency and Mode notation				
17.1 GHz TM_{100}	27.3 GHz TM_{110}	36.5 GHz TM_{120}	39.3 GHz TM_{200}	45.4 GHz TM_{130}
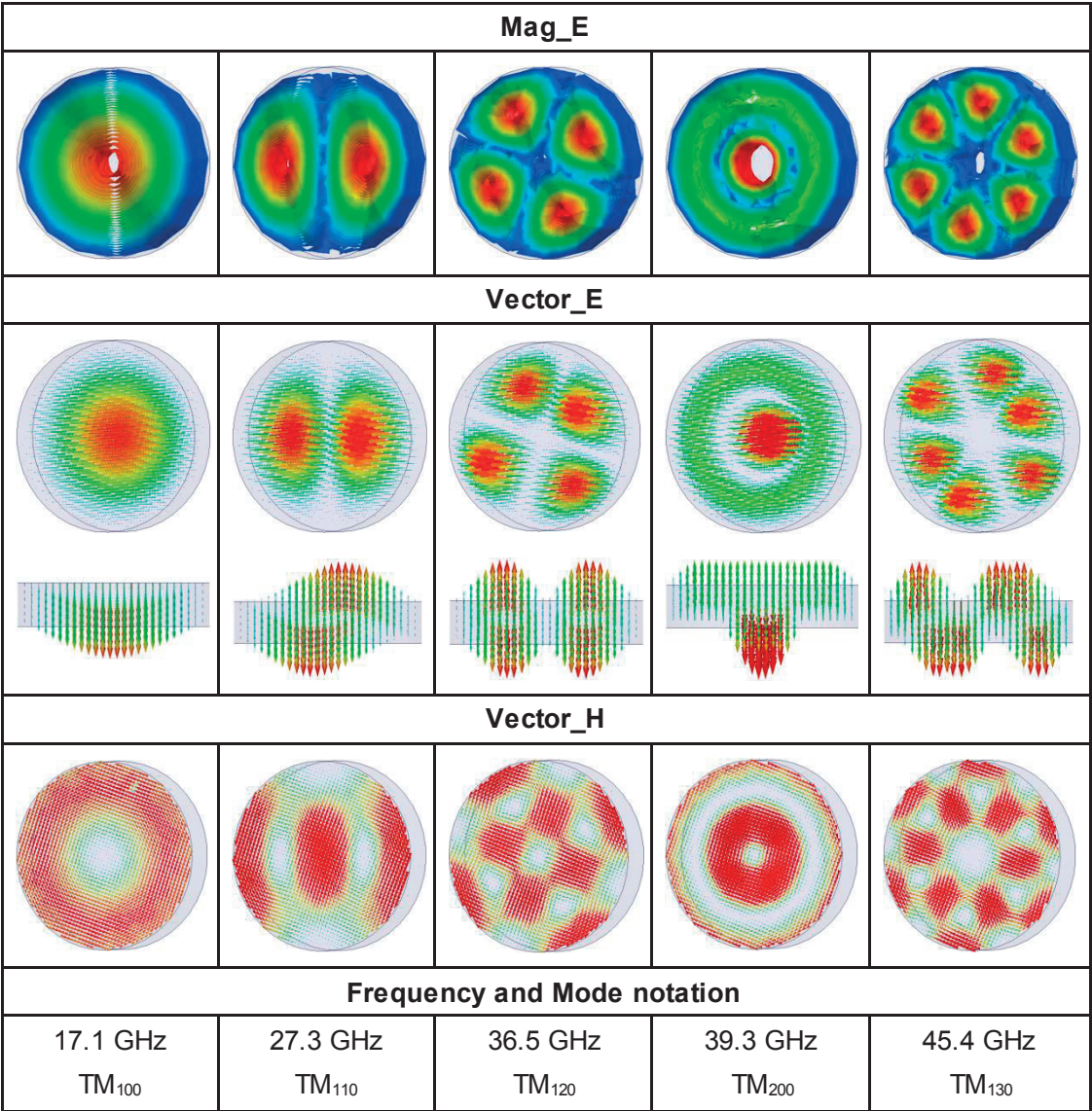
2. Secondly, we consider the effect of the feeding pins. Due to the vertical orientation of these pins, they will couple energy to the TM modes of the cavity naturally, as they

induce an electric field which is parallel to them. It is important to highlight that the sequential excitation of the pins will not allow the excitation of all the modes presented in Table 5.II. The feeding technique used in this antenna can be easily interpreted by the scheme presented in Fig. 5.8. The antenna can be considered as the quadrature combination of the two schemes of Fig. 5.8, that are identical and rotated geometrically 90°. The first scheme has two (blue) pins that have a phase difference of 180° between them, and it produces LP along x. In the second scheme the pair of (green) pins produce LP along y. When combined in quadrature, CP is thus achieved (right or left in function of the sign of the summation).

Thus, for the understanding of the antenna, it is enough to consider the antenna operation under the excitation of two pins with inverse currents. These two pins excite modes in which the electric field is parallel to them, thus TM modes, that respect the boundary conditions (BC) depicted in Fig. 5.9. This means that the modal fields must present at least a phase variation of 180° in half-cavity geometrical move. Therefore, the pins do not excite the modes TM_{100} and TM_{200} (see Table 5.II), since the present no phi-variation.
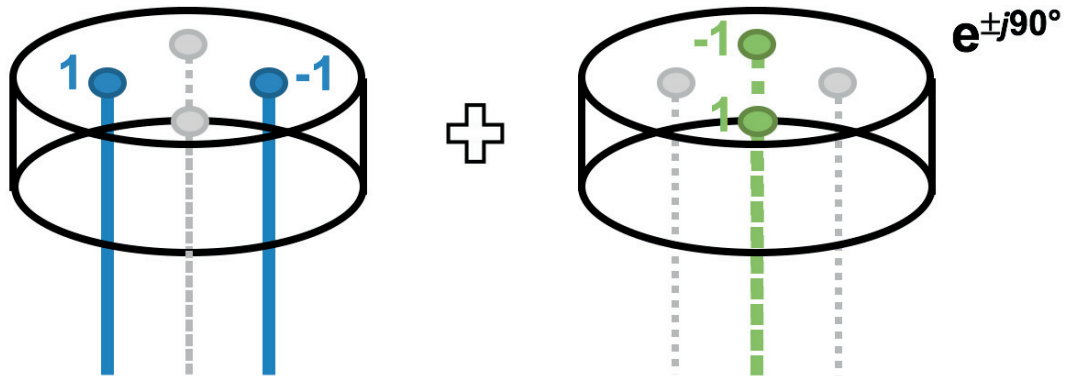
Fig. 5.8 – Sequential rotation feeding o±f Ka-RiCSA. Weight "1" or "-1" refer respectively to ingoing and outgoing currents throught the pins.
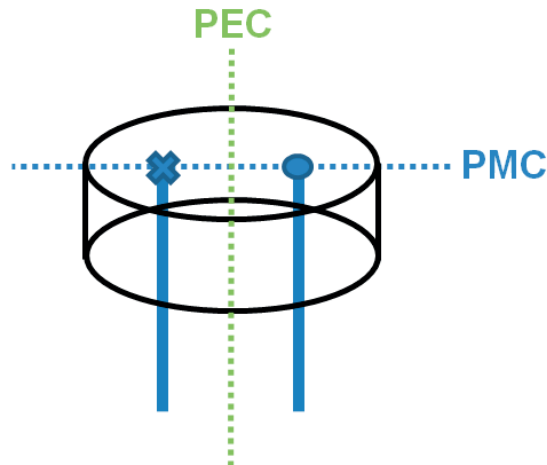
Fig. 5.9 – Simplified scheme of Ka-RiCSA for the modal analysis.

As a result, the modes excited by the pins in our circular cavity (that respect the previous BC) are shown in Table 5.III. Here, the vector of the electric field is represented by a circle (when its direction is towards the paper) and by a cross (when it points to the reader). The light red lobes aim to represent the azimuthal variations of the modes. The BC are coherent with the ones depicted in Fig. 5.9.

Table 5.III – Eigenmode analysis of the empty cavity respecting the BC shown in Fig. 5.9.

TM_{110} f = 27.3 GHz	TM_{120} f = 36.5 GHz	TM_{130} f = 45.4 GHz

3. Next we will include and understand the effect of the ridges. The starting point is the adoption of only four ridges (marked in black in Fig. 5.10). Three different examples are

documented in Table 5.IV and also compared with the corresponding results of the empty cavity. The ridges perturb the modes previously analyzed in the empty cavity but they still preserve the same phi, rho and z variations. Therefore, we have named the perturbed modes in the ridged cavity according to the following: Mode A ~ TM_{110}, Mode B ~ TM_{120} and Mode C ~ TM_{130}. This notation is used in Table 5.IV where it is visible that both the height and the length of the ridges have a significant influence in the resonance of the first mode (Mode A), shifting it from 27.3 GHz to 20.3 GHz. In other words, the resonance of Mode A can be tuned by appropriately selecting the dimensions of the four ridges.

The next analysis concerns the cavity with eight ridges (by adding the ones marked in red in Fig. 5.10) instead of only four. This time, two examples are shown in Table 5.V and they are compared with the last example shown in Table 5.IV (last column: L_B = 4.53 mm, H_B = 2.3 mm and W_B = 2 mm). Please note that for the two 8R-examples presented, the size of the black ridges was kept as the 4R-example shown in the same table. Again we verify that both the height and the length of these ridges allow to tune the resonances of Mode B (from 40.4 GHz to 25.8 GHz) and Mode C (from 42 GHz to 26.7 GHz).

Thanks to this eigenmodal analysis, we are able to understand the influence of the ridges and their corresponding geometry, which is extremely helpful for a good starting point of a later full-wave optimization. In fact, the optimization carried on is successfully made thanks to a parallel analysis between both eigenmode and full-wave solutions. The outcome of this combined optimization results in the antenna previously shown in Fig. 5.6 that presents a dual-band behavior covering the entire downlink and uplink Ka bands as shown in Fig. 5.7. For the sake of completeness and aiming to explain the notch behavior at 25 GHz we present the modal analysis of both final cavity and final slot in, respectively, Table 5.VI and Table 5.VII. In the slot analysis, we use the same BC depicted in Fig. 5.9.

(a)   (b)
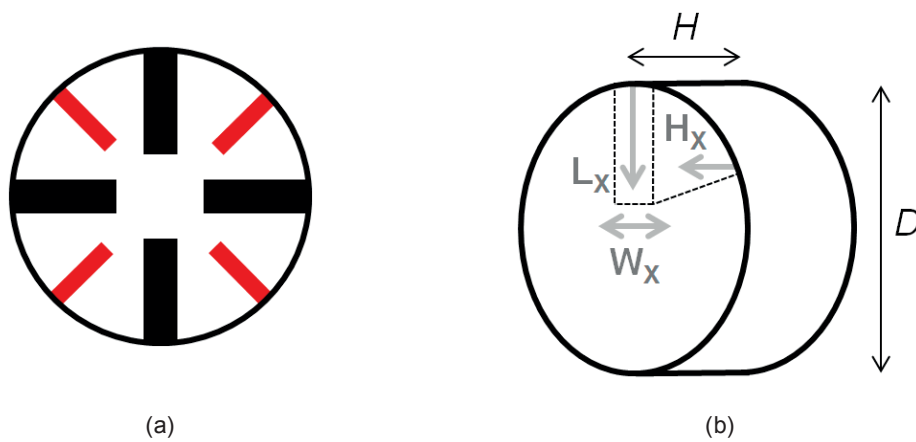
Fig. 5.10 – Ridged cavity: (a) first approach counts only on black ridges (4R configuration) and second approach counts on both black and red ridges (8R configuration); (b) notation for the dimensions of the ridges: L_X = length, H_X = height and W_X = width. Cavity inner dimensions: D = 13.6 mm; H = 3 mm

Table 5.Ⅳ – Eigenmode analysis of the 4R configuration.

EMPTY CAV.	4R configuration		
	L_B = 2.27 mm (D/6) H_B = 1.15 mm (H/2.6) W_B = 2 mm	L_B = 4.53 mm (D/3) H_B = 1.15 mm (H/2.6) W_B = 2 mm	L_B = 4.53 mm (D/3) H_B = 2.3 mm (H/1.3) W_B = 2 mm
TM_{110}			
27.3 GHz	~ f_A = 27.2 GHz	↓ f_A = 24.8 GHz	↓ f_A = 20.3 GHz
TM_{120}			
36.5 GHz	~ f_B = 36.9 GHz	↑ f_B = 37.8 GHz	↑ f_B = 40.4 GHz
TM_{130}			
45.4 GHz	↓ f_C = 42.1 GHz	↓ f_C = 43.1 GHz	↓ f_C = 42 GHz

Table 5.V – Eigenmode analysis of the 8R configuration.
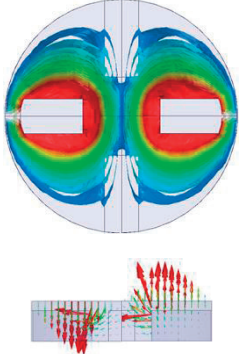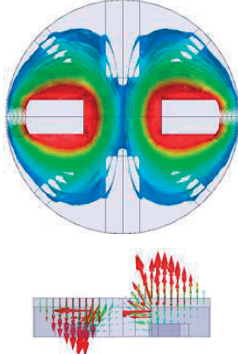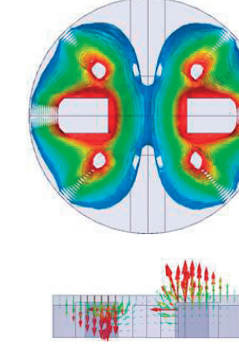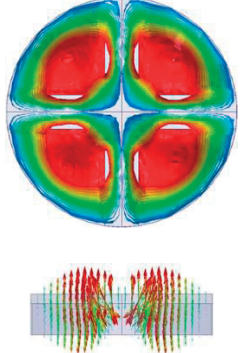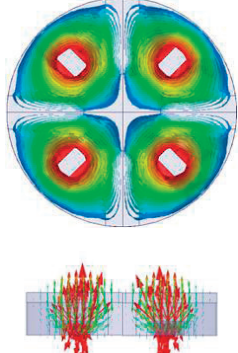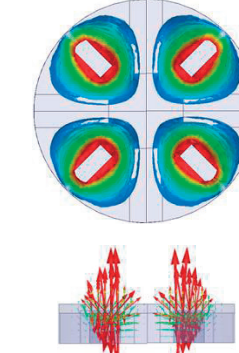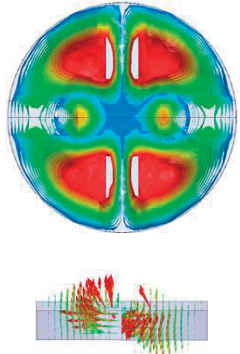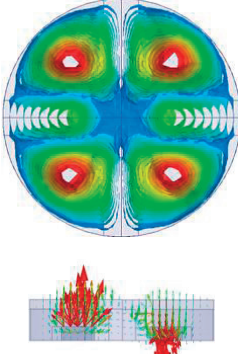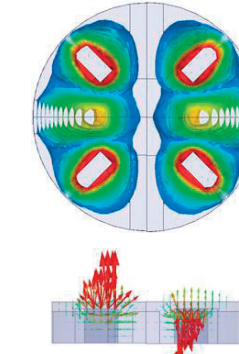
EMPTY CAV.	4R configuration	8R configuration	
	L_B = 4.53 mm (D/3) H_B = 2.3 mm (H/1.3) W_B = 2 mm	L_R = 3.4 mm (D/4) H_R = 1 mm (H/3) W_R = 1 mm	L_R = 3.4 mm (D/4) H_R = 2.5 mm (H/1.2) W_R = 1 mm
TM_{110}			
27.3 GHz	f_A = 20.3 GHz	~ f_A = 20.4 GHz	~ f_A = 20.7 GHz
TM_{120}			
36.5 GHz	f_B = 40.4 GHz	↓ f_B = 37 GHz	↓ f_B = 25.8 GHz
TM_{130}			
45.4 GHz	f_C = 42 GHz	↓ f_C = 38.2 GHz	↓ f_C = 26.7 GHz
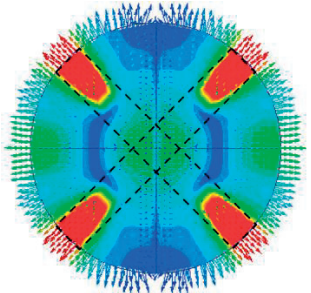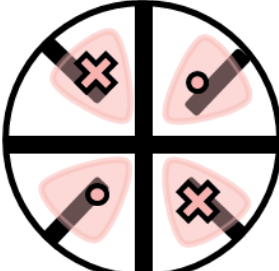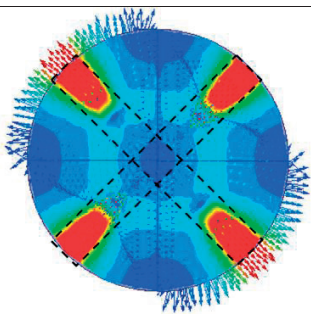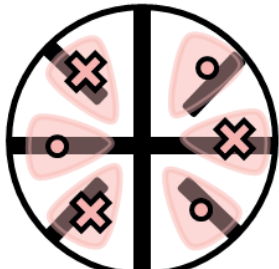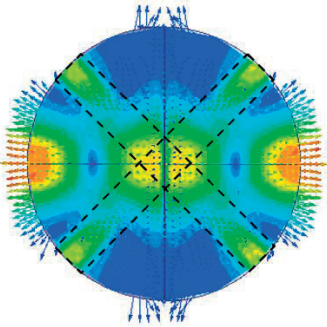
Table 5.VI – Eigenmode analysis of final cavity (D = 13.6 mm, H = 3 mm, L_B = 6.8 mm, H_B = 2.3 mm, W_B = 2 mm, L_R = 3.5 mm, H_R = 2.8 mm, W_R = 1 mm).

MODE A ($\sim$TM$_{110}$) – f_A = 22.7 GHz		
Mag_E	Vector_E	Vector_H
MODE B ($\sim$TM$_{120}$) – f_B = 23.4 GHz		
Mag_E	Vector_E	Vector_H
MODE C ($\sim$TM$_{130}$) – f_C = 27.4 GHz		
Mag_E	Vector_E	Vector_H
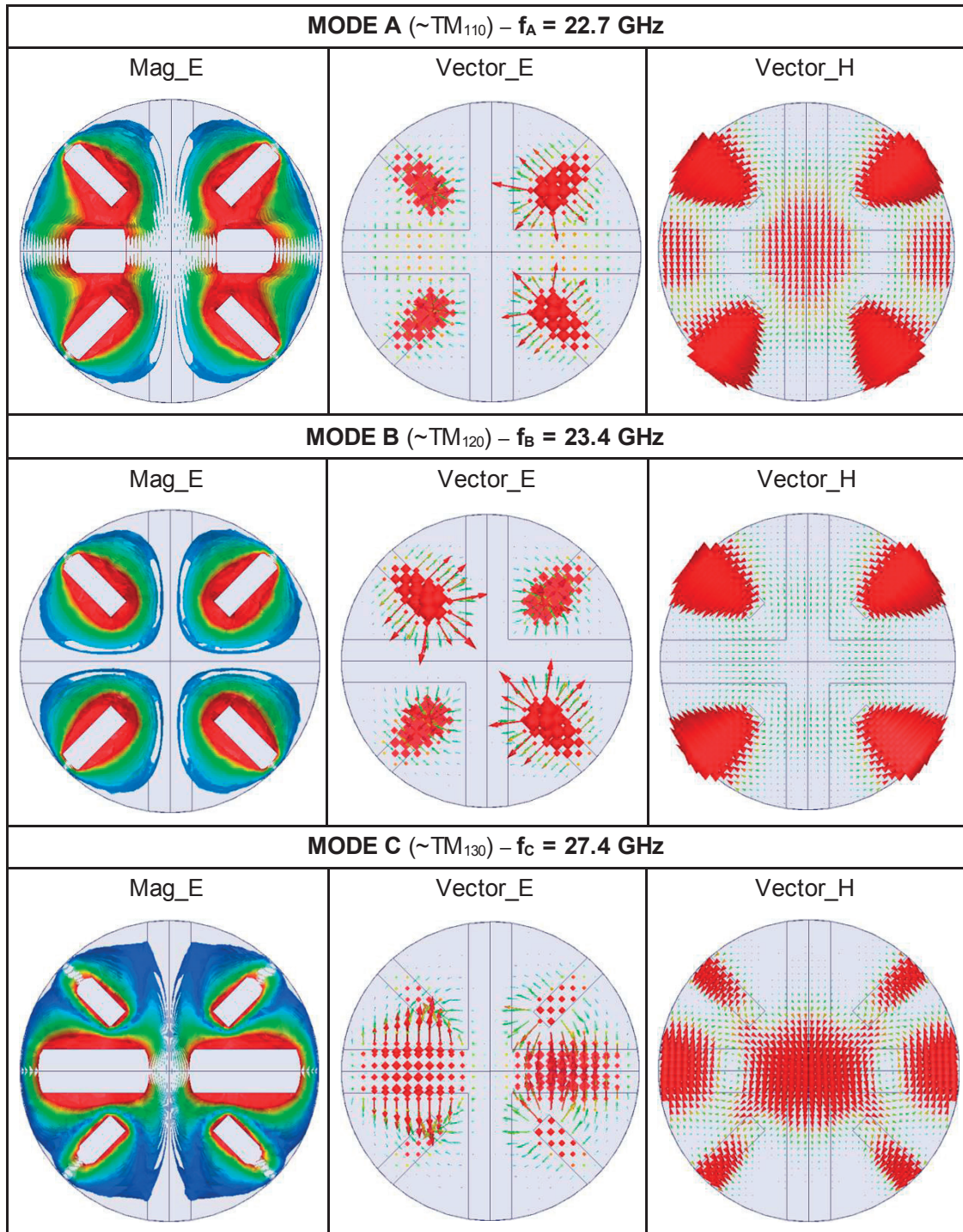
4. Finally, we consider the effect of the radiating crossed-slot. This slot interacts with the currents induced by each of the modes in the top of the cavity. The antenna radiates when the currents are exciting the slot (being perpendicular to it). Table 5.VII shows the currents induced in the top pf the cavity by the three modes. As we can see in the third column, both Mode A and Mode C interact with the slot, as there is some current perpendicular to it excited in the center of the cavity. The two Ka bands are thus allocated to these two pass-band resonances. However, Mode B excites currents that are always parallel to the crossed-slot, and therefore they do not interact with it. This singularity behaves as a notch in our antenna, since when Mode B is excited, it reflects all the energy back to the source.

Table 5.VII – Summary of the modal analysis of Ka-RiCSA.

	Ridged cavity	Surface electric currents induced on the top
1st resonance, downlink Ka (pass-band)	f_A = 22.7 GHz	
2nd resonance (notch)	f_B = 23.4 GHz	
3rd resonance, uplink Ka (pass-band)	f_C = 27.4 GHz	

So, in summary, the ridges in our antenna allow us to tune the two radiative pass bands and the notch. In the next figure we can see an example of how it is possible to shift the notch by changing the parameter Hr.
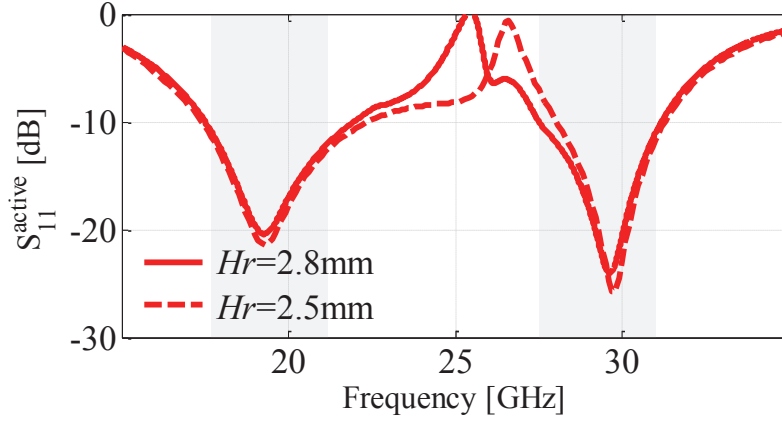
Fig. 5.11 – Example of the tuning of the notch.

5.4 Dedicated beam-forming network

For the sake of completeness and with the sole propose of allowing our new antenna to be measured, a dedicated BFN was designed in collaboration with Dr. Tomislav Debogovic (former LEMA-EPFL currently at Swissto12) to provide this antenna with the aforementioned required phase differences. The scheme of the complete antenna system is shown in Fig. 5.12. The proposed 2-ports BFN comprises two microstrip circuits, where each one is linked to a different frequency. Both are depicted in Fig. 5.13a and Fig. 5.13b. These circuits share the same ground plane, an aluminum plate, as presented in Fig. 5.13c. As it can be seen, the first part of both circuits consists of a series of well-known building blocks such as quadrature and rat-race hybrids. The four outputs generated by this first part in both sides of the BFN correspond to the phase arrangement needed by the sequential rotation feeding. Then, a combination between the signals coming from both circuits is needed in order to feed the 4-ports of the antenna for both frequency bands. In order to combine the signals, diplexers were designed on each circuit. Two signals of the downlink side of the BFN pass to the uplink side and vice-versa through the insertion of pins in holes in the aluminum plate. The diameter of the holes and pins ensures 50Ω characteristic impedance. This second part of the circuits is highlighted in both Fig. 5.13a and Fig. 5.13b by a dashed border white line. In this way it is possible to provide Right Hand Circular Polarization (RHCP) in downlink (0°, 270°, 180°, 90°) and Left Hand Circular Polarization (LHCP) in uplink (0°, 90°, 180°, 270°) to the antenna. The circuits were optimized through full wave simulations [161].

For the sake of completeness an explanatory block diagram of the proposed BFN is presented in Fig. 5.14 where the rat-race hybrids are represented by the π block, the quadrature hybrids by the π/2 block and finally the diplexers by the *D* block.
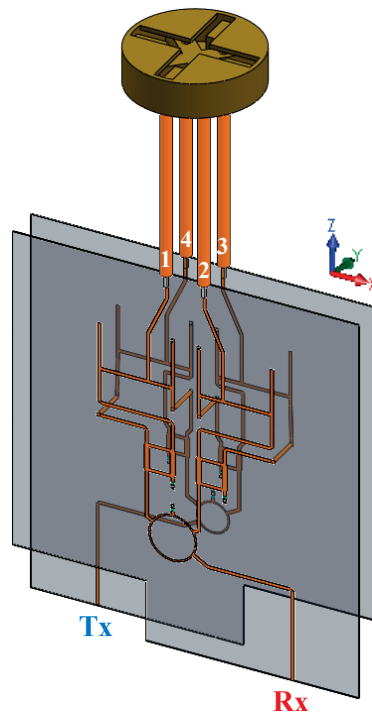
Fig. 5.12 – Complete antenna system: Ka-RiCSA and its dedicated BFN (the aluminum plate between both circuits is not shown here for the sake of simplicity).
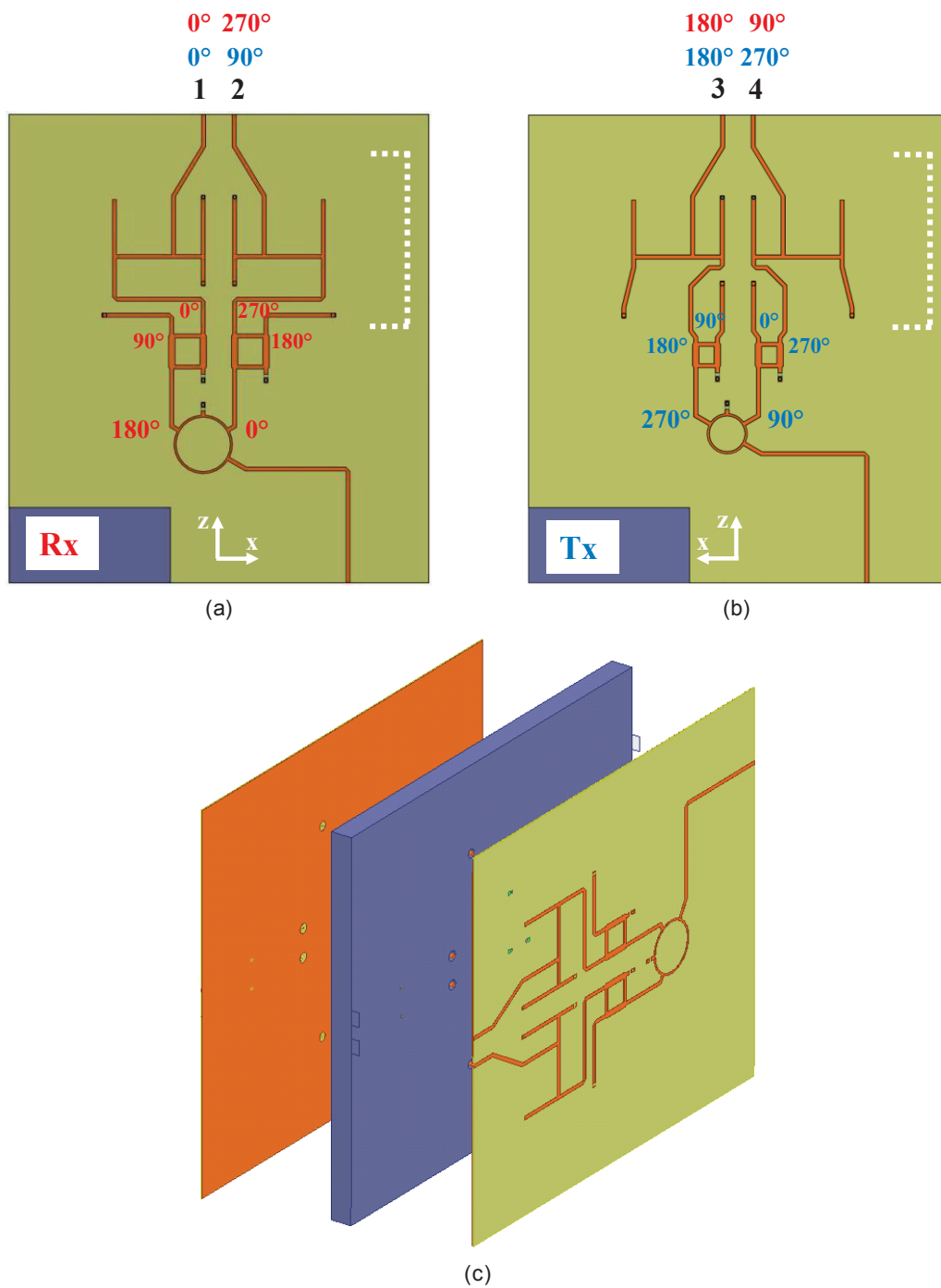
Fig. 5.13 – BFN circuits with phases at different stages included: (a) RX side; (b) Tx side; (c) two circuits sharing the same ground plane.
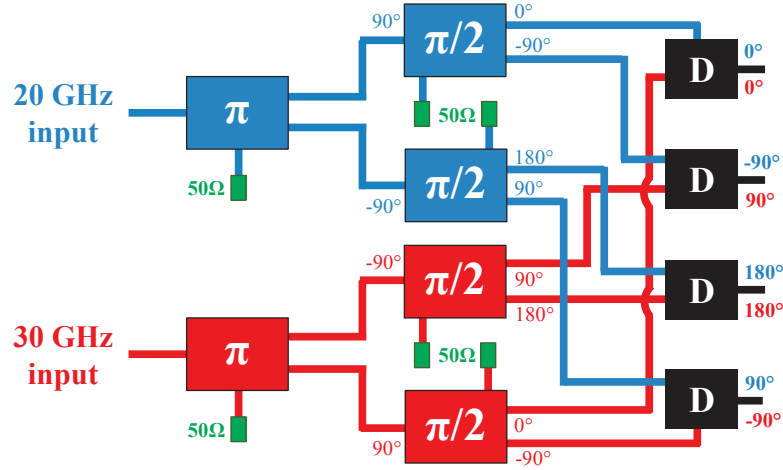
Fig. 5.14 – Explanatory block diagram of the BFN (π block is the rat-race hybrid, $\pi/2$ block is the quadrature hybrid and D block is the diplexer).

The radiation produced by the antenna at both 20 GHz and 30 GHz is represented in Fig. 5.15 and Fig. 5.16, respectively. These pictures were indeed animations made to clearly depict the different paths of the signal while feeding the antenna with either Rx or Tx ports. Therefore, they are here plotted purely as a complement to the previous detailed analysis with the aim of illustrating the operation of the complete antenna system. The comparison of simulated and measured results are presented ahead in this document. However, we can already extract some information and as it can be observed from Fig. 5.15a and Fig. 5.15b, a cardioid RHCP pattern is generated at 20GHz (frequency sample at downlink) when Rx-port is active. Analogously, Fig. 5.16a and Fig. 5.16b show that LHCP is produced at 30GHz (frequency sample at uplink) when Tx-port is active. Moreover, both bands are very well isolated, as shown in Fig. 5.15c and Fig. 5.16c. Please note that all the pictures have the same dynamic range.
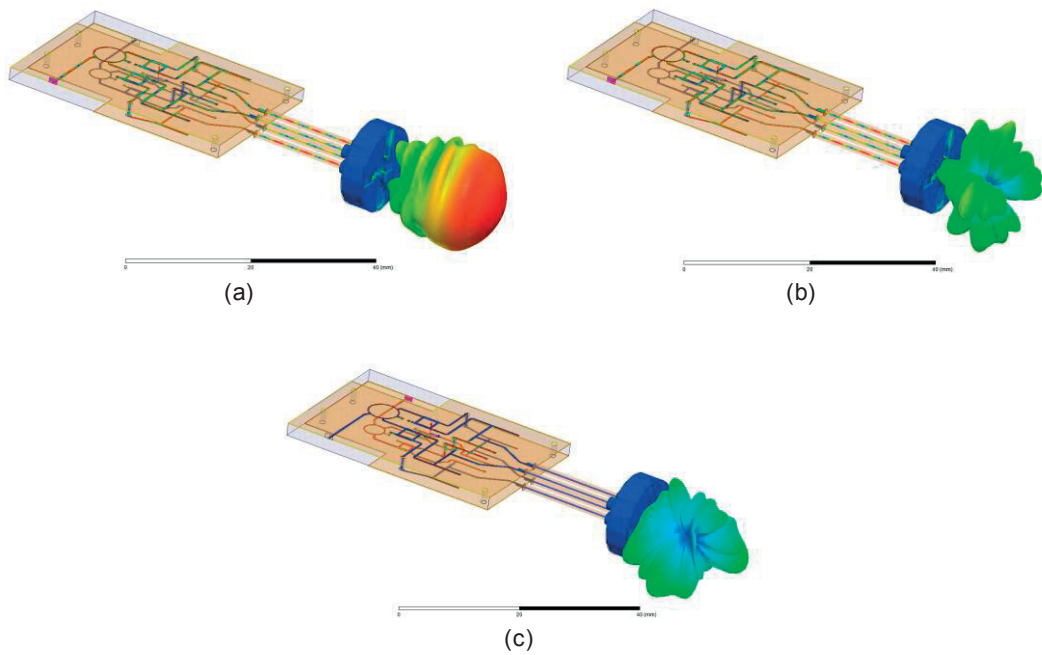
Fig. 5.15 - Radiation at 20 GHz (Rx-band): (a) RHCP (co-pol) w hen feeding Rx port; (b) LHCP (cross-pol) w hen feeding Rx port; (c) total field w hen feeding Tx port.
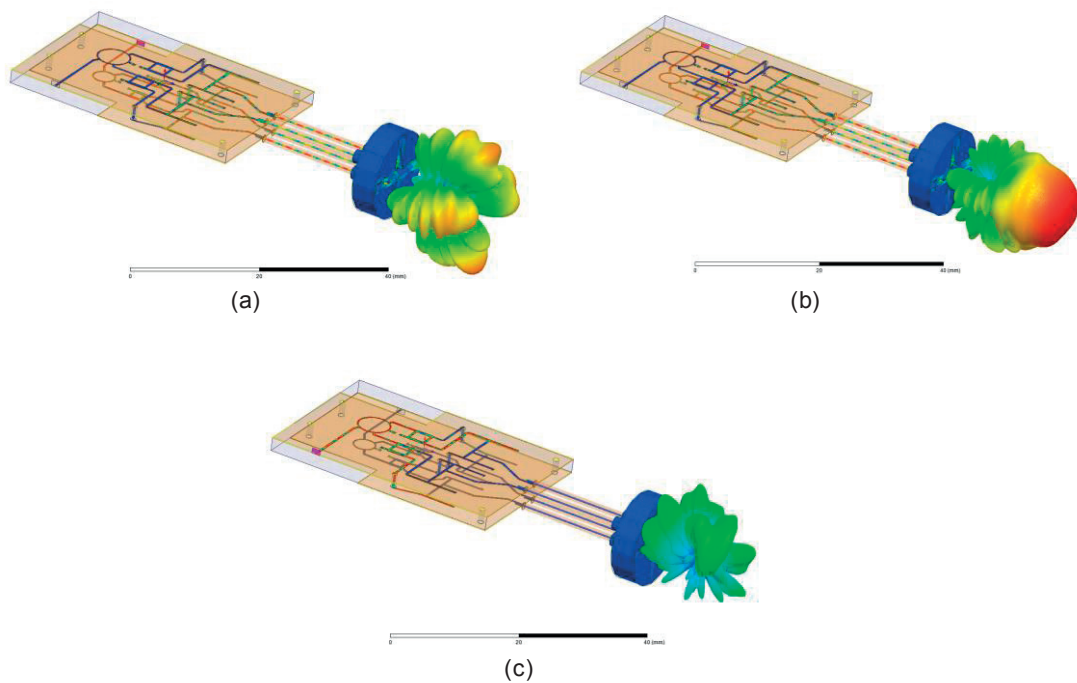
Fig. 5.16 - Radiation at 30 GHz (Tx-band): (a) RHCP (cross-pol) w hen feeding Tx port; (b) LHCP (co-pol) w hen feeding Tx port; (c) total field w hen feeding Rx port.

119

5.5   Prototypes and measurements

The experience acquired with the previous feed antennas in the previous chapters encouraged the authors to manufacture this new antenna directly with the same SLA technique successfully used for the quad-ridged horn system. Several other considerations reinforced that choice and are discussed next.

The available CNC milling workshop offered manufacturing tolerances in the order of 50 μm, while the used SLA technique is five times more accurate. In such a compact device as this cavity antenna where a great accuracy is mandatory, the enhanced precision of the SLA was already enough valuable to opt for this technology. In addition to this fact, the SLA brings in this case other important advantages like resulting in a monolithic prototype. A more sophisticated CNC workshop providing higher precision milling techniques could be selected; however, this largely increase the machining costs and, most important, would continue to prevent a single monolithic prototype. CNC techniques will always require a rigorous post-manufacturing step in order to assemble the parts with the danger of band contacts, misalignments and inaccuracies.

The final SLA prototype of the Ka-RiCSA is shown in Fig. 5.17. Its corresponding weight is 0.5 g, which is a remarkable achievement for a waveguide/cavity-based device. The fact of being a monolithic device able to avoid any screw and alignment pin allows it to benefit from the inherent lightweight of the non-metallic polymers used to print the antenna.
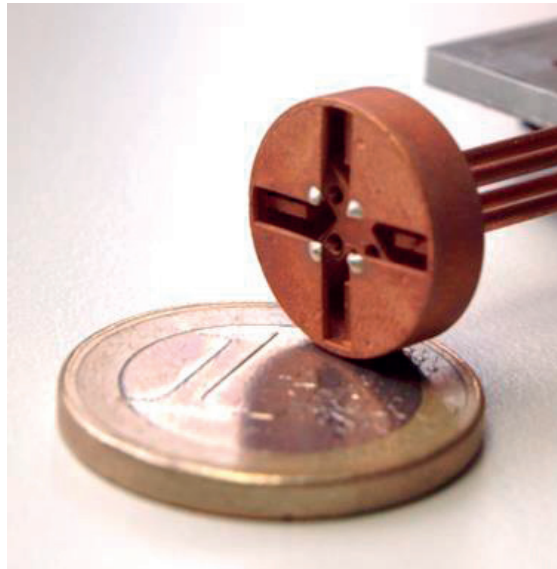
(a)
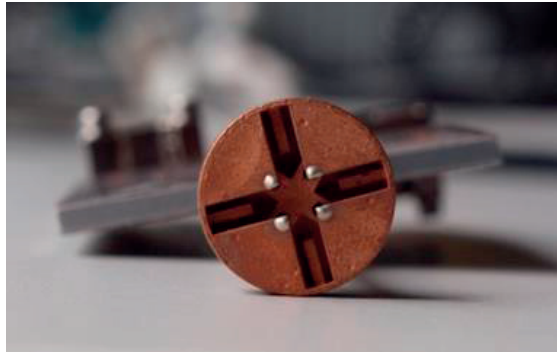
(b)

Fig. 5.17 – SLA Ka-RiCSA prototype: (a) perspective view ; (b) front view .

Regarding the conventional proof-of-concept BFN, it was manufactured using PCB technology. Both circuits are printed on Rogers Duroid 5870 substrate and the aluminum plate was fabricated using CNC milling technology. The BFN and the radiating cavity are connected through four semi-rigid EZ-47 coaxial cables. These coaxial cables were precisely cut using a dedicated tool [158] and attached to the antenna using silver epoxy glue. The Rx and Tx ports (see Fig. 5.12) are implemented using two high precision 2.92 mm connectors, thus providing access to the downlink and uplink signals, respectively.

Photographs of the complete prototype are shown in Fig. 5.18.
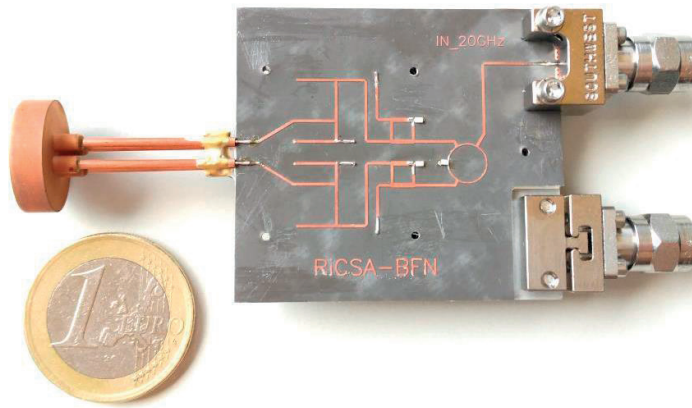
(a)
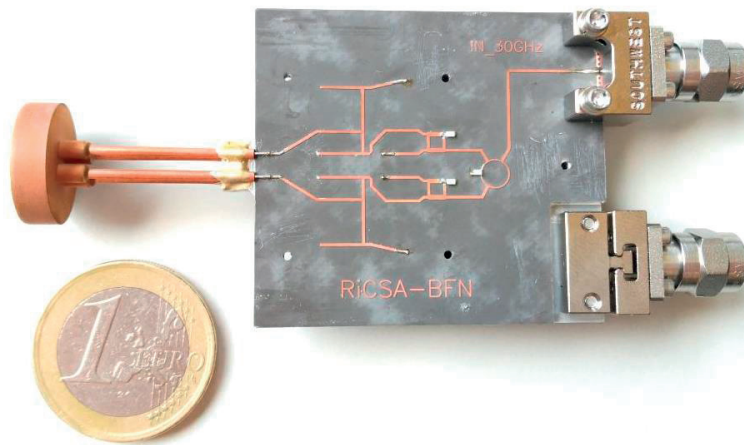
(b)
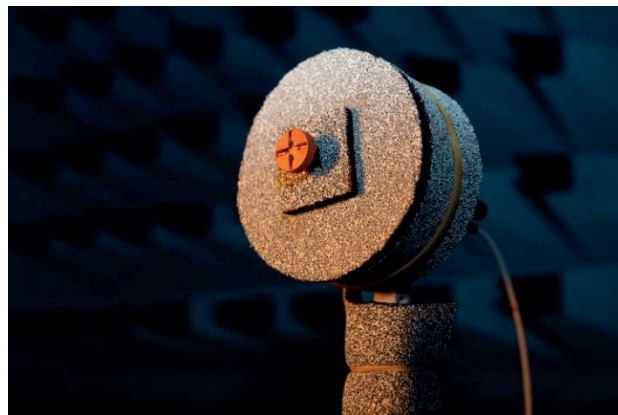
(c)

Fig. 5.18 – Final prototype: (a) complete structure with Rx BFN side up; (b) complete structure with Tx BFN side up; (c) complete structure with absorbers in the anechoic chamber.

The reflection coefficient obtained for each antenna input ports is plotted in Fig. 5.19. As desired, each port is well matched at its corresponding band of operation (Rx-port at downlink and Tx-port at uplink), thus preserving the antenna dual-band behavior. The isolation between ports is presented in Fig. 5.20 and it remains below -15dB in both downlink and uplink bands.

The insertion losses associated to each of the 4-coaxial outputs of the BFN have been measured before connecting them to the radiating cavity, they are plotted in Fig. 5.21. This figure shows that, after discarding -6 dB related to the split of power into the four ports, the losses and unbalances associated to the BFN are in the order of 1.19-1.46 dBs at 20 GHz and 1.14-1.63 dBs at 30 GHz. This order of losses is observed in the overall downlink and uplink bands, both in simulations and measurements.
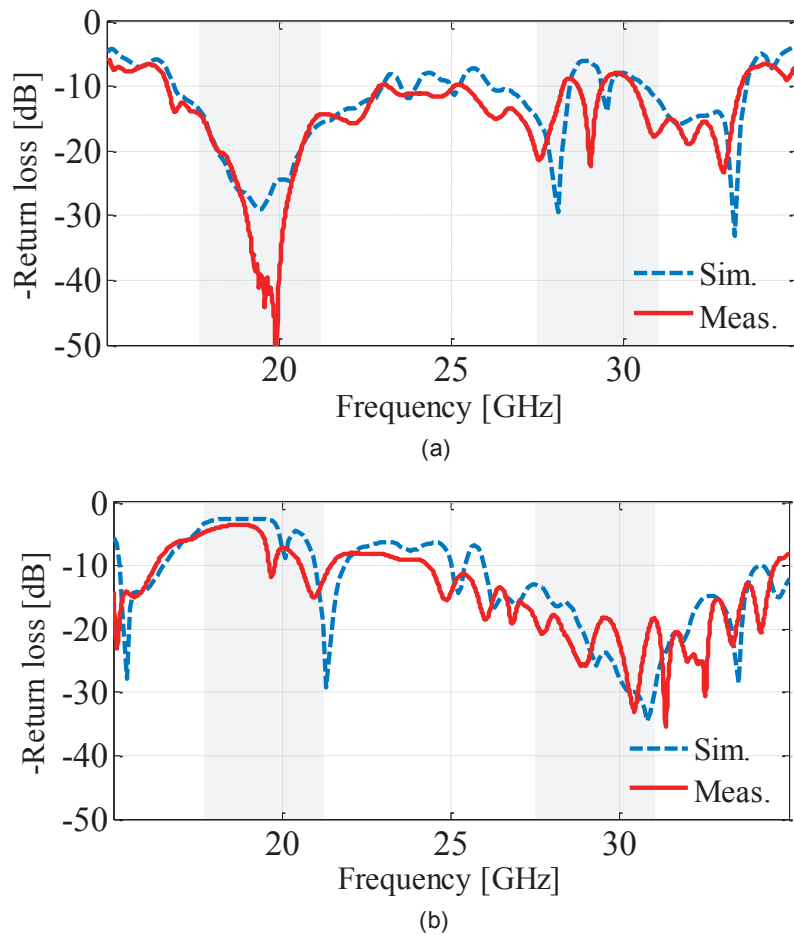
Fig. 5.19 – Simulated (dashed line) and measured (solid line) return loss of the complete structure: (a) Rx (downlink) port; (b) Tx (uplink) port.
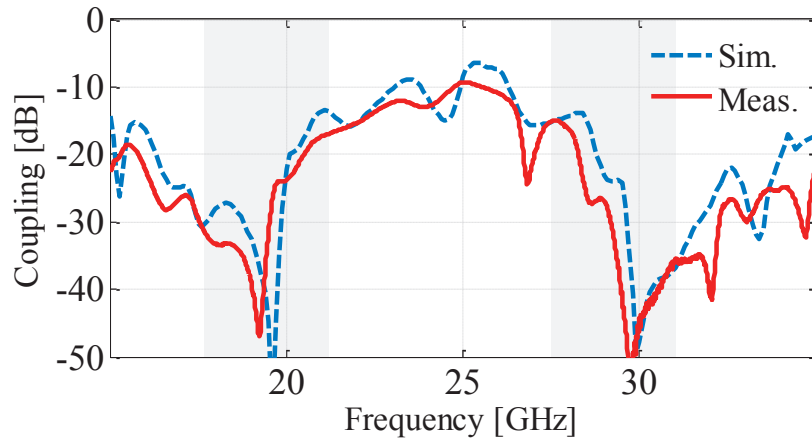
Fig. 5.20 – Simulated (dashed line) and measured (solid line) coupling between both ports.
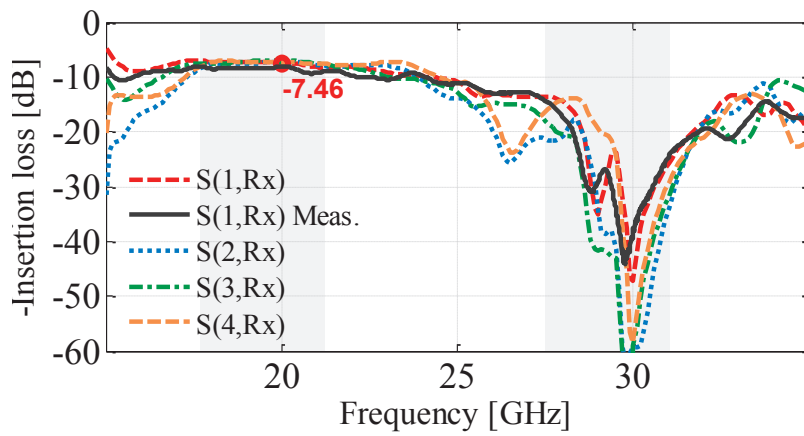
(a)
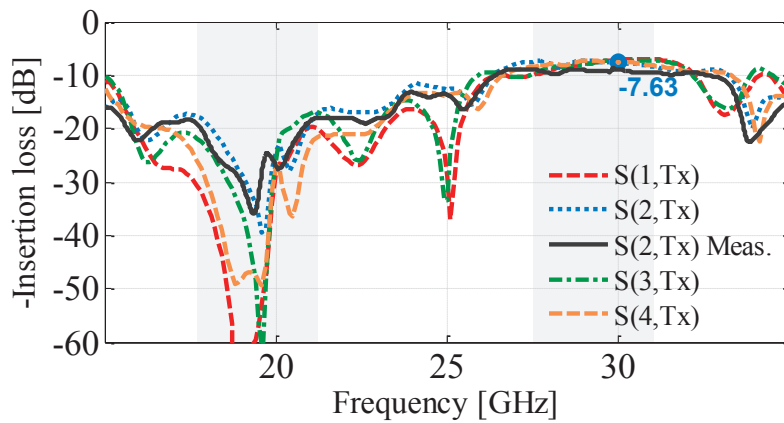
(b)

Fig. 5.21 – Simulated (dashed lines) and measured (solid line) BFN losses: (a) downlink port; (b) uplink port.

The simulated and measured normalized radiation patterns of the complete antenna system in the plane cut phi=0° are shown in Fig. 5.22. Measurements were performed only in the front side of the antenna (theta values from -90° to 90°) as the theory cannot adequately predict the back-side radiation of this prototype, where the BFN was not encapsulated but only imperfectly screened by some absorbers as seen in Fig. 5.18c. The antenna radiation was also measured in different phi-cuts and the normalized radiation patterns are shown in Fig. 5.23 with the angle phi as parameter. The different cuts show a good rotational symmetry, especially at 20 GHz.
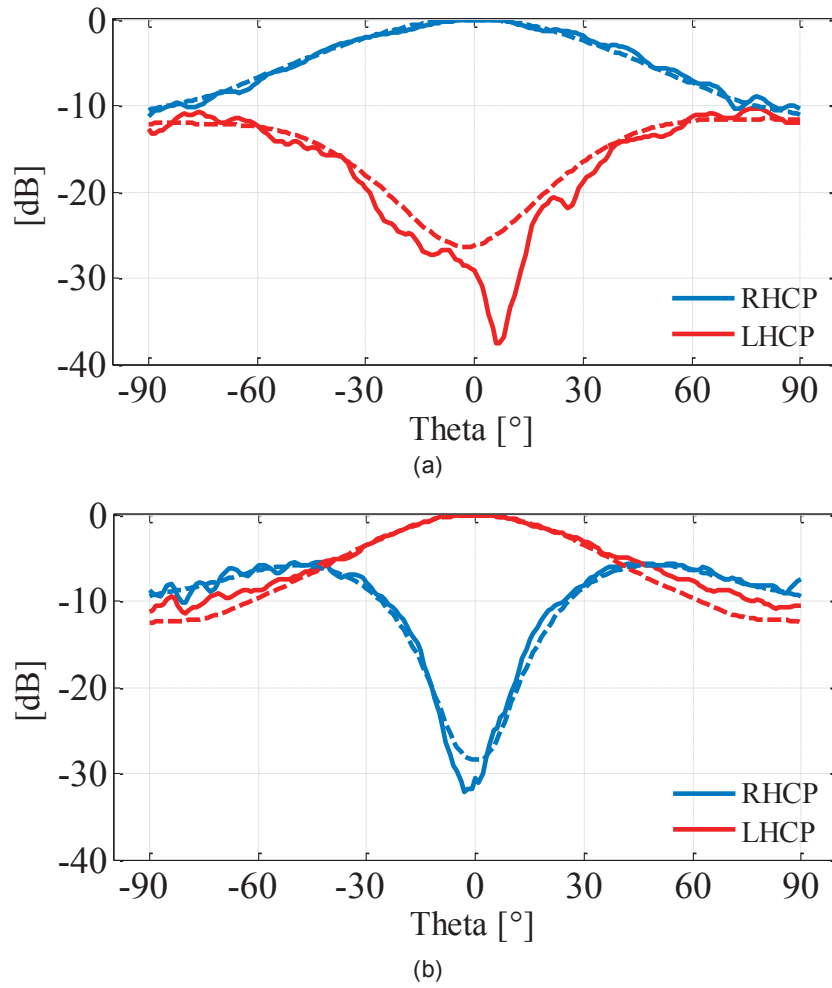
Fig. 5.22 – Simulated (dashed lines) and measured (solid lines) radiation patterns in the ϕ=0° plane. (a) at 20GHz, Rx-port active, (b) at 30GHz, Tx-port active.
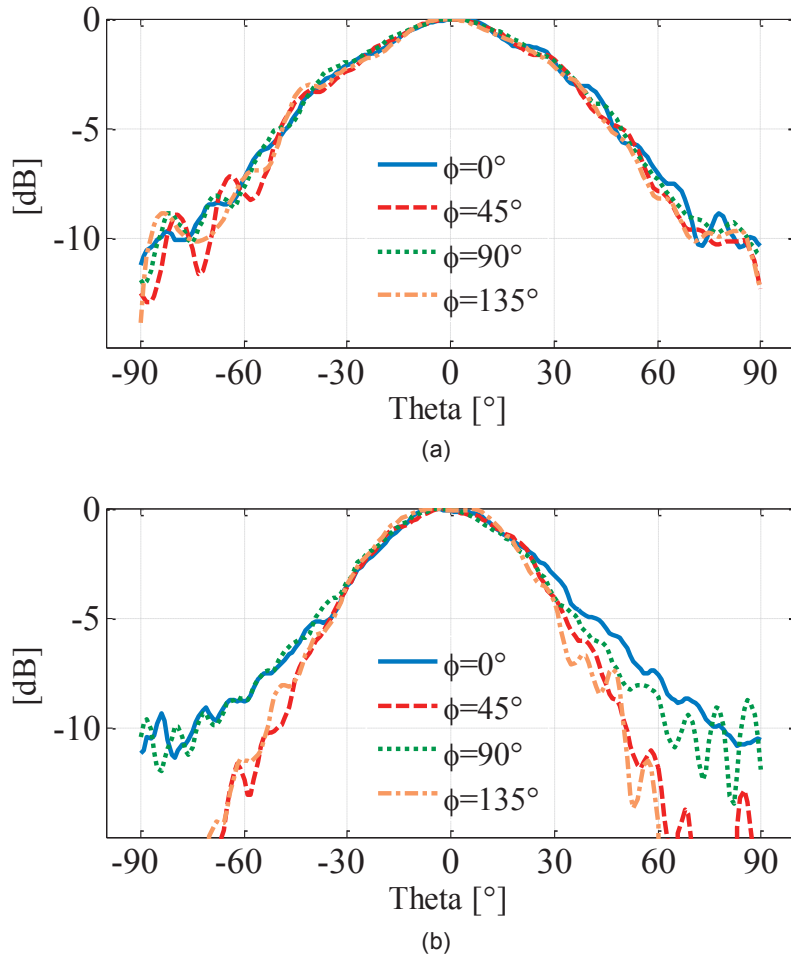
Fig. 5.23 – Co-polar normalized radiation patterns, measured for different azimuthal cuts ($\phi = 0°$, 45°, 90°, 135°): (a) RHCP at 20 GHz (Rx); (b) LHCP at 30 GHz (Tx).

Finally, plots of the antenna subsystem gain versus frequency for both Rx and Tx operation are presented in Fig. 5.24. The maximum measured gain value in both Rx and Tx modes is approximately 5 dBi, and it occurs at, respectively, 19.5 GHz and 30 GHz, as expected. The gain difference between simulations and measurements are 1.22 dB at 20 GHz and 1.75 dB at 30 GHz.

All previous figures show good agreement between measured results and theoretical predictions, thus validating the antenna operation mechanism and confirming the potential of SLA for antenna prototyping at Ka band.
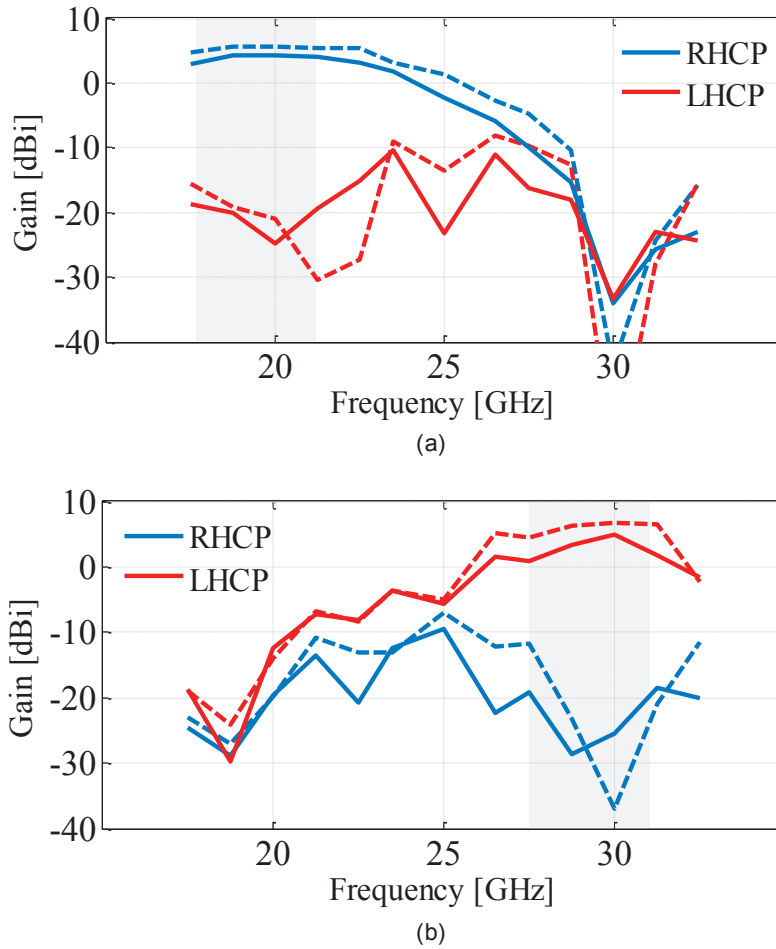
Fig. 5.24 – Simulated (dashed lines) and measured (solid lines) antenna gain: (a) Rx; (b) Tx.

5.6   SOTM application: feeder of a transmitarray

The benefits of Ka-band systems have directed research towards SOTM applications as already explained earlier in this document. Although the focus of this thesis is the feed antenna, we aim to test them together with a directive device.

For instance, in the Chapter 3, the horn antenna was tested with a dielectric lens. This lens-based system operates at both 20 GHz and 30 GHz and allows tilting the beam from 0° to 70° in relation to the zenith. Although both simulations and measurements validated the concept, there was still plenty of room to improve it, especially regarding the size of both feeder and lens. This specific goal was examined in Chapter 4, where a feeder much smaller in than the horn is proposed. In the same chapter, some preliminary tests with a planar lens were also performed and presented.

The successive efforts to obtain an optimized planar feed are documented in this chapter. The good simulated standalone performances of Ka-RiCSA were validated by the corresponding measurements. This was an decisive incentive to explore its behaviour as feeder of a planar directive device, and for the reasons explained here below a transmitarray (Tx-array) was selected.

The results presented in this section were possible thanks to the existing research of Dr. Hamed Hasani, former post-doc at LEMA, who designed the dual-band Tx-array presented in Fig. 5.25a. Thus, the logical next step was to test our RiCSA as a Tx-array feeder. The final assessment of the ongoing collaboration resulting from this idea should result in a coming publication [159], where all the technical details about this device are given. Here we will limit ourselves to a short explanation for the sake of completeness.

(c)   (d)
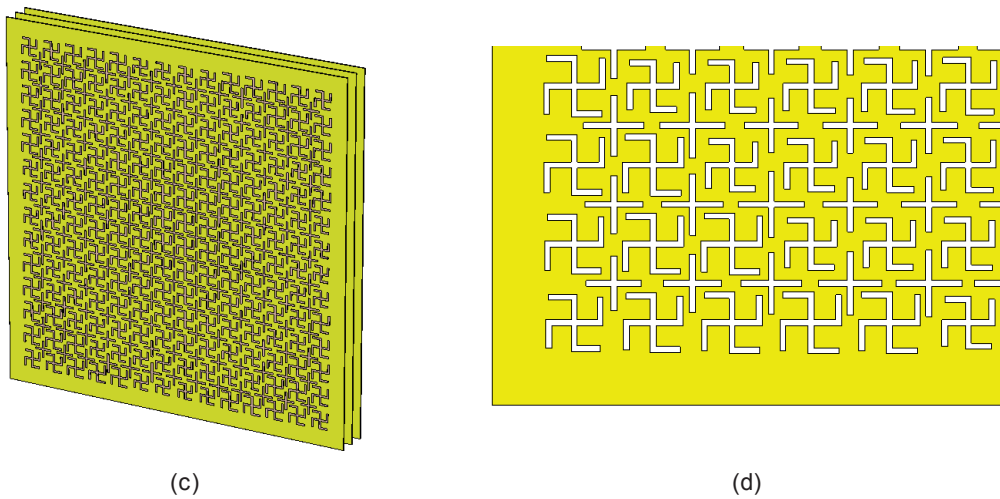
Fig. 5.25 – Tx-array: (a) final design; (b) Tx-array pattern.

While a simple cross-slot element has been chosen for operation at 30 GHz, a swastika cross is picked for operation at 20 GHz due to miniaturization purposes. Both cells are interleaved which results in the pattern shown in Fig. 5.25b. The cells are composed of three layers of dual-polarized slot elements; and therefore they are capable of operation in circular polarization as desired for the target application. The cell size of 5.3 mm would allow beam deviation up to 60° from the broadside direction at 30 GHz without originating grating lobes.

The slot elements are printed on Rogers 5870 (with 0.254 mm of thickness and ε_r = 2.33). The separation between the layers is 3.6 mm, which makes the total array thickness of 8 mm, approximately.

A square of 8 x 8 cm of the Tx-array pattern was used for simulations in order to test the validity of the concept especially in terms of beam steering at both frequency bands. It is important to highlight here that the mesh needed for this Tx-array is very dense. Therefore, due to ressources limitations, we needed to consider a Tx-array of 8 x 8 cm in an infinite plane of both metal and Rogers dielectric in the three layers. With this arrangement, only the slot apertures are meshed and the full wave solver [162] uses the structure Green functions to compute the fields. In addition, the Ka-RiCSA also here considered without the BFN for the same reason. Considering that this was a purely research initiative, we were not driven by some requirements. Therefore, for the sake of demonstrating the potential of the design we considered the Tx-array as a square of 8 x 8 cm and we took into account the feed characteristics. In line with this, the computed focal point is 55 mm below the bottom layer of the Tx-array. As done for the previous configurations presented in the document, in this case both Tx-array focal point and Ka-RiCSA phase center are also overlapped aiming to achieve the best performance. Here, again, we consider the average of both 20 GHz and 30 GHz phase center positions as the final value.

The complete system composed of both Ka-RiCSA and Tx-array is presented in Fig. 5.26. In this case, the beam is tilted thanks to a translational movement of the Tx-array, while the Ka-RiCSA is kept at the same position.

(a)   (b)
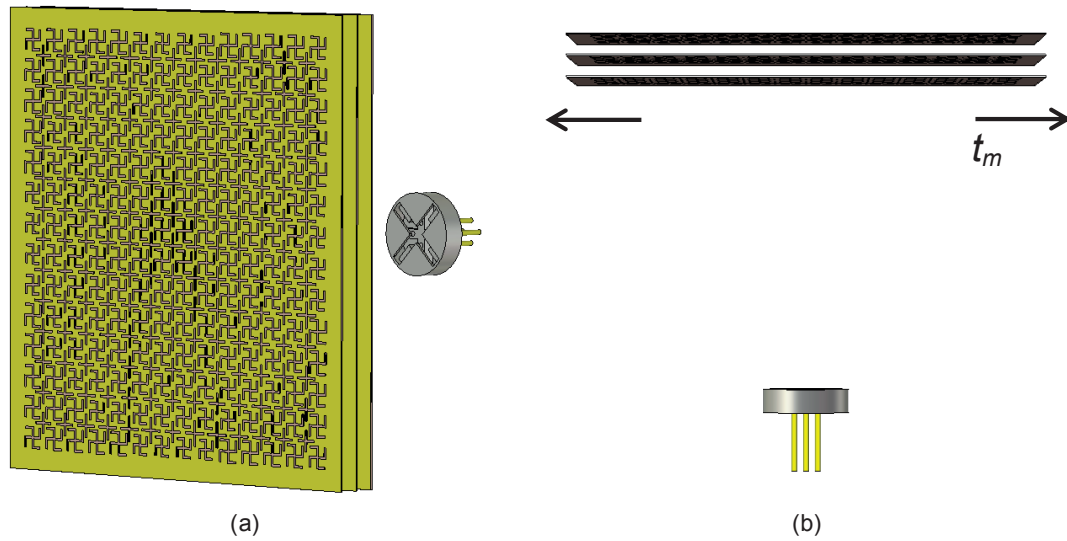
Fig. 5.26 – Complete antenna system composed of Ka-RiCSA and Tx-array: (a) perspective view; (b) front view (arrows indicate the translational movement needed to tilt the beam).

The simulated radiation patterns at both 20 GHz and 30 GHz are presented in Fig. 5.27. The Tx-array was deviated from the reference position (when both Tx-array and Ka-RiCSA are aligned, Fig. 5.26b) each 10 mm until a maximum of 30 mm (0 mm < t_m < 30 mm). As it is

possible to verify, the beam followed the movement of the Tx-array at both frequencies. It is also possible to check that the gain is higher at 30 GHz. The simulated performance indicators for both frequencies are summarized in Table 5.VIII, where t_m is the translational movement of the Tx-array, α_{beam} is the beam tilt angle, G is the gain, ΔG is the scan loss and $\Delta\alpha_{beam}$ is half of the beam pointing difference between the two frequencies. Please note that the first gain value corresponds to the simulation without the BFN, where we used four waveguide ports with 90° phase shift between them. However, as we have previously shown, the BFN will contribute to slight decrease this value due to the insertion losses. Therefore, between parentheses, we have added the expected gain accounting with the BFN losses for each frequency (1.46 dB at 20 GHz and 1.63 dB at 30 GHz, see Fig. 5.21).
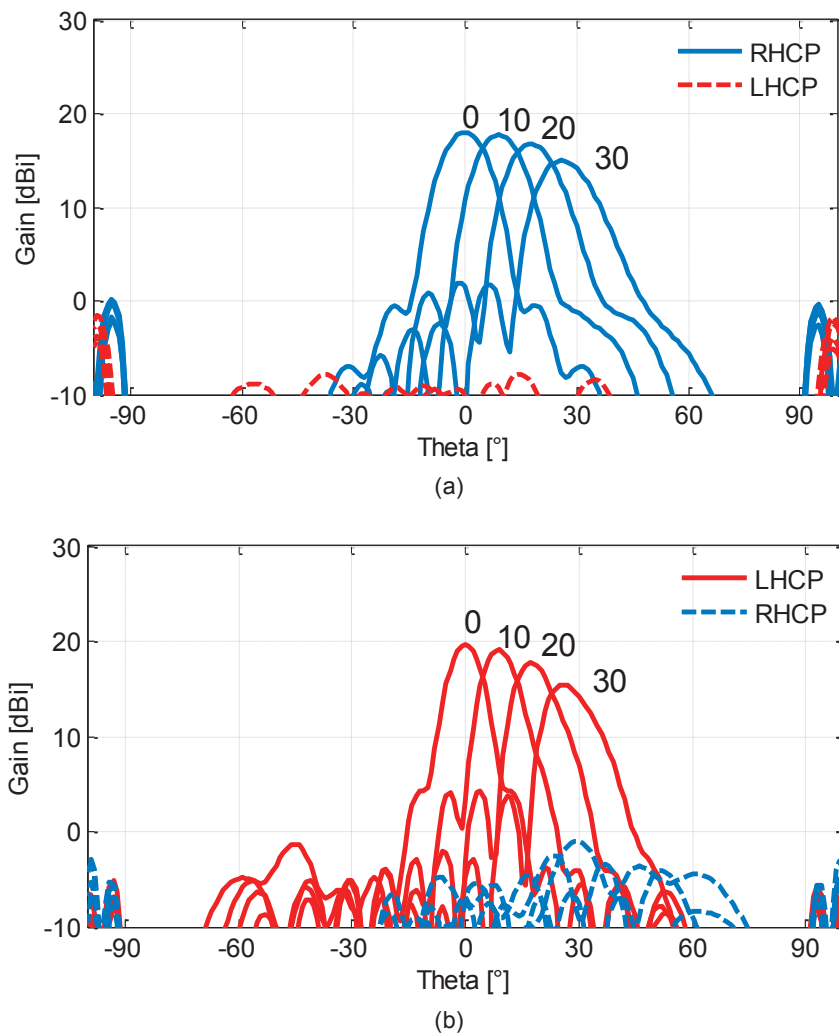
Fig. 5.27 – Simulated radiation patterns for different positions of the Tx-array (0 mm < t_m < 30 mm, with steps of 10 mm): (a) at 20 GHz; (b) at 30 GHz. Please note that the units (mm) are not written in the plots for a clear reading.

Table 5.VIII — Simulated performance indicators of the complete antenna system.

t_m [mm]	20 GHz			30 GHz			$\Delta\alpha_{beam}$ [°]
	α_{beam} [°]	G [dBi]	ΔG [dB]	α_{beam} [°]	G [dBi]	ΔG [dB]	
0	0	18 (16.54)	0	0	19.6 (17.97)	0	0
10	9	17.7 (16.24)	0.3	9	19.1 (17.47)	0.5	0
20	18	16.7 (15.24)	1.3	17	17.7 (16.07)	1.9	0.5
30	26	15 (13.54)	3	26	15.4 (13.77)	4.2	0

This Tx-array design is a compromise between size, simplicity and performance. The perfomance could be improved by increasing the number of layers and/or changing the unit-cells, which will lead to a more complex structure. On the other hand, the size of the Tx-array could be larger in order to achieve higher gain and larger scan range; however, in order to really profit from these changes, the focal distance would need to be bigger which means that the final system would not be so compact. The current design is a promising solution since it is even more challenging to accommodate all these desired functionalities for operation at both downlink and uplink Ka bands.

The Tx-array was manufactured in order to validate the design. At this point, our main goal was to verify the scanning performance. As aforementioned, the simulations were done in special conditions considering an infinite plane of both metal and Rogers dielectric (where diffraction is not considered) due to ressources limitations and that cannot be replicated in a real prototype. Therefore, in addition to the BFN losses, in the real case we will have diffraction, and therefore, a lower gain is expected. Thus, in order to have a fair comparison, the BFN losses were subtracted to the simulations for comparison between measured results.

The prototype is shown in Fig. 5.28. A comparison between measured and simulated radiation patterns for one specific position is shown in Fig. 5.29 for both frequencies. Similar agreement was verified for the other positions. The measured plots for all the positions are presented in Fig. 5.30 and the measured performance indicators for both frequencies are summarized in Table 5.IX. If we compared both Table 5.VIII (accounting with BFN losses) and Table 5.IX, we can see that there is a difference in gain of 1.24 dB at 20 GHz and 2.47 dB at 30 GHz. As aforementioned this can be justified by the different scenarios considered in simulations and measurements. The most important factor is the efficiency of the feed, since in the simulation array is fed with a feed having 100% efficiency (due to the employment of lossless materials) whereas in practice it is around 60% and 70 % at 20 and 30 GHz, respectively. Besides, the foam used between the layers, edge diffraction, fabrication tolerance and conductor losses in the transmitarray also have their own negative effect on the gain. The influence of these factors is more severe at 30 GHz.
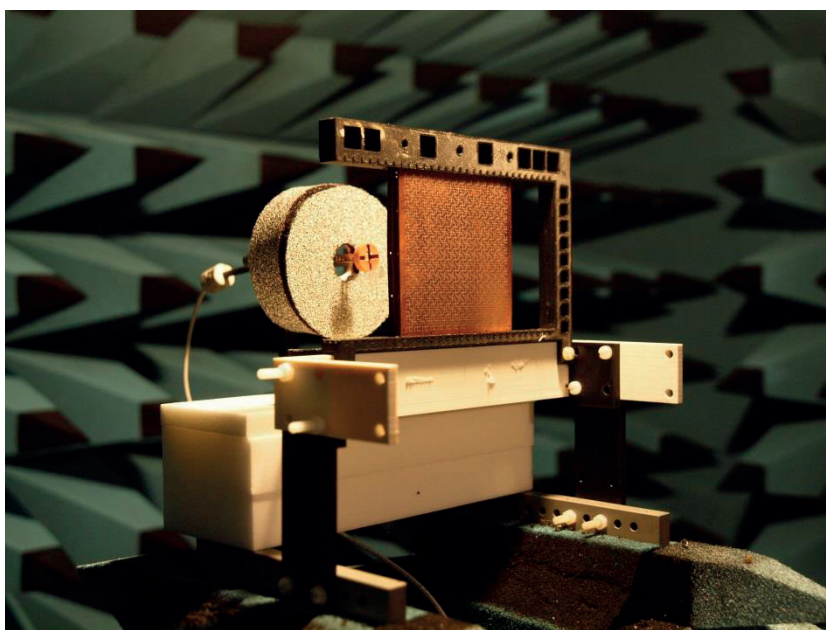
Fig 5.28 – Antenna prototype (Tx-array and Ka-RiCSA).
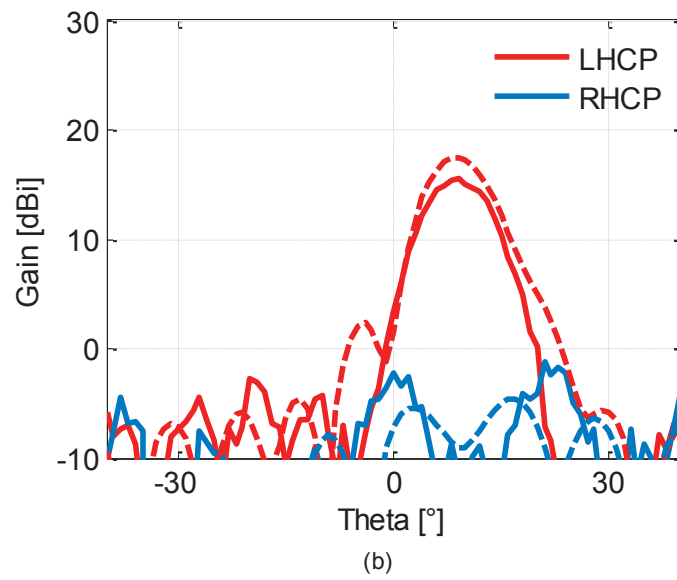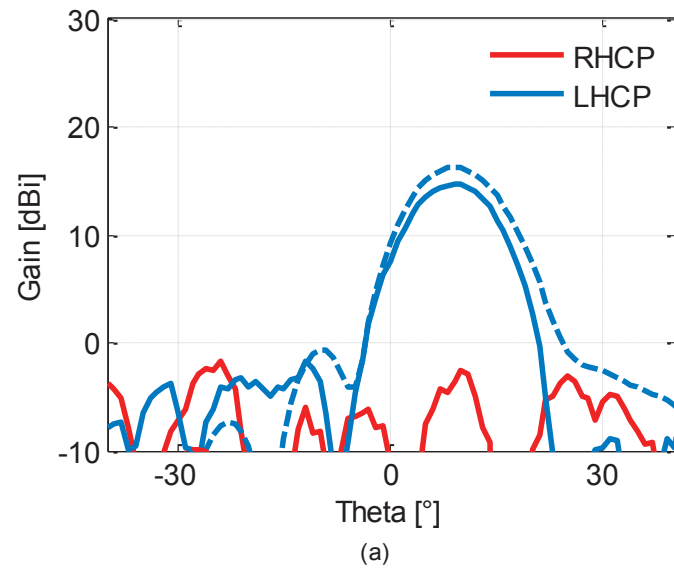
Fig. 5.29 – Simulated including BFN losses (dashed lines) and measured (solid lines) radiation patterns of complete antenna system, t_m =10 mm: (a) at 20 GHz; (b) at 30 GHz.
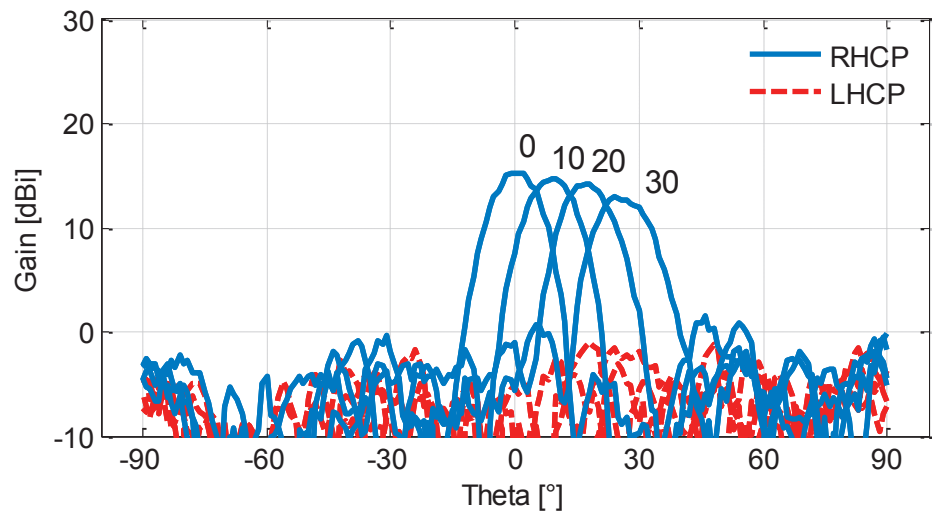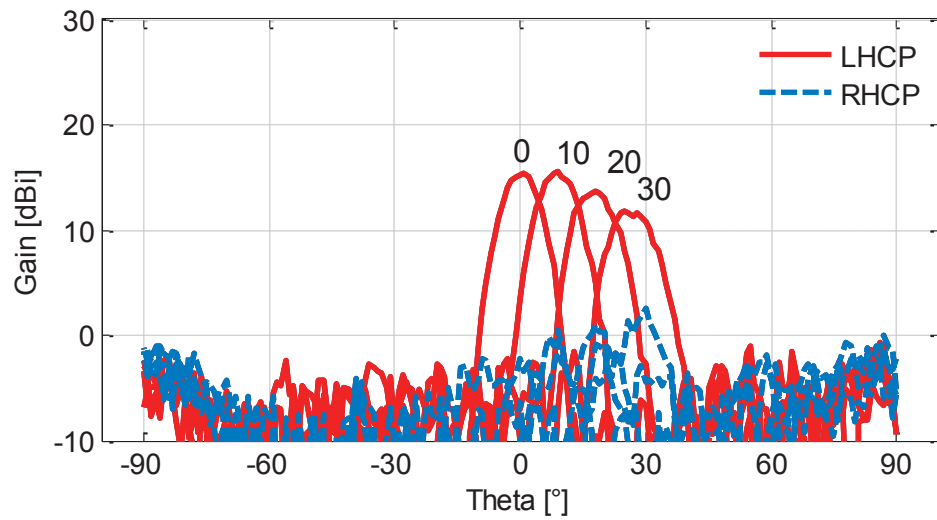
Fig. 5.30 – Measured radiation patterns for different positions of the Tx-array (0 mm < t_m < 30 mm, with steps of 10 mm): (a) Rx; (b) Tx. Please note that the units (mm) are not written in the plots for a clear reading.

Table 5.IX – Simulated performance indicators of the complete antenna system.

t_m [mm]	20 GHz			30 GHz			$\Delta\alpha_{beam}$ [°]
	α_{beam} [°]	G [dBi]	ΔG [dB]	α_{beam} [°]	G [dBi]	ΔG [dB]	
0	0	15.3	0	0	15.3	0.2	0
10	10	14.7	0.6	9	15.5	0	0.5
20	18	14.1	1.2	18	13.7	1.8	0
30	24	13	2.3	25	11.9	3.6	0.5

5.7   Conclusions

The work presented in this chapter addressed the design and manufacturing of a compact feed antenna. The structure is composed of a ridged cavity with a crossed-slot on his top aperture (Ka-RiCSA). The antenna is fed in sequential rotation through four coaxial cables that are inserted from the bottom of the cavity until the slot. In order to provide the phase differences needed by each coaxial, a printed substrate BFN was designed.

The outer diameter and height of the Ka-RICSA are 14.6 mm and 4 mm, respectively. The height of the antenna if 0.27λ at 20 GHz, which denotes a dramatic reduction of more than 93% with respect to the previous horn feed presented in Chapter 3. As it was explained and documented, the price to pay for the size reduction is lower gain values.

The good simulated results boosted the fabrication of the complete device, both Ka-RICSA and BFN. The Ka-RICSA was manufactured resorting to SLA, the same AM technique used in the horn case. In this case, due to the experience with prototypes reported in this thesis, the AM prototype was directly the first option. Concerning the BFN, it was manufactured using PCB technology. The measurements were performed after assembling both components through four coaxial cables and the results show a good agreement with the theoretical predictions.

Although the focus of this thesis is the feed antenna, its final usefulness can be completed by testing it together with a directive device. In Chapter 3, the horn antenna was tested with a dielectric lens. Here, in this chapter, we proposed a more compact solution by combining the Ka-RiCSA with a Tx-array. The height of this system is approximately 65 mm (4.3λ at 20 GHz and 6.5λ at 30 GHz), which is smaller than just the dielectric lens and its corresponding focal point (F+T = 75 mm in Chapter 3). On the other hand, there is a trade off regarding size, gain and scanning range. This system is more compact but the gain and the scanning range are smaller.

The Tx-array was manufactured and measured fed by the Ka-RiCSA. The performance of the complete system confirmed the theoretical predictions. Nevertheless, the measured gain was lower than expected, since the real finite Tx-array could not be simulated due to computer ressources limitations. In addition, misalignements in the set-up are also prone to contribute to this fact.

Conclusions and Perspectives

Valeu a pena? Tudo vale a pena
Se a alma não é pequena.

Fernando Pessoa

Exploitation of the electromagnetic spectrum is expanding towards the upper part of the microwave band and millimeter-wave frequencies mainly due to the growing capacity demand from end-users and markets. The adoption and migration to Ka-band has been the new direction for satcom and it has impacted strongly this industry, implying significant architectural changes and considerable investments.

One of the most significant changes is related to the beam configuration. Although the first spot-beam satellite systems were developed at C band (4-8 GHz) and then also used at Ku band (12-18 GHz), the regional beam coverage is dominant in these frequencies. In contrast, most part of the Ka-satellites provides spot-beam coverage allowing frequency reuse operation. Moreover, Ka-band enables narrower beams which then allow more beams per area, leading to higher frequency reuse and consequently higher capacity. Evident advantages of moving towards higher frequencies are related to gain, size and cost of the antennas, since equivalent services are now provided by smaller, lighter and, in many cases, lower-priced devices.

Intensive research activity is therefore carried out these days towards the development of Ka-band antennas and components, and main challenges concern dual-band operation (both in downlink and uplink) and CP operation. Several antenna elements based on PCB technology are already available in the literature, allowing ease of fabrication and low profile, cost and weight. Their use is typically restricted to ground applications, since they are mainly based on the use of dielectric materials. Metal-based antennas such as horns keep being the most desirable solution for the

space segment; in contrast to the previous PCB examples, they provide higher gain at the price of increased size, cost and weight. Hybrid structures combining waveguide parts with PCBs have been recently proposed in order to alleviate this trade off.

The exploitation of higher frequencies brings new challenges to the antenna design and especially to the fabrication and assembling processes of the corresponding prototypes. The devices are smaller and the required precision is higher. Traditional manufacturing techniques can achieve such accuracies but normally at higher prices. Moreover, in many cases, the devices needed to be split in several blocks and assembled afterwards which decreases the original accuracy.

These issues contributed to push research and investment towards new techniques. Recently, AM has been mentioned as one of the most promising techniques for RF components. In fact, AM techniques seem to be the enabling technology when aiming at both compactness and high precision, especially when conceiving RF components involving complex shapes at Ka-band and above. AM techniques offer the possibility to create monolithic devices, thus avoiding assembling processes that are often a source of errors and the justification for extra external material. This fact can be even more attractive when the piece is printed using light non-metallic polymers, as it is the case of SLA, leading to a dramatic weight reduction. In addition to reduced volume, weight and cost, SLA fabrication process is also recognized by high precision and inherently low surface roughness. These two aspects are crucial to attain good performance when fabricating devices that operate at high-microwave and millimeter-wave frequencies.

The questions concerning the design challenges at Ka-band and also the fabrication issues have been addressed in more detail in both Chapter 1 and Chapter 2. The aim of this thesis was to propose new feed antennas at Ka-band, comparing different design solutions and manufacturing techniques to arrive to a final and fair trade off. The second goal of the thesis, for the sake of completeness, was to test these antennas having in mind a SOTM scenario.

This thesis proposes three different antenna designs. The first one has been presented in Chapter 3. The feed system is composed by a quad-ridged horn and its dedicated coaxial-to-waveguide transition. The ridges allow achieving larger bandwidth, thus the antenna is working from downlink to uplink Ka-bands. However, the adoption of a single coaxial cable in the transition limits the operation to LP, which is a drawback. Nevertheless, its two symmetry planes allows a 90° rotation with respect to the horn and therefore, it is possible to obtain the results for two orthogonal LPs, which followed by a proper post-processed combination allows getting the expected CP response of the device. Good simulated results encouraged the fabrication of the corresponding prototype. First, the feed system was manufactured using a CNC milling technique; however the matching results of this prototype were not the expected ones. Thanks to the fact that at both 20 GHz and 30 GHz we obtained a satisfactory matching we could still perform radiation measurements at

these frequencies. Regarding these measurements, we obtain a very good agreement with simulations. Nevertheless, another prototype was manufactured but this time using a SLA technique. In addition of being more accurate than the previous one, we could fabricate a monolithic device which reduces dramatically the assembling errors as previously mentioned. Thus, we were able to recover the simulated matching response of the feeder, validating the design of the antenna. As aforementioned, one of the goals in the thesis is to test the feeders in systems intended for SOTM applications and in this case, the horn antenna was integrated with a lens. Again, it is important to highlight that the design of the lens antenna used in this system is out of the scope of this thesis. Here, more than the size of the complete system, we were interested to test the beam tilting at both 20 GHz and 30 GHz while achieving a large scanning performance. Both feeder prototypes were measured together with the lens and good agreements between simulated and measured results were obtained.

The next step was to invest in reducing the size of the feed, while keeping a good trade off regarding the electromagnetic characteristics. A more compact feed antenna is presented in Chapter 4. The structure is a cavity-backed patch antenna. Two circular patches are placed inside the circular cavity and each one is associated to one Ka-band. The antenna is fed in sequential rotation through four coaxial cables that are inserted from the bottom of the cavity. In this chapter, this new design is compared with the previous horn and the positive and negative points are fairly highlighted. Moreover, this antenna is also tested with the same lens and the results are compared with the previous ones obtained with the horn. In the end of the chapter, a preliminary study with a planar lens is performed only for uplink Ka-band. Despite the good simulated results, the tentative prototype, fabricated with CNC milling machine and PCB technology, was not performing well. At this point of the thesis, considering the experience acquired until here, we decided that the best path would be to invest in a new compact fully metallic feed design in order to fabricate it using the aforementioned SLA technique.

Hence, in Chapter 5, we present the last feed antenna proposed in this thesis. The antenna is a ridged cavity with a crossed slot on its top aperture. Here, again, the antenna is fed in sequential rotation with four coaxial cables. This time, we also invest in the design of a dedicated BFN that would provide the required phase shifts to the antenna. This BFN was a proof of concept and therefore it was done using microstrip circuits. After a theoretical analysis and an optimization of the design, the feeder was manufactured resorting the same SLA technique and the BFN was fabricated using PCB technology. After assembling both components through the four coaxial cables, we obtained a good agreement with the theoretical predictions. In accordance with the idea introduced in the last chapter, using the feeder with a planar gain enhancement device, we tested this new feed antenna with a Tx-array operating at both Ka-bands. Again, the design of the Tx-array is out of the scope of this thesis. The performance of the complete system confirmed the theoretical study. Nevertheless, as expected, the measured gain is lower once the real case was

not possible to reproduce in the simulations due to ressources limitations. In addition, misalignements in the set-up are also prone to contribute to this fact.

This thesis contributed to the research and development on Ka-band antennas and also to clearly illustrate the crucial role played by AM in the realization of these devices. Our contribution in seeking feed solutions was achieved, highlighting the trade-offs between them. In addition, the good performance obtained with AM prototypes supports and validates its strong potential and pushes for its further assessment.

The work performed in this thesis also leaves space for future research lines such as the ones listed below:

a) Miniaturize the diameter of the ridged cavity antenna and investigate an array configuration. It would be a solution to increase the gain and still be a compact solution in terms of height;
b) Investigate the possibility to do a waveguide-based BFN which would allow a complete 3D-printed device.

References

[1]   Union of Concerned Scientists (UCS), "UCS Satellite Database," Feb. 2016 [Online]. Available: http://www.ucsusa.org/nuclear-weapons/space-weapons/satellite-database?_ga=1.133109578.551668857.1469110448#.V5iwSKJznKG, accessed on Aug. 2016.

[2]   B. R. Elbert, "Introduction to Satellite Communications," Norwood, Massachusetts, USA: Artech House, 1987.

[3]   Telesat, "Advantages of Satellites" [Online]. Available: https://www.telesat.com/about-us/why-satellite/advantages-satellites, accessed on Aug. 2016.

[4]   International Telecommunication Union (ITU), "Sir Arthur C. Clarke – space age visionary" [Online]. Available: https://www.itu.int/itunews/manager/display.asp?lang=en&year=2008&issue=03&ipage=Arthur-Clarke&ext=html, accessed on Aug. 2016.

[5]   "The 1945 proposal by Arthur C. Clarke for geostationary satellite communications" [Online]. Available: http://lakdiva.org/clarke/1945ww/, accessed on Aug. 2016.

[6]   European Space Agency (ESA), "Satellite Frequency Bands," Nov. 2013 [Online]. Available: http://www.esa.int/Our_Activities/Telecommunications_Integrated_Applications/Satellite_frequency_bands, accessed on Aug. 2016.

[7]   J. R. Freer, "Computer Communications and Networks," London, United Kingdom: CRC Press, Taylor & Francis, 1996.

[8]   National Aeronautics and Space Administration (NASA), "Ka-band represents the future of space communications," May 2014 [Online]. Available: http://www.nasa.gov/mission_pages/station/research/news/ka_band, accessed on Aug. 2016.

[9] Newsat, "Ka-band," Sep. 2012 [Online]. Available: http://www.newsat.com/whitepapers/572-ka-band-white-paper/file, accessed on Aug. 2016.

[10] Microwave101, "Frequency Letter Bands" [Online]. Available: http://www.microwaves101.com/encyclopedias/frequency-letter-bands, accessed on Aug. 2016.

[11] Rafal Glowgorski, "Planar Antennas for Ka-Band Space Applications," PhD thesis, École Polytechnique Fédérale de Lausanne, Switzerland, and Instituto Superior Técnico - Universidade de Lisboa, Portugal, 2013.

[12] L. S. Chuan, S. Ru-Tian, and Y. P. Hon, "Ka band satellite communications design analysis and optimization," Defense, Science and Technology Agency (DSTA) Horizons 2015 [Online]. Available: https://www.dsta.gov.sg/docs/default-source/dsta-about/ka-band-satellite-communications-design-analysis-and-optimisation.pdf?sfvrsn=2, accessed on Aug. 2016.

[13] European Conference of Postal and Telecommunications Administrations (CEPT), Electronic Communications Committee (ECC) Report 184, "The use of earth stations on mobile platforms operating with GSO satellite networks in the frequency ranges 17.3-20.2 GHz and 27.5-30 GHz," Feb. 2013 [Online]. Available: http://www.erodocdb.dk/docs/doc98/official/pdf/ECCRep184.pdf, accessed on Aug. 2016.

[14] J. Yoh, C. C. Wang, and G. W. Goo, "Survey of Ka-band satellites for wideband communications," in Proc. Military Communications Conf. (MILCOM), Atlantic City, New Jersey, USA, Oct. 1999, pp. 120-125.

[15] CS-1 (Sakura-1) [Online]. Available: http://space.skyrocket.de/doc_sdat/cs-1.htm, accessed on Aug. 2016.

[16] European Space Agency (ESA), Telecommunications and Integrated Applications, "Historical overview" [Online]. Available: http://www.esa.int/Our_Activities/Telecommunications_Integrated_Applications/Historical_overview, accessed on Aug. 2016.

[17] Italsat-1 [Online]. Available: http://space.skyrocket.de/doc_sdat/italsat-1.htm, accessed on Aug. 2016.

[18] Kopernicus-1 [Online]. Available: http://space.skyrocket.de/doc_sdat/dfs-kopernikus-1.htm, accessed on Aug. 2016.

[19] National Aeronautics and Space Administration (NASA), "Advanced Communications Technology Satellite (ACTS)" [Online]. Available:

http://www.nasa.gov/centers/glenn/multimedia/artgallery/art_feature_006_ACTS.html, accessed on Aug. 2016.

[20] International Telecommunication Union (ITU), "Regulation of global broadband satellite communications," Apr. 2012 [Online]. Available: http://www.itu.int/ITU-D/treg/broadband/ITU-BB-Reports_RegulationBroadbandSatellite.pdf, accessed on Aug. 2016.

[21] Telesat, "The exciting potential of Ka-band" [Online]. Available: https://www.telesat.com/exciting-potential-ka-band, accessed on Aug. 2016.

[22] List os satellites at geostationary orbit [Online]. Available: http://www.satbeams.com/satellites, accessed on Aug. 2016.

[23] R. Swinford and B. Grau, "High throughput satellites – delivering future capacity needs," 2015 [Online]. Available: http://www.adlittle.com/downloads/tx_adlreports/ADL_High_Throughput_Satellites-Main_Report.pdf, accessed on Aug. 2016.

[24] Newsat, "Not all Ka-band satellites are the same," Mar. 2013 [Online]. Available: http://www.newsat.com/whitepapers/573-ka-band-satellites-are-not-same-whitepaper/file, accessed on Aug. 2016.

[25] Anik F2 [Online]. Available: https://www.telesat.com/sites/default/files/satellite/telesat_satellitebrochure_anikf2_2.pdf, accessed on Aug. 2016.

[26] G. Maral and M. Bousquet, "Satellite Communications Systems – Systems, Techniques and Technologies," Chichester, United Kingdom: Wiley, 2009.

[27] C. McLain, L. Gonzalez, and W. Hall, "Relative performance of mobile networks in the Ku, commercial Ka and government Ka bands," in Proc. Military Communications Conf. (MILCOM), Baltimore, Maryland, USA, Nov. 2011, pp. 2081-2086.

[28] J. Merchlinsky, G. Ernst, and R. Kepley, "Ground segment technologies for Ka-band and beyond," Oct. 2013 [Online]. Available: http://www.hughes.com/company/newsroom/stories/ground-segment-technologies-for-ka-band-and-beyond?locale=en, accessed on Aug. 2016.

[29] EM Solutions, "Satcom-on-the-move – a terminal engineered to sing," Aug. 2012 [Online]. Available: http://www.emsolutions.com.au/attachments/article/85/Satcom%20on%20the%20move%20terminal%20-%20engineered%20to%20hum.pdf, accessed on Aug. 2016.

[30] Y. Rahmat-Samii and A. C. Densmore, "Technology trends and challenges of antennas for satellite communication systems," IEEE Trans. Antennas Propag., vol. 63, no. 4, pp. 1191-1204, Apr. 2015.

[31] W. Fang, P. Fei, F. Nian, Y. Yang, and K. Feng, "A compact dielectric rod antenna array for wideband millimeter-wave applications," in Proc. 44th Eur. Microw. Conf., Rome, Italy, Oct. 2014, pp. 1636-1639.

[32] S. Y. Stroobandt, "An X-band high-gain dielectric rod antenna," report from the Catholic University of Leuven, Belgium, Aug. 1997 [Online]. Available: http://www.stroobandt.com/antennas/diel-rod/dielectric_rod_antenna.pdf, accessed on Aug. 2016.

[33] K. W. Leung, E. H. Lim, and X. S. Fang, "Dielectric resonator antennas: from the basic to the aesthetic," Proc. IEEE, vol. 100, no. 7, pp. 2181-2193, Jul. 2012.

[34] A. A. Long, M. W. McAllister, and L. C. Shen, "The resonant cylindrical dielectric cavity antenna," IEEE Trans. Antennas Propag, vol. 31, no. 3, pp. 406-412, May 1983.

[35] M. G. Keller, J. Shaker, A. Petosa, A. Ittipiboon, M. Cuhaci and Y. M. M. Antar, "A Ka-band dielectric resonator antenna reflectarray," in Proc. 30th Eur. Microw. Conf., Paris, France, Oct. 2000, pp. 1-4.

[36] M. H. Jamaluddin, R. Gillard, R. Sauleau, T. Koleck, and X. Castel, "Dielectric resonator antenna reflectarray in Ka band," in Proc. Int. Symp. Antennas Propag. Society (AP-S), Toronto, Ontario, Canada, Jul. 2010, pp. 1-4.

[37] D. Guha and Y. M. M. Antar, Eds., "Microstrip and Printed Antennas – New Trends , Techniques and Applications," Chicester, United Kingdom: Wiley, 2011.

[38] J.-F. Zürcher and F. E. Gardiol, "Broadband Patch Antennas," Norwood, Massachusetts, USA: Artech House, 1995.

[39] D. M. Pozar, "A review of aperture coupled microstrip antennas: history, operation, development, and applications," May 1996 [Online]. Available: http://www.ecs.umass.edu/ece/pozar/aperture.pdf, accessed on Aug. 2016.

[40] D. M. Pozar, "A microstrip antenna aperture coupled to a microstrip line," Electronic Lett., vol. 21, no. 2, pp. 49-50, Jan. 1985.

[41] Y-C. L. Liu and Y. E. Wang, "A 16x16 Ka band aperture-coupled microstrip planar array," in Proc. Int. Symp. Antennas Propag. Society (AP-S), Honolulu, Hawaii, USA, Jun. 2007, pp. 4373-4376.

[42] G. L. Dai, S. L. Lü, and M. Y. Xia, "A microstrip patch array with aperture-coupled feeding for Ka-band applications," in Proc. Global Symp. Millimeter Waves (GSMM), Nanjing, China, Apr. 2008, pp. 1-3.

[43] Y. Wang, L. Wang, and Y. Sun, "Design of L-circularly polarized microstrip antenna array at Ka-band," in Proc. Int. Conf. Microw. Millimeter Wave (ICMMT), Chengdu, China, May 2010, pp. 15-17.

[44] A. Geise and A. F. Jacob, "A ring-coupled patch antenna for broadband polarization multiplex at Ka-band," in Proc. 3rd Eur. Conf. Antennas Propag (EuCAP), Berlin, Germany, Mar. 2009, pp. 1260-1263.

[45] A.-S. Hussam, F. Mohmmad, W. M. Abdel-Wahab, G. Rafi, and S. Safavi-Naeini, "A 4x4 circularly polarized aperture coupled antenna array for Ka-band satellite communication," in Proc. Int. Symp. Antennas Propag. Society (AP-S), Vancouver, British Columbia, Canada, Jul. 2015, pp. 1896-1897.

[46] R. Glogowski, J.-F. Zürcher, J. R. Mosig, and C. Peixeiro, "Circularly polarized aperture coupled stacked patch antenna element for Ka-band," in Proc. Int. Symp. Antennas Propag. Society (AP-S), Spokane, Washington, USA, Jul. 2011, pp. 911-914.

[47] M. Zawadzki, "A circularly polarized Ka-band stacked patch antenna with increased gain," in Proc. Int. Symp. Antennas Propag. Society (AP-S), 2002, pp. 870-873.

[48] P. Gorski, J. S. Silva, and J. R. Mosig, "Wideband, low profile and circularly polarized K/Ka band antenna," in Proc. 9th Eur. Conf. Antennas Propag. (EuCAP), Lisbon, Portugal, Apr. 2015, pp. 1-3.

[49] R. B. Waterhouse, D. Novak, A. Nirmalathas, and C. Lim, "Broadband printed sectorized coverage antennas for millimeter-wave wireless applications," IEEE Trans. Antennas Propag., vol. 50, no. 1, pp. 12-16, Jan. 2002.

[50] D. Wolanský, P. Vsetula, J. Puskely, and Z. Raida, "Broadband small patch antenna array for Ka-band application," in Proc. 7th Eur. Conf. Antennas Propag. (EuCAP), Gothenburg, Sweden, Apr. 2013, pp. 907-910.

[51] F. J. Wang and J. S. Zhang, "Wide band cavity-backed patch antenna for PCS/IMI2000/2.4 GHz WLAN," Progress Electrom. Res. (PIER), vol. 74, pp. 39-46, 2007.

[52] W. Yang and J. Zhou, "Wideband circularly polarized cavity-backed aperture antenna with a parasitic square patch," IEEE Antennas Wireless Propag. Lett., vol. 13, pp. 197-200, Jan. 2014.

[53] Y.-J. Ren and K. Chang, "An ultrawideband microstrip dual-ring antenna for millimeter-wave applications," IEEE Antennas Wireless Propag. Lett., vol. 6, pp. 457-459, Oct. 2007.

[54] M. H. Awida and A. E. Fathy, "Design guidelines of substrate-integrated cavity-backed patch antennas," IET Microw. Antennas Propag., vol. 6, no. 2, pp. 151-157, Jan. 2012.

[55] J. McSpadden, L. Fan and K. Chang, "Ka-band cavity-backed inverted circular patch antenna," in Proc. Int. Symp. Antennas Propag. Society (AP-S), Montreal, Quebec, Jul. 1997, pp. 2504-2507.

[56] K. Wu, "Integration and interconnect techniques of planar and non-planar structures for microwave and millimiter-wave circuits – current status and future trend," in Proc. Asia Pacific Microw. Conf. (APMC), Taipei, Taiwan, Dec. 2001, pp. 411-416.

[57] M. Bozzi, A. Georgiadis, and K. Wu, "Review of substrate-integrated waveguide circuits and antennas," IET Microw. Antennas Propag., vol. 5, no.8, pp. 909-920, Jun. 2011.

[58] Y. J. Cheng, "Substrate Integrated Antennas and Arrays," London, United Kingdom: CRC Press, Taylor & Francis, 2016.

[59] L. Wang, M. Garcia-Vigueras, and J. R. Mosig, "Matching and gain enhancement of leaky-wave dielectric horn antenna," in Proc. 10th Eur. Conf. Antennas Propag. (EuCAP), Davos, Switzerland, Apr. 2016, pp. 1-4.

[60] L. Wang, M. Esquius-Morote, X. Yin, and J. R. Mosig, "Gain enhanced H-plane gap SIW horn antenna with phase correction," in Proc. 9th Eur. Conf. Antennas Propag. (EuCAP), Lisbon, Portugal, Apr. 2015, pp. 1-5.

[61] T. Ke-Jun and L. Xiu-Zhen, "Millimeter wave circularly polarized substrate integrated waveguide antenna," in Proc. Int. Microw. Millimeter Wave Technology (ICMMT), Nanjing, China, Apr. 2008, pp. 1058-1061.

[62] C. Kalialakis and A. Georgiadis, "A dual band circularly polarized SIW interleaved antenna array," in Proc. 10th Eur. Conf. Antennas Propag. (EuCAP), Davos, Switzerland, Apr. 2016, pp. 1-4.

[63] Y. Cai, Y. Zhang, Z. Qian, W. Cao, and S. Shi, "Compact wideband dual circularly polarized substrate integrated waveguide horn antenna," IEEE Trans. Antennas Propag., vol. 64, no. 7, pp. 3184-3189, Jul. 2016.

[64] R. Glogorski, C. Peixeiro, J.-F. Zürcher, and J. R. Mosig, "Design and optimization of a shaped-beam Ka-band substrate integrated waveguide antenna array," in Proc. Global Symp. Millimeter Waves (GSMM), Montreal, Quebec, Canada, May 2015, pp. 1-3.

[65] H. Bayer, A. Krauss, R. Stephan, and M. A. Hein, "A compact planar feed structure for Ka-band satcom-on-the-move tracking antennas," in Proc. 10th Eur. Conf. Antennas Propag. (EuCAP), Lisbon, Portugal, Apr. 2015, pp. 1-5.

[66] W. A. Imbriale, S. Gao, and L. Boccia, "Space antenna handbook," Hoboken, New Jersey, USA: Wiley, 2012.

[67] A.D. Olver, P.J.B. Clarricoats, A.A. Kishk, L. Shafai, "Microwave Horns and Feeds," Stevenage, United Kingdom: IEEE Press, 1994.

[68] C. A. Balanis, "Antenna Theory – Analysis and Design," Hoboken, New Jersey, USA: Wiley, 1997.

[69] Ian Poole, "Microwave horn antenna," [Online]. Available: http://www.radio-electronics.com/info/antennas/horn_antenna/horn_antenna.php, accessed on Aug. 2016.

[70] Ducommun, Circular and Rectangular Horn Antennas [Online]. Available: http://www.ducommun.com/pdf/mmw-antennas-ach-arh.pdf, accessed on Aug. 2016.

[71] MVG, Standard Gain Horns [Online]. Available: http://www.mvg-world.com/en/system/files/datasheet_antenna_2016_hd_standard_gain_horns.pdf, accessed on Aug. 2016.

[72] Satimo, Closed wideband quad ridge horns (QR18000) [Online]. Available: www.satimo.com/sites/www.satimo.com/files/Closed_Wideband_2013.pdf, accessed on Aug. 2016.

[73] MVG, Closed Boundary Quad-Ridge Horns [Online]. Available: http://www.mvg-world.com/en/system/files/closed_boundary_quad-ridge_horns_july_2016.pdf, accessed on Aug. 2016.

[74] O. Sotoudeh, P.-S. Kildal, P. Ingvarson, and C. Mangenot, "Dual band hard horn for use in cluster-fed multi-beam antennas in Ka-band," in Proc. Int. Symp. Antennas Propag. Society (AP-S), Jul. 2005, pp. 379-382.

[75] U. Schwerthoeffer, H. Adel, and R. Wansch, "Design and implementation of a Ka-band corrugated feed horn for reflector antennas," in Proc. Int. Symp. Antennas Propag. Society (AP-S), Orlando, Florida, USA, Jul. 2013, pp. 396-397.

[76] Y. B. Karandikar and P.-S. Kildal, "X-Ka dual band prime focus feed for satellite earth terminals," in Proc. 3rd Eur. Conf. Antennas Propag. (EuCAP), Berlin, Germany, Mar. 2009, pp. 3085-3089.

[77] J. Su and G. Zhao, "Ka/W dual frequency band dual polarization horn antenna," in Proc. 6th Int. Symp. Microw. Antenna Propag. Technologies (MAPE), Shanghai, China, Oct. 2015, pp. 129-132.

[78] N. Seong, C. Pyo, J. Chae, and C. Kim, "Ka-band satellite active phased array multi-beam antenna," in Proc. 59th Vehicular Technology Conf. (VTC), May 2004, pp. 2807-2810.

[79] Y.-B. Jung and S.-Y. Eom, "Dual-band horn array design using a helical exciter for mobile satellite communication terminals," IEEE Trans. Antennas Propag., vol. 60, no. 3, pp. 1336-1342, Mar. 2012.

[80] A. O. Salman, "Millimeter-wave sinusoidal slotted waveguide antenna," in Proc. Int. Kharkov Symp. Physics Eng. Microw. Millimeter Submillimeter Waves (MSMW), Kharkov, Ukraine, Jun. 2010, pp. 1-4.

[81] I. P. Theron and J. H. Cloete, "On slotted waveguide antenna design at Ka-band," in Proc. South African Symp. Communications Signal Processing, Rondebosh, South Africa, Sep. 1998, pp. 7-8.

[82] T. Chaloun, C. Waldschmidt, and W. Menzel, "Wide-angle scanning cavity antenna element for mobile satcom applications at Ka band," in Proc. 10th Eur. Conf. Antennas Propag. (EuCAP), Davos, Switzerland, Apr. 2016, pp. 1-5.

[83] J. Zackrisson and M. Ohgren, "GNSS receive antennas on satellites for precision orbit determination," in Proc. 25th AIAA/USU Conf. Small Satellites, Logan, UT, USA, Aug. 2011, pp. 1-9.

[84] H. E. King and J. L. Wong, "A shallow ridged-cavity crossed-slot antenna for the 240- to 400-MHz frequency range," IEEE Trans. Antennas Propag., vol. 23, no. 5, pp. 687-689, Sep. 1975.

[85] M. Manteghi and Y. Rahmat-Samii, "Multiport characteristics of a wide-band cavity backed annular patch antenna for multipolarization operations," IEEE Trans. Antennas Propag., vol. 53, no. 1, pp. 466-474, Jan. 2005.

[86] M. Garcia-Vigueras and J. R. Mosig, "Low profile antennas for GNSS and S-band TM/TC," final report of the collaborative project of EPFL, Lausanne and RUAG Space, Sweden, funded by the Swiss Space Office, 2013.

[87] Y. J. Cheng, P. Chen, W. Hong, T. Djerafi, and K. Wu, "Substrate-integrated-waveguide beamforming networks and multibeam antenna arrays for low-cost satellite and mobile systems," IEEE Antennas Propag. Mag., vol. 53, no. 6, pp. 18–30, Dec. 2011.

148

[88] A. Greda and A. Dreher, "Tx-terminal phased array for satellite communication at Ka-band," in Proc. 37th Eur. Microw. Conf., Munich, Germany, Oct. 2007, pp. 266–269.

[89] Chaloun, W. Menzel, F. Tabarani, T. Purtova, H. Schumacher, M. Kaynak, Q. Luo, S. Gao, R. Starec, and V. Ziegler, "Wide-angle scanning active transmit/receive reflectar-ray," IET Microw. Antennas Propag., vol. 8, no. 11, pp. 811—818, Aug. 2014.

[90] C. Viganó, D. L. del Río, F. Bongard, J. Padilla, and S. Vaccaro, "One-bit phased array with wide scan and linear polarization control for mobilesatellite applications," in Proc. 6th Eur. Conf. Antennas Propag. (EuCAP), Prague, Czech Republic, Mar. 2012, pp. 1641–1644.

[91] G. Bellaveglia, L. Marcellini, R. Lo Forti, A. Arcidiacono, and B. Ray, "Low profile Ku-band VSAT antenna system for high-speed trains," in Proc. 29th ESA Antenna Workshop Multiple Beams Reconfigurable Antennas ESA/ESTEC, Noordwijk, The Netherlands, May 2007, pp. 303–306.

[92] R. Lo Forti, G. Bellaveglia, A. Colasante, E. Shabirow, and M. Greenspan, "Mobile communications: High-speed train antennas from Ku to Ka," in Proc. 5th Eur. Conf. Antennas Propag. (EuCAP), Rome, Italy, Apr. 2011, pp. 2354–2357.

[93] iNetVu Mobile Internet, "Ka-75V, technical specifications" [Online]. Available: http://www.c-comsat.com/antenna/ka-75v/, accessed on Aug. 2016.

[94] H. Bayer, A. Krauss, T. Zaiczek, R. Stephan, O. Enge-Rosenblatt, and M. A. Hein, "Ka-band user terminal antennas for satellite communications," IEEE Antennas Propag. Mag., vol. 58, no. 1, pp. 76-88, Feb. 2016.

[95] J. R. Costa, C. A. Fernandes, G. Godi, R. Sauleau, L. Le Coq, and H. Legay, "Compact Ka-band lens antennas for LEO satellites," IEEE Trans. Antennas and Propag., vol. 56, no. 5, pp. 1251–1258, May 2008.

[96] J. R. Costa, E. B. Lima, and C. A. Fernandes, "Compact beam-steerable lens antennas for 60-GHz wireless communications," IEEETrans. Antennas Propag., vol. 57, no. 10, pp. 2926–2933, Oct. 2009.

[97] J. S. Silva, J. R. Costa, E. B. Lima, and C. A. Fernandes, "Ground terminalantenna for Ka-band satellite communications," in Proc. 7th Eur. Conf.Antennas Propag. (EuCAP), Gothenburg, Sweden, Apr. 2013, pp. 1613–1616.

[98] J. Thornton, D. Smith, S. J. Forti, and Y. Y. Jiang, "Reduced height luneberg lens antennas for satellite communications-on-the-move," *in Proc. Conf. Microw. Techn. (COMITE)*, Pardubice, Czech Republic, Apr. 2015, pp. 1-4.

[99] T. Maruyama, K. Yamamori, and Y. Kuwahara, "Design of multibeam dielectric lens antennas by multiobjective optimization," IEEE Trans. Antennas Propag., vol. 57, no. 1, pp. 57–63, Jan. 2009.

[100] E. B. Lima, S. A. Matos, J. R. Costa, C. A. Fernandes, and N. J. G. Fonseca, "Circular polarization wide-angle beam steering at Ka-band by in-plane translation of a plate lens antenna," IEEE Trans. Antennas Propag., vol. 63, no. 12, pp. 5443-5455, Dec. 2015.

[101] L. Di Palma, A. Clemente, L. Dussopt, R. Sauleau, P. Potier, and P. Pouliguen, "Circularly polarized transmitarray with sequential rotation in Ka-band," IEEE Trans. Antennas Propag., vol. 63, no. 11, pp. 5118-5124, Nov. 2015.

[102] J.-M. Baracco, P. Ratajczak, P. Brachat, and G. Toso, "A dual frequency Ka-band printed fresnel reflector for ground terminal applications," IEEE Trans. Antennas Propag., vol. 63, no. 10, pp. 4352-4366, Oct. 2015.

[103] M. Shelley, J. Vazquez, and D. Moore, "X- and Ka-band low profile antennas for aeronautical and land mobile satcom," in Proc. 8th Eur. Conf. Antennas Propag. (EuCAP), pp. 2619-2622, The Hague, The Netherlands, Apr. 2014.

[104] N. Gagnon and A. Petosa, "Using rotatable planar phase shifting surfaces to steer a high-gain beam," IEEE Trans. Antennas Propag., vol. 61, no. 6, pp. 3086–3092, Jun. 2013.

[105] M. Tripodi, F. DiMarca, T. Cadili, C. Mollura, F. DiMaggio, andM. Russo, "Ka band active phased array antenna system for satellite communication on the move terminal," in Proc. 5th Eur. Conf. Antennas Propag. (EuCAP), Rome, Italy, Apr. 2011, pp. 2628–2630.

[106] I. Gibson, D. W. Rosen, and B. Stucker, "Additive manufacturing technologies," New York City, New York, USA: Springer, 2010.

[107] O. A. Peverini, G. Virone, G. Addamo, and R. Tascone, "Development of passive microwave antenna-feed systems for wideband dual-polarisation receivers," IET Microw. Antennas Propag., vol. 5, no. 8, pp. 1008-1015, Jun. 2011.

[108] S. Srikanth and M. Solatka, "A compact full waveguide band turnstile junction orthomode transducer," in Proc. General Assembly Scientific Symp., Istambul, Turkey, Aug. 2011, pp. 1-4.

[109] D. Henke and S. Claude, "Minimizing RF performance spikes in a cryogenic orthomode transducer (OMT)," IEEE Trans. Microw. Theory Techniques, vol. 62, no. 4, pp. 840-850, Mar. 2014.

150

[110] G. Virone, O. A. Peverini, M. Lumia, M. Z. Farooqui, G. Adamo, and R. Tascone, "W-band orthomode transducer for dense focal-plane clusters," IEEE Microw. Wireless Components Lett., vol. 25, no. 2, pp. 85-87, Dec. 2014.

[111] M. Vaezi, H. Seitz, and S. Yang, "A review on 3D micro-additive manufacturing technologies," Int. J. Adv. Manuf. Technol., vol 67, no. 5, pp. 1721-1754, July 2013.

[112] "Horizon 2020: key enabling technologies (KETs), booster for European leadership in the manufacturing sector," Study for the Industry, Research and Energy (ITRE) Committee, Oct. 2014 [Online]. Available: http://www.europarl.europa.eu/RegData/etudes/STUD/2014/536282/IPOL_STU(2014)536282_EN.pdf, accessed on Aug. 2016.

[113] T. Ghidini, "An overview of current AM activities at the European Space Agency," 2013 [Online]. Available: http://www.3d-printing-additive-manufacturing.com/media/downloads/52-d1-12-20-c-tommaso-ghidini-esa.pdf, accessed on Aug. 2016.

[114] E. Van de Velde, C. Rammer, B. Gehrke, P. Debergh, P. Schliessler, and P. Wassmann, "Key Enabling Technologies (KETs) Observatory," first annual report, May 2015 [Online]. Available: https://ec.europa.eu/growth/tools-databases/kets-tools/sites/default/files/library/kets_1st_annual_report.pdf, accessed on Aug. 2016.

[115] "Additive Manufacturing in FP7 and Horizon 2020," report from the EC workshop on additive manufacturing, Jun. 2014 [Online]. Available: http://www.rm-platform.com/linkdoc/EC%20AM%20Workshop%20Report%202014.pdf, accessed on Aug. 2016.

[116] Gartner's Hype Cycle for 3D Printing, 2015 [Online]. Available: http://www.forbes.com/sites/louiscolumbus/2015/08/28/gartners-hype-cycle-for-3-d-printing-2015-medical-products-driving-market-growth/#ed580775c505, accessed on Aug. 2016.

[117] Sculpteo, "The state of 3D printing," Apr. 2015 [Online]. Available: http://www.sculpteo.com/static/0.30.0-64/download/report/Sculpteo_State_of_3D_Printing.pdf, accessed on Aug. 2016.

[118] M. van der Vorst, J. R. Mosig, E. Menargues, E. de Rijk, M. Favre, and M. Billod, "Metal-coated additive manufactured mm-wave antenna feed chains with integrated orthomode transducers," European Space Agency-GSTP project, 2015-2017.

[119] Project between SWISSto12 and Cobham Antenna Systems funded by European Space agency, Press Release Mar. 2016 [Online]. Available:

http://www.swissto12.ch/resources/Press-Release-ARTES-with-Cobham.pdf, accessed on Aug. 2016

[120] Collaborative EU project, Additive Manufacturing Aiming towards Zero waste and Efficient production of high-tech metal products (AMAZE), 2013-2017 [Online]. Available: http://cordis.europa.eu/project/rcn/105484_en.html, accessed on Aug. 2016.

[121] European Space Agency, "Ten ways 3D printing could change space," Apr. 2014 [Onlin]. Available:
http://www.esa.int/Our_Activities/Space_Engineering_Technology/Ten_ways_3D_printing_could_change_space, accessed on Aug. 2016.

[122] V. T. di Crestvolant, P. M. Iglesias, and M. J. Lancaster, "Advanced butler matrices with integrated bandpass filter functions," IEEE Trans. Microw.Theory Techn., vol. 63, no. 10, pp. 3433-3444, Oct. 2015.

[123] M. Szymkiewicz, Y. Konkel, C. Hartwanger, and M. Schneider, "Ku-band sidearm ortho-mode transducer manufactured by additive layer manufacturing," in Proc. 10th Eur. Conf. Antennas Propag. (EuCAP), Davos, Switzerland, Apr. 2016, pp. 1-4.

[124] L. G. Menéndez, O. S. Kim, F. Persson, M. Nielsen, and O. Breinbjerg, "3D printed 20/30-GHz dual-band offset stepped-reflector antenna," in Proc. 9th Eur. Conf.Antennas Propag. (EuCAP), Lisbon, Portugal, Apr. 2015, pp. 1-2.

[125] "Additive manufacturing and 3D printing state of the industry," Annual worldwide progress report, Fort Collins, Colorado, USA: Wohlers Associates, Inc. 2013.

[126] G.-L. Huang, S.-G. Zhou, T.-H. Chio, and T.-S. Yeo, "Fabrication of a high-efficiency waveguide antenna array via direct metal laser sintering," IEEE Antennas Wireless Propag. Lett.,, vol. 15, pp. 622-625, Aug. 2015.

[127] A. Macor, E. de Rijk, S. Alberti, T. Goodman, and J.-Ph. Ansermet, "Three-dimensional stereolithography for millimeter wave and terahertz applications," Rev. Sci. Instrum., vol. 83, no. 4, Apr. 2012.

[128] E. de Rijk, J. S. Silva, S. Capdevila, M. Favre, M. Billod, and A. Macor, "Additive manufac-tured RF components based on stereo-lithography," 36th European Space Agency Work-shop in Antennas and RF Systems, ESA/ESTEC, The Netherlands, Oct. 2015.

[129] Additively, Stereolithography [Online]. Available: https://www.additively.com/en/learn-about/stereolithography, accessed on Aug. 2016.

[130] J. Thornton, B. Dalay, and D. Smith, "Additive manufacturing of waveguide for Ku-band satellite communications antenna," in Proc. 10th Eur. Conf. Antennas Propag. (EuCAP), Davos, Switzerland, Apr. 2016, pp. 1-4.

[131] M. van der Vorst and J. Gumpinger, "Applicability of 3D printing techniques for compact Ku-band medium/high-gain antennas," in Proc. 10th Eur. Conf. Antennas Propag. (EuCAP), Davos, Switzerland, Apr. 2016, pp. 1-4.

[132] G. P. Le Sage, "3D printed waveguide slot array antennas," IEEE Access, vol. 4, pp. 1258-1265, Mar. 2016.

[133] L. Schulwitz and A. Mortazawi, "A compact millimeter-wave horn antenna array fabricated through layer-by-layer stereolithography," Int. Symp. Antennas Propag. Society (AP-S), San Diego, California, USA, Jul. 2008, pp. 1-4.

[134] A. von Bieren, E. de Rijk, J.-Ph. Ansermet, and A. Macor, "Monolithic metal-coated plastic components for mm-wave applications," in Proc. 39th Int. Conf. Infrared, mm- and THz-waves (IRMMW-THz), Tucson, Arizona, USA, Sep. 2014, pp.1-2.

[135] P. T. Timbie, J. Grade, D. Van der Weide, B. Maffei, and G. Pisano, "Stereolithographed mm-wave corrugated horn antennas," in Proc. 36th Int. Conf. Infrared, mm- and THz-waves (IRMMW-THz), Wollongong, New South Wales, Australia, Sep. 2012, pp.1.

[136] A. Macor, B. Maffei, P. Timbie, E. de Rijk, J. Grade, G. Pisano, M. Powers, and D. van der Weide, "High performance stereolithographed W-band waveguide components for large format array instruments," in Proc. 37th Int. Conf. Infrared, mm- and THz-waves (IRMMW-THz), Houston, Texas, USA, Oct. 2011, pp.1-3.

[137] SWISSto12 [Online]. Available: www.swissto12.ch, accessed on Aug. 2016.

[138] J. S. Silva, Master thesis entitled "Antenas compactas baseadas em lentes com feixe orientável para terminais de terra na banda Ka," ISCTE-IUL, Sep. 2012.

[139] D. T. Emerson, "The work of Jagadis Chandra Bose: 100 years of millimeter-wave research," IEEE Trans. Microw. Theory Techniques, vol. 45, no. 12, pp. 2267-2273, Dec. 1997.

[140] W. L. Barrow and L. J. Chu, "Theory of the electromagnetic horn," Proc. IRE, vol. 27, no. 1, pp. 51-64, Jan. 1939.

[141] Horn antennas (pictures) [Online]. Available: https://en.wikipedia.org/wiki/Horn_antenna, accessed on Oct. 2016.

[142] V. Rodriguez, "A brief history of horns, from early history to latest developments," Nov. 2010 [Online]. Available: http://www.ets-lindgren.com/pdf/briefhistoryofhornantennas.pdf, accessed on Oct. 2016.

[143] Millitech, circular waveguide sizes [Online]. Available: http://www.millitech.com/pdfs/circwave.pdf, accessed on Oct. 2016.

[144] Computer Simulation Technology (CST). Darmstadt, Germany [Online]. Available: https://www.cst.com/, accessed on Oct. 2016.

[145] N. Rui-Xing, L. En, G. Gao-Feng, and W. Yi, "Simulation and Design of 18-40GHz Ridge Waveguide to Coaxial Transition," Proc. ICMTCE, pp. 183-185, Beijing, China, May 2011.

[146] A. R. Mallahzadeh and A. Imani, "Double-Ridged Antenna for Wideband Applications," Prog. in Electromagnetics Research (PIER), vol. 91, pp. 273-285, 2009.

[147] A. Peebles, "A dielectric bifocal lens for multibeam antenna applications," IEEE Trans. Antennas Propag., vol. 36, no. 5, pp. 599-606, May 1988.

[148] G. A. Deschamps, "Microstrip microwave antennas," 3rd USAF Symp. Antennas, Oct. 1953.

[149] H. Gutton and G. Baissinot, "Flat aerial for ultra high frequencies," French Patent No. 70313, 1955.

[150] D. M. Pozar, "Microwave Engineering," Chichester, United Kingdom: Wiley, 2009.

[151] W. H. Watson, "The Physical Principles of Waveguide Transmission and Antenna Systems," Oxford, UK: Oxford Clarendon Press, 1947.

[152] A. F. Stevenson, "Theory of slots in rectangular waveguides," J. Appl. Physics, vol. 19, pp. 24-38, Jan. 1948.

[153] M. H. Cohen, "On the bandwidth of cavity antennas," J. Appl. Physics, vol. 25, no. 5, pp. 582-587, May 1954.

[154] A. Vasiliadis and R. L. Tanner, "Evaluating the impedance broadbanding potential of antennas," IRE Trans. Antennas Propag., vol. 6, no. 3, pp. 226-231, Jul. 1958.

[155] A. T. Adams, "Flush mounted rectangular cavity slot antenna - theory and design", IEEE Trans. Antennas Propag., vol. 15, no. 3, pp. 342–351, May 1967.

[156] J. Galejs, "Antennas in inhomogeneous media," Oxford, UK: Pergamon Press, 1969.

[157] V. Deillon, J.-F. Zürcher, and A. K. Skrivervik, "A compact dual-band dual-polarized antenna element for GSM/DCS/UMTS base stations," IEEE Microw. Opt. Technol. Lett., vol. 40, no. 1, Jan. 2004.

[158] Cable stripping tool Huber+Suhner W157 (74_Z-0-0-157).

[159] H. Hasani, J. S. Silva, S. Capdevila, M. Garcia-Vigueras, and J. R. Mosig, "Dual-band transmitarray for satellite communications in Ka band," (provisory title) *in preparation*.

[160] P. Ingvarson, U. Jostell, and P. Svedjenas, "Patch-excited cup elements for satellite-based mobile communication antennas," in Proc. Int. Conf. Phased Array Systems and Technol., Dana Point, California, USA, May 2000, pp. 215-218.

[161] ANSYS HFSS. Canonsburg, Pennsylvania, USA [Online]. Available: http://www.ansys.com/Products/Electronics/ANSYS-HFSS, accessed on Mar. 2017.

[162] Altair Engineering - FEKO. Troy, Michigan, USA [Online]. Available: https://www.feko.info, accessed on Mar. 2017.

List of Figures

158

160

Cavity inner dimensions: D = 13.6 mm; H = 3 mm

List of Tables

Joana Santos Silva

Schlosshofstrasse 23, 8600 Winterthur, Switzerland
+41 78 677 24 40 | joanarassilva@gmail.com
Nationality: Portuguese | Birth: 14 March 1988 | Driving license: B | Status: Single

I have four years of research experience in Antennas and during that time I have focused on the design of compact feeders for Ka-band satellite-on-the-move applications with an output of more than 10 papers in international peer-reviewed journals and conferences. In addition to the experience with different software products, I also have acquired experience in different manufacturing techniques (computer numerical control milling machine, printed circuit board and additive technologies), laboratory measurements and public speaking.

Work experience

Development Engineer on Antennas | Jan. 2017 –

HUBER+SUHNER, Herisau, Switzerland

Education

PhD degree | Jan. 2013 – Mar. 2017

Joint initiative of École Polytechnique Fédéral de Lausanne (EPFL), Switzerland and Instituto Superior Técnico – Universidade de Lisboa (IST-UL), Portugal in the focus area of Antennas and EM devices for Wireless Applications.

Experience : - Participation in the project KALens, *Compact Lens-based Mechanically Steered Ka-band User Terminal Antenna*, funded by the European Space Agency (ESA);
- Participation in the project mm-SatCom, *Millimeter Wave Antennas for Next-Generation Satellite Mass Services*, funded by the Fundação para a Ciência e a Tecnologia (FCT);
- Participation in the European Cooperation in Science and Technology (COST) Action IC1102: *Versatile, Integrated and Signal-aware Technologies for Antennas (VISTA)*;
- Teaching assistant on bachelor-level courses at EPFL.

MSc degree | Sep. 2010 – Sep. 2012

Telecommunications and Computer Engineering at ISCTE – Instituto Universitário de Lisboa (IUL), Portugal.
Master thesis: Lens-based steerable-beam compact antennas for Ka-band ground terminals.

BSc degree | Sep. 2006 – Jun. 2010

Telecommunications and Computer Engineering at ISCTE – Instituto Universitário de Lisboa (IUL), Portugal.

Skills

Languages Portuguese (mother tongue), English (proficient user, C1), French (independent user, B1), Spanish (basic user, A2), German (basic user, A1).

Software Good command of Microsoft Windows, Mac OS X, Microsoft Office Suite, Matlab, Ansys HFSS, CST Microwave Studio and SolidWorks.

Social Excellent team spirit and communication skills due to my experience as a Students' Association and IEEE Student Branch member at ISCTE-IUL as well as a volunteer staff member at international conferences. Very good ability to adapt to multicultural environments due to my experience abroad.

Additional information

Awards & Honors
Oct. 2015: Best Poster Award in the 36th ESA Antenna Workshop with the work *Additive Manufactured RF components based on Stereo-lithography.*
Nov. 2012: Honorable Mention of ANACOM-URSI Portugal Prize with the work *Lens-based steerable-beam compact antennas for Ka-band ground terminals*.

Training
Mar. 2011: European School of Antennas (ESoA) course, *Antenna Project Management* at EPFL.

Publications & Peer-review
Author of several publications in journals (2 published, 1 accepted for publication) and conference proceedings (12 published).
Reviewer for IEEE and IET journals as well as for international conferences in Antennas and Propagation.

Personal interests

I love travelling, reading, sports (cycling, snowboarding, pilates, TRX), interior design and socializing with friends.